Preparation and Characterization of New Materials for the Storage of Electric Energy

2005

Takahiro Morishita

Contents

Chapter 3

Preparation of carbon-coated metallic tin powders and their anode performance for lithium ion rechargeable batteries

Chapter 4

Preparation of porous carbons from thermoplastic precursors without activation process and their performance for electrode materials of electric double layer capacitors

Chapter 5

Preparation of carbon-coated tungsten and molybdenum carbides and their performance for electrode materials of electrochemical capacitors

Chapter 6

Conclusions

Abstract in English

Electric energy storage devices, such as lithium ion rechargeable batteries and electrochemical capacitors, are used in various equipments. They are going to be used more in various systems, for examples, electric vehicles, but for these applications better performances, such as higher power density and better rate characteristics, are strongly required. In the present thesis, new materials for these electric energy storage devices were investigated.

For two materials, manganese vanadate and carbon-coated metallic tin, their synthesis procedures were established by referring to their characteristics in structure and performance for the anode of lithium ion rechargeable batteries.

Manganese vanadate MnV_2O_6 is one of the candidates for anode materials of lithium ion rechargeable batteries, which might be possible to replace graphite (Chapter 2). Crystalline powders of anhydrous MnV_2O_6 were successfully synthesized at a temperature below 200 °C under autogenous hydrothermal condition and by coprecipitation method. MnV_2O_6 powders, which were synthesized using a high concentration solutions, more than 0.1 mol/L, gave relatively high reversible capacity as 600 mAh/g and interesting cyclic performance, reversible capacity increasing to more than initial charge capacity after 3rd or 4th cycle of charge-discharge. The powders showing this interesting performance were characterized by strong 110 diffraction peak relative to other peaks and by thin rod-like morphology. The Oxidation state of anhydrous MnV_2O_6 synthesized was investigated by different techniques, such as XPS, XAFS, TEM, etc.

Carbon-coated metallic tin powders were prepared through the heat treatment of the powder mixtures of poly(vinyl alcohol) (PVA) as a carbon precursor, SnO_2 as a Sn precursor and MgO in different mass ratios in N_2 gas flow (Chapter 3). SnO_2 was reduced to metal, which wetted with the surface of MgO particles and so could not flow to coagulate. After carbonization of PVA, MgO was dissolved out using 1 M HCl. The carbon-coated Sn powders was found to give a high capacity as 500 mAh/g and a stable cyclic performance as an anode of lithium ion rechargeable batteries, though they showed relatively large irreversible capacity at the first cycle of charge-discharge. The reasons for this good performance for the anode of lithium ion rechargeable batteries were a small particle size of Sn, which was possible by the existence of MgO particles during carbonization process, the inhibition of coagulation of small Sn particles during charge-discharge cycles because they are coated by carbon, and the existence of spaces neighboring to Sn metal particle in carbon shells, which could absorb a large volume expansion of Sn particle due to Li alloying during charging.

Two materials, mesoporous carbons and carbon-coated metal carbides, were developed for the electrode of electrochemical capacitors for electric energy storage, by establishing the synthesis procedures

and measuring their structural and electrochemical characteristics.

Electric double layer formation on large surface area of activated carbons has been employed for capacitors. In the present work, novel process for the synthesis of porous carbons, rich in mesopores, from thermoplastic precursors was newly developed (Chapter 4). BET surface area of the carbons synthesized through this process reached to 2000 m^2/g, even though no activation process was employed. The mixtures of MgO precursor (MgO, magnesium acetate and magnesium citrate) and thermoplastic carbon precursor (PVA, poly(ethylene terephtarate) PET and hydroxyl propyl cellulose HPC) were carbonized at 700-1000 °C in inert atmosphere. After carbonization, carbon was isolated by dissolution of MgO formed from its precursors using diluted acid. MgO particles formed from magnesium acetate and citrate were very fine and left a large amount of mesopores with a sharp distribution in size of around 10 and 5 nm, respectively. The mesoporous carbons synthesized gave relatively high capacity, as about 300 F/g, and excellent rate characteristics in 1 M H_2SO_4 electrolyte. Mesopores in the electrode carbons were shown to have an important role for their rate performance.

The mixtures of HPC with K_2WO_4 and K_2MoO_4 were found to give carbon-coated tungsten carbide WC and molybdenum carbide Mo_2C after heat treatment at 1000 and 850 °C, respectively (Chapter 5). Cyclic voltammogram for these carbon-coated metal carbides showed a clear box-shaped curve even in the first cycle, which was known to be characteristic for electric double layer capacitor, no redox peak being observed. The capacity was about 210 F/g, which suggested the overlap of redox capacity due to either tungsten or molybdenum hydroxide, which was formed during the first cycle of charge-discharge, to the capacity due to the formation of electric double layers on porous carbons. Carbon coating kept carbide particles small, as 30 to 100 nm, which made the transformation of carbides to hydroxides possible in the first charge-discharge cycle, and inhibited the coagulation of metal hydroxide particles during cycles of charge-discharge. Carbon-coated metal carbides thus prepared have very high capacitance based on the volume of electrode film, 500 ~ 700 F/cm^3, which is much higher than about 140 F/cm^3 for carbon electrode.

In the present thesis, MnV_2O_6 and carbon-coated Sn fine particles were developed for anode materials of lithium ion rechargeable batteries, and also mesoporous carbons and carbon-coated WC and Mo_2C were developed for electrode materials of electrochemical capacitors. These materials showed either larger electric energy storage and/or better charge-discharge performance than the conventional materials. These materials are believed to contribute the future development of electric energy storage devices. The process for the preparation of porous carbons from thermoplastic precursors is expected to be developed as a novel process for the production of activated carbons.

Abstract in Japanese

蓄電デバイスは、小型電子機器に限らず様々な電源として、需要が非常に高く、新規開発や改質が早急に望まれている。このような中で、リチウムイオン二次電池には、高容量、長寿命、高効率化が強く求められ、電極の開発、改質は非常に重要な課題として取り上げられている。また、二次電池に並んで、電気化学キャパシタが近年様々な用途に期待され、高容量化、レート特性の改良などが強く求められている。いずれのデバイスに対しても国内外で多数の報告がなされている中、未だ現状に変わる次の主流となる材料が決まらないという事実がある。これには、工業的な問題やコスト、プロセスなどいろいろな課題が存在することが大きい。そこで本研究では、電極材料のより簡便でかつ経済性の高い合成方法を開発し、それらデバイスのより高性能化に寄与することを目的とした。

複合酸化物である MnV_2O_6 は、リチウムイオン二次電池負極材の一つとして期待されている材料である。本研究では、エネルギーコストが低く、装置が簡便な水熱法および共沈法により 200°C 以下という低温で、その無水物を直接合成することに成功した。得られた試料は 10 回目のサイクル時においても 600mAh/g と比較的良好な容量が確認された。さらに 0.1mol/L 以上の濃度条件下で合成した試料は、3 回目もしくは 4 回目のサイクル時に一旦減少した充放電容量が初期容量近くまで回復するというサイクル特異性を見出だした。このサイクル特異性を引き起こす試料は、いずれも X 線による 110 回折線のピーク強度が他の回折線に比べて強く出ていることが共通して確認された。その構造について各種の手法(XPS, XAFS,TEM)による解析を行った。

金属スズは、理論容量が 990mAh/g と非常に高く,リチウムイオンニ次電池の負極材として注目されている。しかし、Li 吸蔵時の体積膨張やサイクル寿命に限度があることなどの欠点によりそのままでは使用が難しいとされてきた。本研究では、炭素被覆した微粒子金属スズを作成することによって、リチウムイオン二次電池の高容量および高性能化が可能であることを示した。熱可塑性樹脂を SnO_2 および MgO と混合した後、不活性ガス気流中で 900 °C に加熱、炭素化し、MgO を希酸により溶解、除去した。SnO_2 は、熱処理によって金属スズに還元され、混在する MgO との親和性から凝集が妨げられ、30 から 100nm の微粒子に保たれる。その電極性能は、500mAh/g とグラファイト電極より優れ、リチウム挿入による金属スズの体積膨張は、MgO の溶解後に残った空隙によって吸収されていると考えられる。

電池と並び蓄電デバイスとして、キャパシタが存在する。高比表面積を有する活性炭を電極とした電気二重層を利用したキャパシタが様々な用途に期待さている。この高表面積を持つ活性炭を作る工程は非常に複雑であり環境に与える影響も大きい。本研究では、MgO 上へ炭素被覆した後、その MgO を取り除くことで、多孔質炭素を調製する新しい活性炭の製造方法を開発することに成功した。この方法は、活性炭製造では通常では用いられない熱可塑性樹脂を使用するため、様々な樹脂を選択できる利点がある。また、得られた炭素の表面積は 2000 m^2/g 以上と非常に高く、表面積および細孔構造は、炭素前駆体および MgO 前駆体そしてそれらの混合比を選択することにより簡単に制御可能であることを見出した。特に、従来の方法では直接的には作成しにくいメソ孔を作ることができることが

特徴的である。この多孔質炭素をキャパシタ電極に用いた場合 300 F/g と非常に高い容量が得られ、高速充放電時にも損失が少ないという利点を有することを明らかにした。

さらに、熱可塑性炭素前駆体であるヒドロキシプロピルセルロース（HPC）と K_2WO_4 または K_2MoO_4 の水溶液混合物から作ったゲルを 800~1100 °C の温度に 1 時間、不活性ガス中で熱処理することによって、炭素被覆タングステン（WC）またはモリブデンカーバイド(Mo_2C)を作成した。このカーバイドをキャパシタの電極活物質に用い、CV 測定を行ったところ、電気二重層キャパシタ特有のボックス型の挙動を描き、その容量は 210 F/g を示した。これは、1000 m^2/g を超えるような高純度活性炭の電気容量と比較しても遜色のない容量である。現在まで、金属カーバイドをキャパシタ電極に用いたという報告例はない。一方、市販の WC では、このような容量や挙動は得られず、炭素被覆されているためカーバイドが微粒に保たれていることが有利に働いていると考えられる。これらの炭素被覆カーバイドは、電極フィルムの体積あたりの容量としては 500~700F/cm^3 となり、炭素電極の約 140F/cm^3 に比べると極めて高い値を示した。

以上のように、本研究では、電気エネルギー貯蔵のためのデバイスであるリチウムイオン二次電池の負極材としての MnV_2O_6 および炭素被覆金属スズ微粒子、キャパシタの電極材としてのメソポーラス炭素、炭素被覆タングステンおよびモリブデンカーバイドの調製方法を開発した。作製した材料は、いずれも従来のものよりも高い性能（高い貯蔵容量および優れたレート特性）を示し、それぞれのエネルギー貯蔵デバイスの高性能化に対して貢献できると考えられる。また、本研究で開発した熱可塑性炭素前駆体を原料とする多孔炭の製造法は、全く画期的な方法であり、今後活性炭の新しい製造法としての展開が期待できる

Chapter 1

Introduction

1-1 Electric energy storage

High performance devices for electric energy storage are demanded in various electrical equipments, particularly those movable ones, e.g. automobile, portable computers and handy phones. Three possibilities for electric energy storage have been developed, *i.e.*, rechargeable (secondary) batteries, electrochemical capacitors and electrolyte capacitors. In Fig. 1-1, these three devices for electric energy storage are shown on Ragone plot, energy density against power density for devices [1].

Rechargeable storage devices, i.e., secondary batteries, have been investigated for long time from different view points. In the old days, it began with the lead batteries as the auxiliary power of the automobile. Around 1980's, nickel cadmium batteries were commercialized as the power sources for the portable equipments, and then nickel hydrogen batteries have been developed. As modern technology developed, electric energy consumptions for electrical equipments much increased, and new rechargeable storage devices with high capacity and longer cycle life were strongly desired.

Lithium ion rechargeable batteries were successfully developed by selecting suitable electrode materials, $LiCoO_2$ for the cathode and graphite for the anode, where the intercalation and deintercalation processes of lithium ions into the materials at both electrodes were known to be fundamental electrochemical reactions [2, 3]. Lithium rechargeable batteries were at first commercialized in early 1990's by SONY Corporation. Even now, in order to improve battery performance, various electrode materials and electrolyte have been examined [4-14].

Capacitors are another device to store electric energy, which are completely different in storage mechanism and cell performance from batteries. The discovery of the possibility of storing an electrical charge on surface arose from the phenomenon associated with rubbing of amber in ancient time. These phenomena were so-called static electricity. The cell known as Leyden jar was developed as prototype of electrolyte capacitors. After that, Faraday, Thomson, Helmholtz, et al. advocated the mechanism and/or law for different dielectric phenomena. Even now, however, the fundamental construction of these electric energy storage systems has not changed so much, these being called "condenser" in Japan, but "electrolytic capacitor" in other countries. Condensers, *i.e.*, electrolytic capacitors, consist of aluminum, tantalum, and

multilayer alumina [15-17]. The characteristics of capacitor storage were of high power density and long cycle life which the batteries do not possess, but these capacitors have relatively small energy density comparing with various rechargeable batteries. The most common applications for these capacitors are semiconductor memory backup, for electronic equipments, which including CMOS, FLASH RAM etc.

Recently, the applications for auxiliary power supply of large sized equipments such as automobile and electric vehicle were also expected. However, capacity of electrolyte capacitors was not enough for these applications, and so new capacitors called electrochemical capacitors were developed [18-21]. The electric storage modes in these capacitors were the formation of electric double layers on the interface between electrolytic and electrode surface and/or the pseudocapacitance derived form redox reactions. Electric double layer capacitors and redox capacitors have larger capacity than electrolytic capacitors, but can't reach the capacity of batteries. The most important difference between rechargeable batteries and capacitors, both electrochemical and electrolyte capacitors, is basic process for energy storage, in the former Faradic and in the latter non-Faradic, except redox capacitors, which is responsible for the characteristics of two devices.

In Table 1-1 and 1-2, types of batteries and capacitors were shown, respectively. In energy storage by capacitors, only an excess and a deficiency of electron charge on the surfaces of the materials in one electrode and counter part electrode have to be established on charging and reversed on discharging, *i.e.*, no chemical changes are involved. Energy storage by batteries, on the other hand, Faradic reactions, *i.e.*, reversible chemical reactions of the anode and cathode materials, must take place. Recently the orientation of researchers was proposed to develop new materials for electrodes and/or storage devices for high energy and power densities.

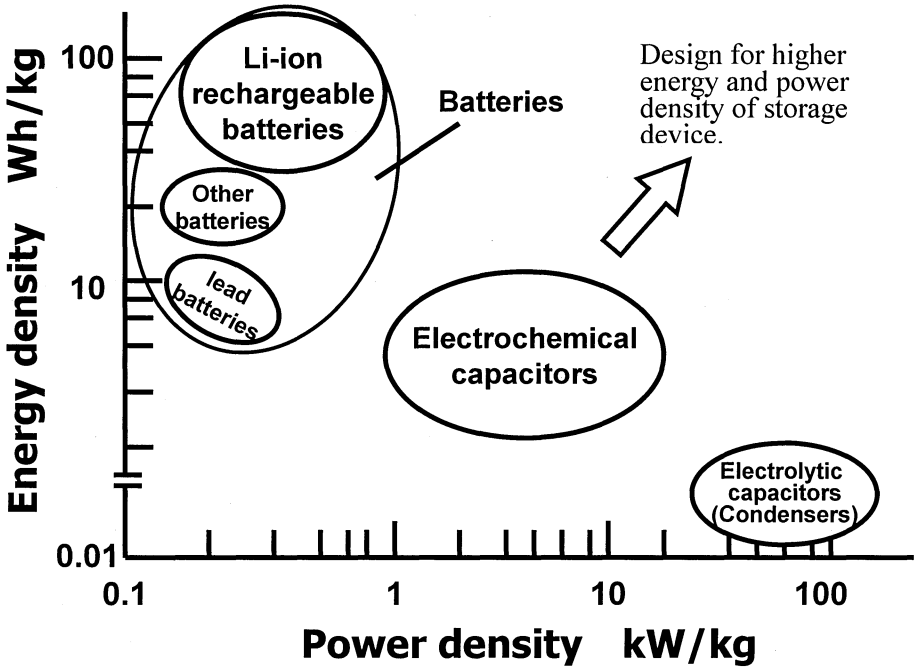

Fig. 1-1 Devices for electric energy storage on Ragone plot [1]

Table 1-1 Types of batteries and mode of energy storage

Cell	Type	Fundamental
Primary batteries	Alkaline, zinc -MnO_2 Mg - AgCl Mg - $PbCl_2$ Li - $SOCl_2$ and other cathodes Li - CF_x Al - air (catalyzed) Zn - air (catalyzed)	Faradic
Rechargeable (Secondary) batteries	Lead acid, Pb - PbO_2 Ni-Cd (Ni·O·OH-Cd) Ni-Hydrogen (Ni·O·OH-metal hydride) HgO - Zn AgO - Zn	Faradic
	Li - TiS Li - MnO_2 Li - CoO_2 Li - C - CoO_2 Na - S	Faradic and intercalated/deintercalated reaction

Table 1-2 Types of capacitors and mode of energy storage

Type of capacitors		Examples for Electrodes and/or products	Fundamental
Electrolytic capacitors	Vacuum	---	Electrostatic
	Dielectric	Mica, Mylar, paper	
	Oxide electrolytic	Ta_2O_5, Al_2O_3 (multilayer condenser)	
Electrochemical capacitors	Electric double layer	Porous or activated carbons, Carbon fibers, Porous oxides	Electrostatic (Charge separation at double-layer at electrode surface)
	Redox reactions	RuO_x, IrO_x, Co_3O_4, NiO_x, MnO_x	Faradic charge transfer (Pseudocapacitance derived from redox reaction)
		polyaniline, polythiophene	
		$V^{2+}/V^{3+}/VO^{2+}$ in solution	

1-2 Li ion rechargeable batteries

Lithium primary batteries were developed using graphite-fluoride $(CF)_n$ and commercialized as small batteries, such as button and coin types [22]. The characteristics of lithium primary batteries are having high voltage, high energy density, low self-electric discharge and wide range temperature of operation. A number of trials had been done these high performances to transfer to the rechargeable batteries, but no success was arrived. By the repetition of charge and discharge, short circuit was often formed in the cell, since dendrites of metallic lithium deposited. Even though various difficulties had been encountered, rechargeable (secondary) batteries were developed by using intercalation/deintercalation process of lithium ions, as explained below (Fig. 1-2). The lithium ion secondary batteries have high current and power densities compared with other secondary batteries. The scheme of the cell of commercially available lithium ion rechargeable batteries is shown in Fig.1-3 [23].

(a) Charge

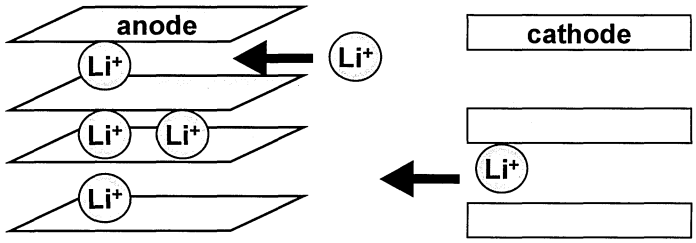

Intercalation of lithium ions into anode and deintercalation from cathode

(b) Discharge

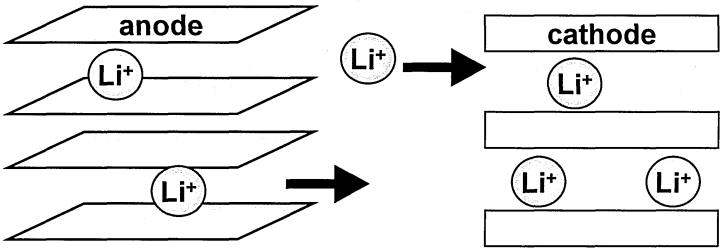

Deintercalation of lithium ions from anode and intercalation into cathode

Fig. 1-2 Intercalation/deintercalation processes of lithium ions for lithium ion rechargeable battery.

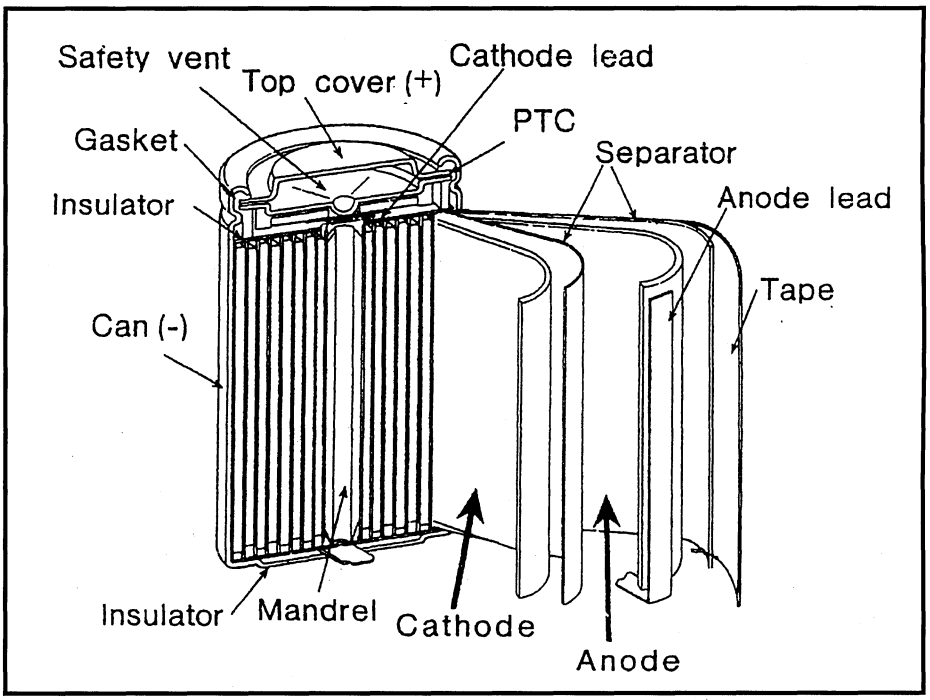

Fig. 1-3 Scheme of commercially available lithium ion rechageable battery.

Commercial cells have developed by selecting suitable electrode materials, either $LiCoO_2$ or $LiMn_2O_4$, for the cathode and graphite for the anode, where the intercalation and deintercalation processes of lithium ions occurred [24]. In Table 1-3, electrochemical reactions in cathode and anode electrode materials in lithium ion rechargeable batteries were shown. In case of the lithium cobaltate $LiCoO_2$ and graphite for cathode and anode, respectively, charge and discharge reactions consist of lithium ion transference between anode and cathode, i.e. intercalation/deintercalation.

Table 1-3 Reaction mechanism of commercial lithium ion secondary battery.

Cathode: $Li_{1-x}CoO_2 + xLi^+ + xe \underset{\text{Charge}}{\overset{\text{Dischage}}{\rightleftharpoons}} LiCoO_2$
Anode: $Li_xC_6 \underset{\text{Charge}}{\overset{\text{Discharge}}{\rightleftharpoons}} xLi^+ + xe + 6C$
Cell reaction: $Li_{1-x}CoO_2 + Li_xC_6 \underset{\text{Charge}}{\overset{\text{Discharge}}{\rightleftharpoons}} LiCoO_2 + 6C$

In order to improve battery performance, various electrode materials have been studied. Lithium compound $LiNiO_2$ and its solid solution with $LiCoO_2$, $Li(Co_{1-x}Ni_x)O_2$ which have the same ordered rock-salt type structure as $LiCoO_2$ [25, 26], and $LiFePO_4$ with olivine structure [27] were investigated for cathode materials. Also MoO_3 and anatase-type TiO_2 were studied as cathode materials for lithium ion rechargeable batteries [28, 29]. For the anode, graphite has been used. However, graphite anode materials commonly used in lithium ion secondary batteries suffers from small capacity per unit weight (its theoretical capacity is 372 mAh/g) and/or per unit volume due to its low density even though it has low redox potential and good cyclic performance. In Fig. 1-4, charge and discharge curves of graphite anode were shown. In order to get high capacity per weight or volume, various types of carbon materials were used, a wide range of carbon materials from low-temperature carbons with amorphous structure to well-crystallized natural graphite [30], surface modified carbons [31], and carbon nanotubes [32]. The carbon materials mixed with tin [33-36] and silicon [37, 38] were also proposed. Instead of carbon materials, metal oxides also have been investigated [39-41]. For many of these new materials studied their synthesis and preparation methods had to be newly developed.

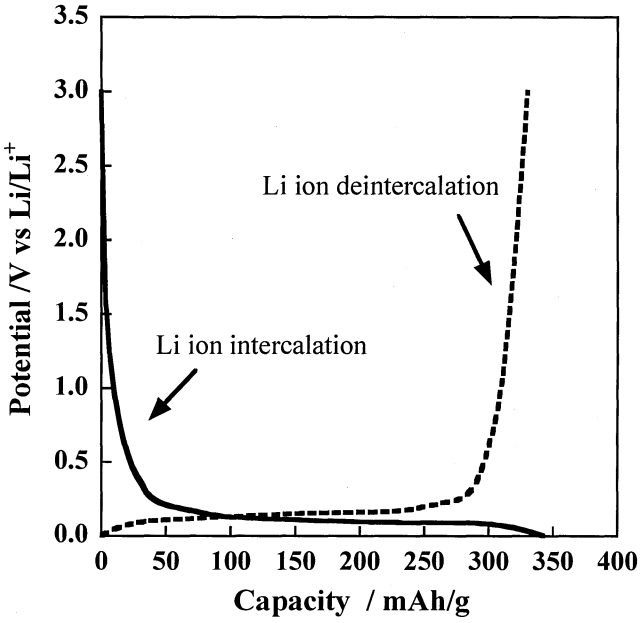

Fig. 1-4 Charge and discharge curves of graphite electrode for lithium ion rechargeable battery.

1-3 Electrochemical capacitors

In Table 1-4, electrochemical capacitors classified into two types based on electrolyte used.

Among these, the capacitors using electric double layers on the surface (electric double layer capacitor, EDLC) were reported in enormous numbers of investigation [42-49]. In Fig. 1-5, charge and discharge process in EDLC is shown schematically. In general, positive and negative charges are arrayed at counter position with an extremely short distance at the interface between two different phases, such as solid electrode and electrolyte solution. EDLC consists of a pair of polarized electrodes with high surface area (e.g. activated carbons) and electrolyte solution. In order to get a high surface area, activation process of carbon has usually been employed [50-53].

Table 1-4 Electrolytes used for electrochemical capacitors.

Type	Electrolytes	Basis of reaction
Aqueous	H_2SO_4, KOH, Na_2SO_4	Electric double layer
		Redox
Nonaqueous	Et_4NBF_4-propylene-carbonate (PC)	Electric double layer
	$LiBF_4$-Polyaniline, etc	Intercalation/ deintercalation

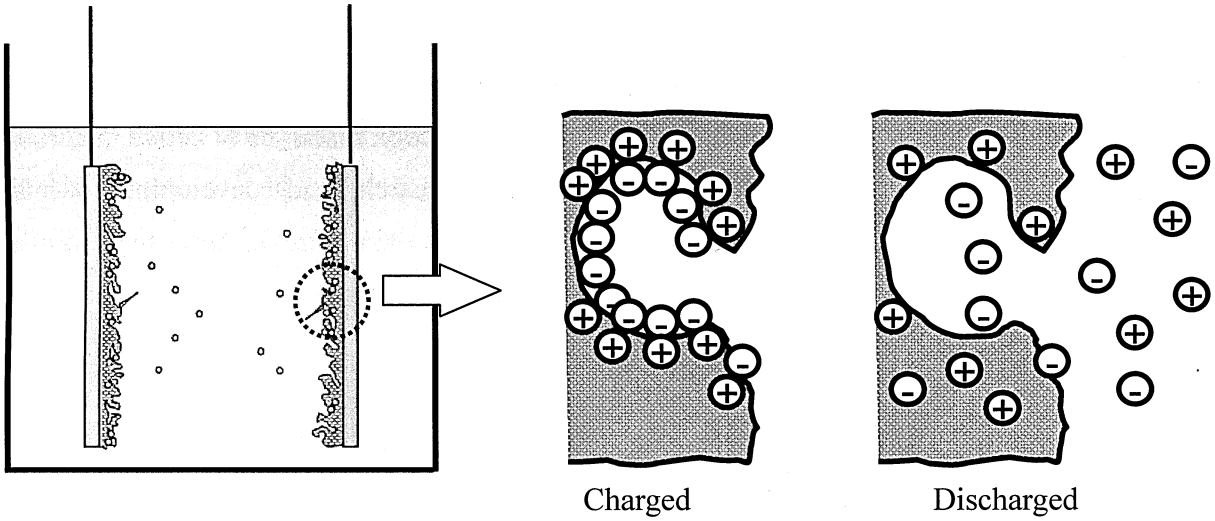

Fig. 1-5 Charge and discharge processes for EDLC.

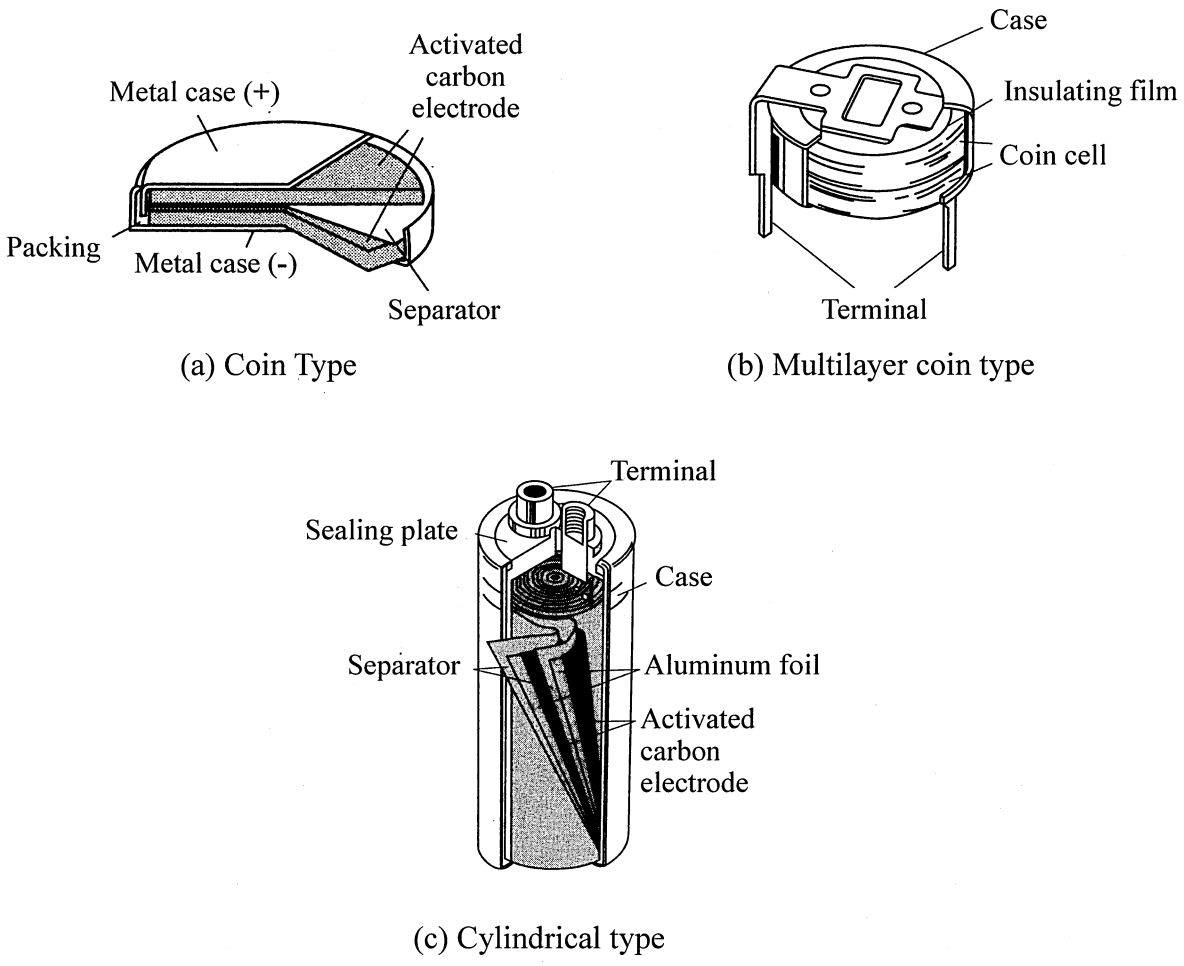

Fig. 1-6 Scheme of commercially available electric double layer capacitors.

In Fig. 1-6, various types of commercially available EDLC are shown. The shapes of electrochemical capacitors were similar to traditional electrolytic capacitors and also various batteries. It is possible to design shapes just for their purposes.

On the other hand, the redox capacitors which are using redox reactions of active materials in electrodes were also developed. Recent trend in research and developments related electrochemical capacitors is the hybridization of EDLC with redox one, in order to obtain high capacity. There was a report to very high capacity using activated carbon which mounted a ruthenium oxide [50-53]. This is the capacitor which used the electric double layers on activated carbon with the redox reaction of ruthenium oxide. Even though the capacity is so attractive, ruthenium is not a material suitable for the use in industrial scale because of high cost and poor resources.

1-4. Purpose of the present thesis

Electric energy storage devices, lithium ion rechargeable batteries and electrochemical capacitors, are used in various equipments, and going to be used more in various systems, for examples, electric vehicles. For these new applications, however, better performances, such as higher power and energy densities and better rate characteristics, are strongly required. Although enormous numbers of studies were reported, there were still possibility to develop new materials for these devices.

The objectives of the present thesis are the development of new electrode materials are developed for the electrodes of lithium ion rechargeable batteries and electrochemical capacitors. Preparation methods of these materials were established; direct synthesis of complex oxide, MnV_2O_6, and fine particles of carbon-coated Sn for anode materials of lithium ion rechargeable batteries, and also mesoporous carbons and carbon-coated WC and Mo_2C were developed for electrode materials of electrochemical capacitors. Charge and discharge mechanism of these new electrode materials for lithium batteries and capacitors was discussed on the basis of crystal structure, morphology and electrochemical examinations.

1-5. Construction of the present thesis

The present thesis consists of 6 chapters.

In Chapter 1, background and fundamental knowledge on energy storage systems was briefly described, and then purpose and construction of the present thesis were shown.

In Chapter 2 and 3, anodic materials for lithium ion rechargeable batteries, *i.e.*, anhydrous MnV_2O_6 and carbon-coated metallic Sn, respectively, were studied, and in Chapter 4 and 5, new electrode materials for electrochemical capacitors, *i.e.*, mesoporous carbon and carbon-coated

metal carbides, respectively, were developed. The materials, preparation methods and applications were listed in Table 1-4

In Chapter 2, manganese vanadium oxide (anhydrous MnV_2O_6) as oxide electrode was synthesized under autogenous hydrothermal condition and also by coprecipitation method. Synthesis conditions and process, structural characteristics, as well as anodic performance, of resultant anhydrous MnV_2O_6 were examined.

In Chapter 3, carbon-coated Sn powders were prepared through carbon coating process from thermoplastic resins. For the synthesis of fine particles of metallic tin with carbon coating, preparation conditions and process were established. Anodic performance of carbon-coated Sn for lithium rechargeable batteries was studied by charge and discharge cycles.

In Chapter 4, preparation procedure of porous carbons from thermoplastic precursors without activation process was newly developed. Mesoporous carbons thus prepared were used for the electrodes of electric double layer capacitors. Novel process of porous carbons was advocated and discussed.

In Chapter 5, carbon-coated tungsten and molybdenum carbides were synthesized through carbon-coating process and applied for the electrode of supercapacitors. Phase changes of metal carbide to metal hydroxide in sulfuric acid electrolyte was investigated and discussed.

In Chapter 6, conclusion and discussion on the results of the present thesis were described in the relation to electric energy storage and preparation method of electrode materials.

Table 1-4 Materials and preparation in the presentthesis

Chapter	Materials	Synthesis or preparation methods	Applications for energy storage
2	Anhydrous MnV_2O_6	Autogenous hydrothermal coprecipitation conditions	Anode for Li ion rechargeable batteries
3	Carbon-coated metallic Sn	Carbon-coating process	
4	Mesoporous carbons derived from thermoplastic	Carbon-coating process	Electrode for electric double layer capacitors
5	Carbon-coated tungsten and molybdenum carbides	Carbon-coating process	Electrode for supercapacitors

References

1. D. V. Ragone, Proc. Soc. Automotive Engineers Conference on Rev. of Battery System for Electrically Powered Vehicles, Society of Automotive Engineers, Warrendale, 1968
2. T.Ohzuku, A.Ueda, M. Nagayama, Y. Iwakoshi and H. Komori, *Electrochim. Acta* **38** (1993) 1159-1165.
3. K. Sawai, A. Ueda, M. Nagayama, Y. Iwakoshi and H. Komori, *Denki Kagaku* **61** (1993) 715-721.
4. Y. P. Wu, C. Jiang, C. Wan, R. Holez, *J. Power Sources*, **111** (2002) 329-334.
5. T. Ohzuku, S Kitano, M. Iwanaga, H. Matsuno, A. Ueda, *J. Power Sources*, **68** (1977) 646-651.
6. C. Y. Yang, C. H. Cheng, S. M. Ho, J. C. Chen, W. M. Hurng *J. Power Sources*, **68** (1977) 440-442.
7. Y. Nishi, *J. Power Sources*, **100** (2001) 101-106.
8. J. Read, D. Foster, J. Wolfenstine, W. Behl, *J. Power Sources*, **96** (2001) 277-281.
9. J. Wolfenstine, *J. Power Sources*, **124** (2003) 241-245.
10. S. H. Yoon, H. Yang, Y. Korai, I. Mochida, R. T. K. Baker, N. M. Rodriguez, *Carbon* **42** (2004) 21-32.
11. P. Arora, B. N. Popov, R. E. White, J. Electrochem. Soc., **145**, (1998) 807-815.
12. C. H. Lu, W. C. Lee, S. J. Liou, G. T. K. Fey, *J. Power Sources*, **81/82** (1999) 696-699.
13. T. Nakajima, M. Koh, R. N. Singh, M Shimada, *Electrochim. Acta*, **44** (1999) 2879-2888.
14. Y. S. Hong, K. S. Ryu, Y. J. Park, S. H. Chang, M. G. Kim, J. M. Lee, J. Mater. Chem., **12** (2002) 1870-1874.
15. L. G. Feinstein, R. J. Pagano, *IEEE Trans Components Hybrid Manuf. Technol.* **4** (1981) 140-147.
16. P. K. Reddy, S. R. Jawalekar, *Thin Solid Films*, **109** (1983) 339-343.
17. Y. Shimada, *Fine Ceramics* **8** (1987) 65-73.
18. T. Morimoto, M. Suhara, K. Haratuka, Y. Sanada, M. Tushima, T. Kawasato, Electrochemical Soc. 96 (1996) 138-145.
19. S. Trasatti, P. Buzzanca, *J. Electroanal. Chem.*, **29** (1971) 1-12.
20. S.H. Jordanov, H.A. Kozlowska, M. Vukovic, B.E. *Conway, J. Electrochem. Soc.* **125** (1978) 125-131.
21. B.E. Conway, *J. Electrochem. Soc.* **138** (1991) 138-144.
22. Y. Asami, K. Tsuchiya, H. Nose, S. Suzuki, K. Mizuhina, *J. Power Sources* **54** (1995) 146-450.
23. M. Wakihara, *Material Sci. and Engineering* **33** (2001) 109-134.
24. D. Wainwright, R. Shimizu, *J. Power Sources* **35** (1991) 56-60.

25. T.Ohzuku, A.Ueda, M. Nagayama, Y. Iwakoshi and H. Komori, *Electrochim. Acta* **38** (1993) 1159-1164.
26. T. Tsumura, A Simizu and M. Inagaki, *Solid State Ionics* **90** (1996) 197-202.
27. H. Buqa, P. Golob, M. Winter, and J. O. Besenhard, *J. Power Sources* **97-98** (2001) 122-126.
28. T. Tsumura, M. Inagaki and K. Yanagisawa, Trans. *Mater. Res. Soc. Jpn* **23** (1998) p.48.
29. J. R. Dahn, A. K. Sleegh, H. Shi, B. M. Way, W, J, Weydanz, J.N. Reimers, Q, Zhong, U. von Sacken,Lithium Batteries, G. Pistoia, *editor, Elsevier* (1993) p.1-44.
30. J. R. Dahn, A. K. Sleegh, H. Shi, B. M. Way, W, J, Weydanz, J.N. Reimers, Q, Zhong, U. von Sacken, Lithium Batteries, G. Pistoia, *editor, Elsevier* (1993) 1.
31. T. Nakajima, K. Yanagida, *Tanso* **174** (1996) 195-200.
32. T. Takeda, R.Takahata, Y. J. Kim, K. Koshiba, K. Ishii, T. Kasai and M. Endo. *Tanso* **196** (2001) 14-20.
33. B. Veeraraghevan, A. Durairajan, B. Haran, B. Popov and R. Guidotti, *J. Electrochem. Soc.* 149 (2002) A675-681.
34. Y. Wang, J. Y. Lee, B-H. Chen, *J. Electrochem. Soc.* **151** (2004) A563-570.
35. A. Sivashanmugam, T. Kumar, N.Renganathan, S. Gopukumar, M. Wohlfathrt -Mehrens, J. Grarche, *J. Power Sources* **144** (2005) 197-203.
36. N. Tamura, M. Fujimoto, M. Kamino, S. Fujitani, *Electrochimica Acta*, **49** (2004) 1949-1956.
37. A. Ulus, Y. Resenberg, L. Burstein, D. Peled, *J. Electrochem. Soc.* **149** (2002) A635-643.
38. M. Yoshio, N. Dimov, H. Wang, Z. Ogumi, T. Umemoto, *J. Electrochem. Soc.* **149** (2002) 1598-1603.
39. Y. Piffard, F. Leroux, D. Guyomard, J-L. Mansot and M. Tournoux, *J. Power Sources* **68** (1997) 698-704.
40. S. S. Kim, S. Ogura, H. Ikuta, Y. Unimoto, M. Wakihara, **146** (2002) 249-256.
41. T. Morishita, K. Nomura, T. Inamasu, M. Inagaki, *Solid State Ionics* **176** (2005) 2235-2341.
42. K. Szabo, J. Mika, Acta Chim. Hung. **128** (1991) 195-205.
43. H. B. Gu, J. U. Kim, H. W. Song, G. C. Park, B. K. Park, *Electrochimca Acta* **45** (2000) 1533-1536.
44. I. B. Fonseca, J. Aggar, C. Sarrazin, P. Simon, J. F. Fauvarque, *J. Power Sources* **79** (1999) 238-241.
45. M. Endo, T. Maeda, T. Takeda, Y. J. Kim, K. Koshiba, H. Hara, M. S. *Dresselhaus, J. Electrochem. Soc.* **148** (2001) 910-914.
46. J. H. Chen, Z. W. Li, D. Z. Wang, S. X. Yang, J. G. Wen, Z. F. Ren, *Carbon* **40** (2002) 1193-1197.
47. O. Tanaike, H. Hatori, Y. Yamada, S. Shiraishi, A. Asao, *Carbon* **40** (2003) 1759-1764.

48. S. E. Moulton, J. N. Barisci, G. G. Wallace, A. Bath, R. Stella, *Electorchim. Acta* **49** (2004) 4223-4230.
49. Y. Z. Wei, B. Fang, S. Iwasa, M. Kumagai, J. Power Sources, **141** (2005) 386-391.
50. I. Abe, O. Iwasaki, *Kagaku to Kougyo*, **75** (2001) 437-440.
51. F. Derbyshire, M. Jagtoyen, M. Thwaiter, Activated Carbons -Production and Application, in Porosity in Carbons. Patrick JW Ed., Edward Arnold. 1995.
52. Y, Sanada, M. Suzuki, K. Fujimoto, Activated Carbons. Fundamentals and Applications. Koudannsha, 1992.
53. M. Inagaki M. Porous carbons, in New Carbons -Control of Structure and Functions. Elsevier, 2000.
54. M. Ramani, B. S. Haran, R. E. White, B. N. Popov and L.Arsov, *J. Power Sources*, **93**, (2001) 209-212.
55. Y. Takasu, T. Ohnuma, W. Sugimoto and Y. Murakami, *Electrochem.*, **67**, (1999) 1187-1193.

Chapter 2

Synthesis of MnV_2O_6 and anode performance for lithium ion rechargeable batteries

2-1 Introduction

Lithium ion rechargeable batteries have high current and power densities compared with other rechargeable batteries, such as nickel hydrogen, nickel cadmium and lead batteries. Commercial cells have developed by selecting suitable electrode materials, either $LiCoO_2$ or $LiMn_2O_4$ for the cathode and graphite for the anode, where the intercalation and deintercalation processes of lithium ions were known to be fundamental electrochemical reactions [1-4]. In order to improve battery performance, various electrode materials have been studied. Lithium compound $LiNiO_2$ and its solid solution with $LiCoO_2$, $Li(Co_{1-x}Ni_x)O_2$,which have the same ordered rock-salt type structure as $LiCoO_2$ [1, 5], and $LiFePO_4$ with olivine structure [6] were investigated for cathode materials. Also MoO_3 and anatase-type TiO_2 were studied as cathode materials for lithium ion batteries [7, 8]. For the anode, various types of carbon materials were used, a wide range of carbon materials from low-temperature carbons with amorphous structure to well-crystallized natural graphite [9], surface modified carbons [10], and carbon nanotubes [11]. The carbon materials mixed with tin [12] and silicon [13] were also proposed.

Instead of carbon materials, metal oxide materials also have been investigated. The compound MnV_2O_6 with brannerite structure was proposed to be used for the anode. Synthesis of anhydrous MnV_2O_6 was carried out through solid state reaction between Mn_2O_3 and V_2O_5 [14], but nonstoichiometric composition of $MnV_2O_{6+\delta}$ was required in order to have anodic activity [15]. The synthesis of manganese vanadate powder was performed by coprecipitation method through aqueous solution of $Mn(NO_3)_2 \cdot 4H_2O$ and $NaVO_3$, and hydrous $MnV_2O_{6+\delta} \cdot nH_2O$ powders with different n values were obtained [15,16]. In order to get anodic activity for lithium ion rechargeable batteries, anhydrous manganese vanadate had to be obtained by the heat treatment of hydrous MnV_2O_6 synthesized by coprecipitation, but these powders prepared gave relatively low anodic activity, low capacity and low Coulombic efficiency. In order to improve Coulombic efficiency, ozonation of anhydrous manganese vanadate prepared was proposed [15]. The preparation of anhydrous manganese vanadate was also reported through the heat treatment of

aqueous gels containing Mn and V with a polymer at 400 °C [17].

In the present chapter, the fine crystalline powders of anhydrous manganese vanadate were directly synthesized in aqueous solution through two different process, autogenous hydrothermal process and coprecipitation process. The manganese vanadate powders were found to have rather high capacities and also to have an interesting cyclic performance.

2-2 Experimental

2-2-1 Synthesis of MnV_2O_6 powders

The starting materials used were reagent grade manganese acetate $Mn(CH_3COO)_2 \cdot 4H_2O$ (99.0% purity, Nakalai Tesque Ltd.) and vanadium pentoxide V_2O_5 (99.99% purity, High Purity Chemicals Ltd.). Preparation of MnV_2O_6 powders carried out by following two synthesis procedures.

a) Autogenous hydrothermal synthesis: The procedure is schematically shown in Fig. 2-1 (a). Aqueous solutions of $Mn(CH_3COO)_2$ and V_2O_5 were mixed with each other to be the V/Mn ratio of 2 and metal ion concentration was controlled to be 0.01 ~ 1.0 mol/L, where the pH value was about 4.0. In the solution with a concentration of 0.1 ~ 1.0 mol/L, undissolved V_2O_5 particles were suspended in the solution, though the pH value was kept at about 4.0. The mixed solution of 18 mL was taken into a 25 mL container of Teflon-lined stainless steel. After sealing the container, it was heated at 135, 175 and 200℃ for various durations of 0.5～10 hours with a constant rotation of 10 rpm. After this treatment, the precipitates formed were washed by distilled water repeatedly until the pH value of rinsed water became 7.0, separated from the solution by centrifugation and dried in air at 65 °C. Some of these precipitates were annealed in air at 400 and 600 °C for 1h.

b) Coprecipitation synthesis: Preparation of MnV_2O_6 powders under coprecipitation condition was performed in distilled water in the following two processes (Fig. 2-1(b));

Process I: Aqueous solutions of $Mn(CH_3COO)_2$ and V_2O_5, were prepared in various concentrations of 0.01 ~ 0.9 mol/L. For V_2O_5, however, its solubility to water is not so high that V_2O_5 particles were suspended in the solutions with the nominal concentration of more than 0.1 mol/L. These aqueous solutions were mixed with each other to be the V/Mn ratio of 2 at pH value of about 4.0. The mixed solution of 300 mL was heated at 90 °C for 5 h. During this treatment, the precipitates were formed. The precipitates formed were washed with a large amount of distilled water by decantation repeatedly until the pH value of rinsed water became 7.0, separated from the solution by centrifugation and then dried in air at 65 °C. Some of these precipitates were annealed in air at 150 ~ 700 °C for 1 h.

Process II: the powder of V_2O_5 was dispersed in distilled water of 300 mL at 95 °C, the nominal

concentration of V_2O_5 being relatively high as 0.1 mol/L. Into this suspended solution, $Mn(CH_3COO)_2$ powder was added under refluxing until the atomic ratio of Mn to V reaching to 1/2 (i.e., V/Mn = 2). This mixed suspension was kept 100 °C for 5 ~ 168 h under refluxing of water. During refluxing, most of undissolved V_2O_5 particles with orange color looked to dissolve and the precipitates with dark red color were formed. The precipitates formed were washed with distilled water by decantation repeatedly until the pH value of rinsed water became 7.0, separated from the solution by centrifugation and dried in air at 65 °C.

2-2-2 Characterization of samples

The crystal structure of the precipitates thus obtained was examined by X-ray powder diffraction (XRD: Rigaku RINT-2500) with CuKα radiation. The lattice parameters a_0, b_0, c_0 and β of brannerite structure of MnV_2O_6 were determined by referring to the inner standard of high purity silicon. Morphology of the powders was observed from transmission electron microscope (TEM: JEOL JEM-2010) with acceleration voltage of 200 kV. Metals presented in particles were identified by energy dispersive X-ray spectrometry (EDS) in TEM. In order to examine thermal behavior of these samples, thermogravimetry (TG: Rigaku TG-8120) was carried out at heating rate of 2 °C /min from room temperature to 800 °C in air.

In order to understand the change in oxidation state of cations, vanadium and manganese, during lithium ion insertion and de-insertion into manganese vanadate electrode, the anode materials were sampled out at different stages in the 1st cycle of discharge-charge process. Vanadium K-edge spectra were measured by X-ray absorption fine structure analysis (XAFS) at the beam line 12C of Photon Factory in High Energy Accelerator Research Organization in Tsukuba. The storage ring energy was 2.5GeV and the current was between 400 and 290 mA. Si(111) monochromator was used. XAFS measurements were performed at 290 K in transmission mode. The spectra of X-ray photoelectron spectroscopy (XPS) with MgKα X-radiation were also measured on the same samples.

a) Autogenous hydrothermal condition

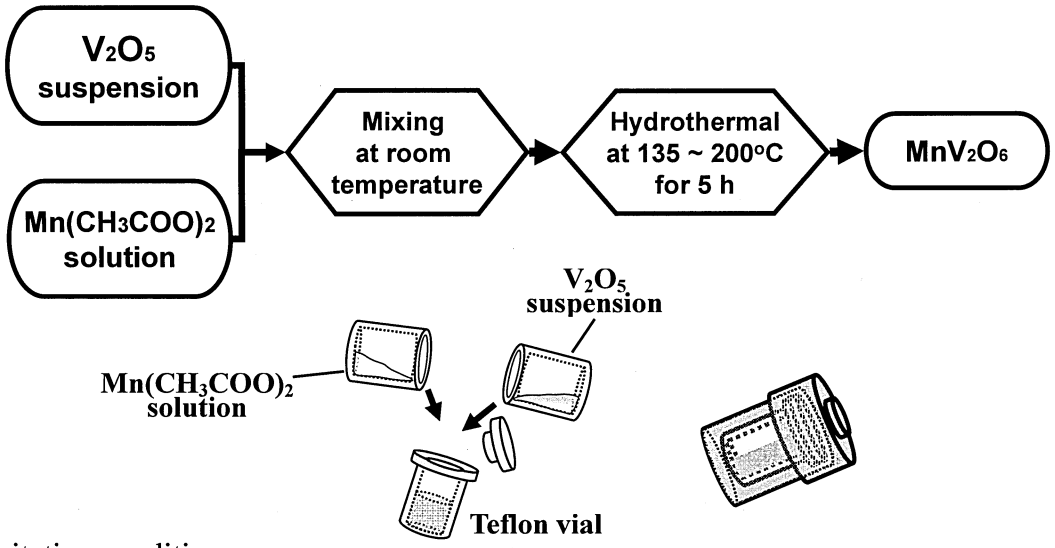

b) Coprecipitation condition

Process I (Solution mixing)

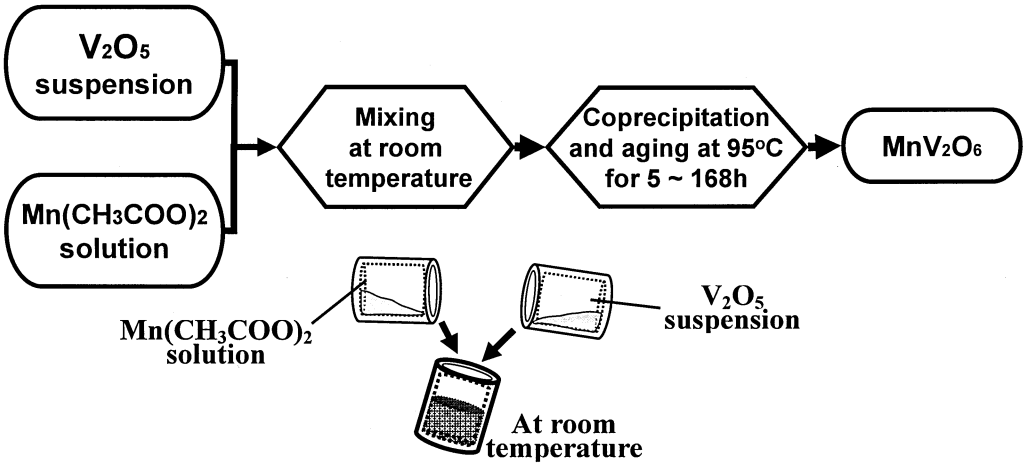

Process II (Powder Mixing)

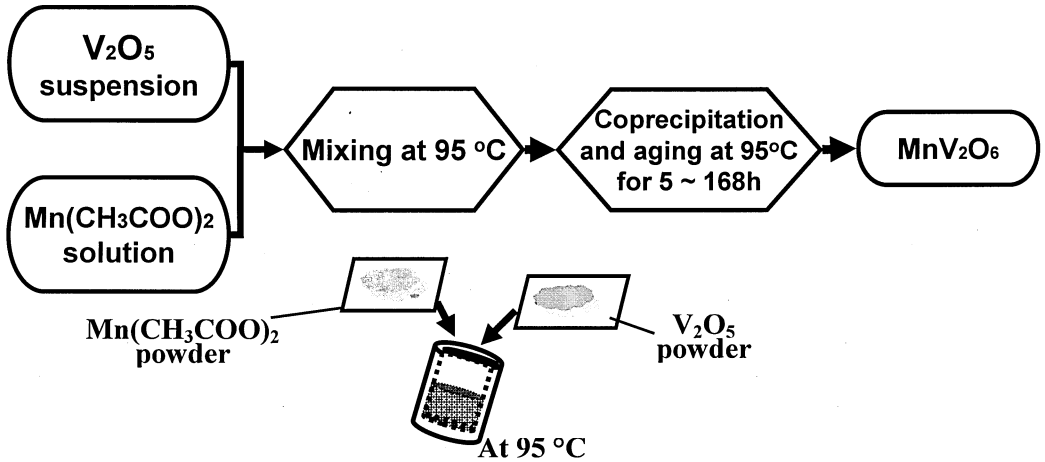

Fig. 2-1 Synthesis procedures of MnV_2O_6 under (a) hydrothermal and (b) coprecipitation condition (Process I and II)

2-2-3 Determination of anodic performance for lithium secondary battery

The electrode to determine anodic performance was prepared by mixing the sample powder with acetylene black as an electrical conductor and polyvinylidene difluoride (PVDF) as a binder in a mass ratio of 70:20:10, and pasting on a thin film of Ni (Fig. 2-2). Li metal was used as counter electrode. The electrolyte solution was the mixture of ethylene carbonate (EC) and diethyl carbonate (DEC) in equal volume ratio, in which 1 mol/L $LiClO_4$ was dissolved. The electrochemical performance was determined in the range of potential at 0.0 - 2.5 V with a current density of 50 mA/g at room temperature in a glove box filled with Ar gas. Discharge and charge cycles were performed up to 50th. In this thesis, the notation of anode was used for the electrode consisting of sample carbons, even though it worked as cathode by coupling with lithium metal as counter electrode, because the words of anode and cathode were premised being used in the actual batteries.

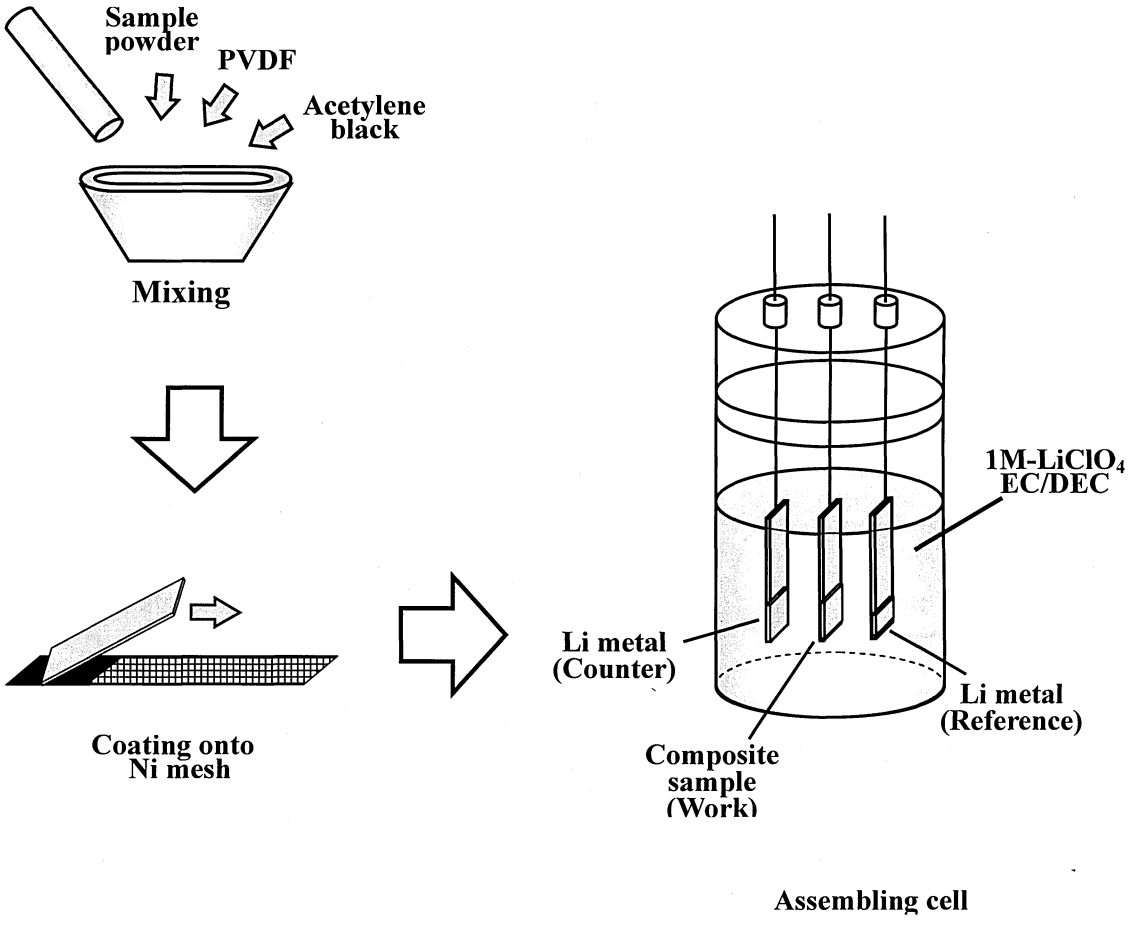

Fig.2-2 Contraction of test cell

2-3 Results and discussion

2-3-1 Synthesis of MnV_2O_6 under autogenous hydrothermal conditions

a) MnV_2O_6 powders synthesized

In Fig. 2-3, XRD patterns of the precipitates obtained are shown. These powder patterns could be indexed based on the data of MnV_2O_6 with brannerite structure which had been synthesized by solid state reaction between Mn_2O_3 and V_2O_5 [13]. No extra peaks were detected on the XRD patterns. The temperature of synthesis seemed to have an effect on crystallinity of the resultant powders, the powders synthesized at 200 °C having sharper diffraction peaks than those at 135°C. Residence time at 200 °C affected a little on crystallinity of the powders, suggesting a rapid precipitation of MnV_2O_6. The XRD pattern of the precipitates obtained from the starting solution with relatively high concentration of metal ions (Fig. 2-3e) could be indexed by the brannerite structure, but relative intensities of diffraction lines are a little different from those observed on the precipitates from low metal concentration (Fig. 2-3c), being clearly revealed among the diffraction lines of 110, $20\bar{2}$, 002 and 201, which is probably represented by strong 110 line relative to $20\bar{2}$ line.

In Fig. 2-4, TG curve is shown on the precipitates obtained from the solution of 0.1 mol/L at 200 °C for 5 h. All TG curves observed on the present samples showed weight loss in three steps, though total weight loss was only a little more than 1 mass%. The first weight loss occurs from room temperature to a little above 100 °C, which is due to the release of adsorbed water on the surface. The amount of weight loss at this step was found to be different from sample to sample. The weight loss at the second step occurs a wide range of temperature from 100 to 400 °C and is about 0.5 mass%. This step seemed to be due to the evaporation of water film on the surface of MnV_2O_6 powder, because it was reported that the surface of ferrite grains was covered with a thin film of water under hydrothermal synthesis and it was released in the temperature range up to 500 °C [18]. The weight loss at the third step was about 0.2 mass%, being almost constant for all samples synthesized under hydrothermal conditions, which will be discussed below.

In Fig. 2-5, XRD patterns for MnV_2O_6 powders annealed at 400 and 600 °C, which corresponds to the temperatures just at the end of 2nd and 3rd steps, respectively, in TG curve of Fig. 2-4. Diffraction patterns of annealed MnV_2O_6 powders are almost the same, except that diffraction peaks become shaper with increasing annealing temperature. The powders annealed at 400 and 600 °C were dark blown and black, respectively, although the as-prepared powders were light brown.

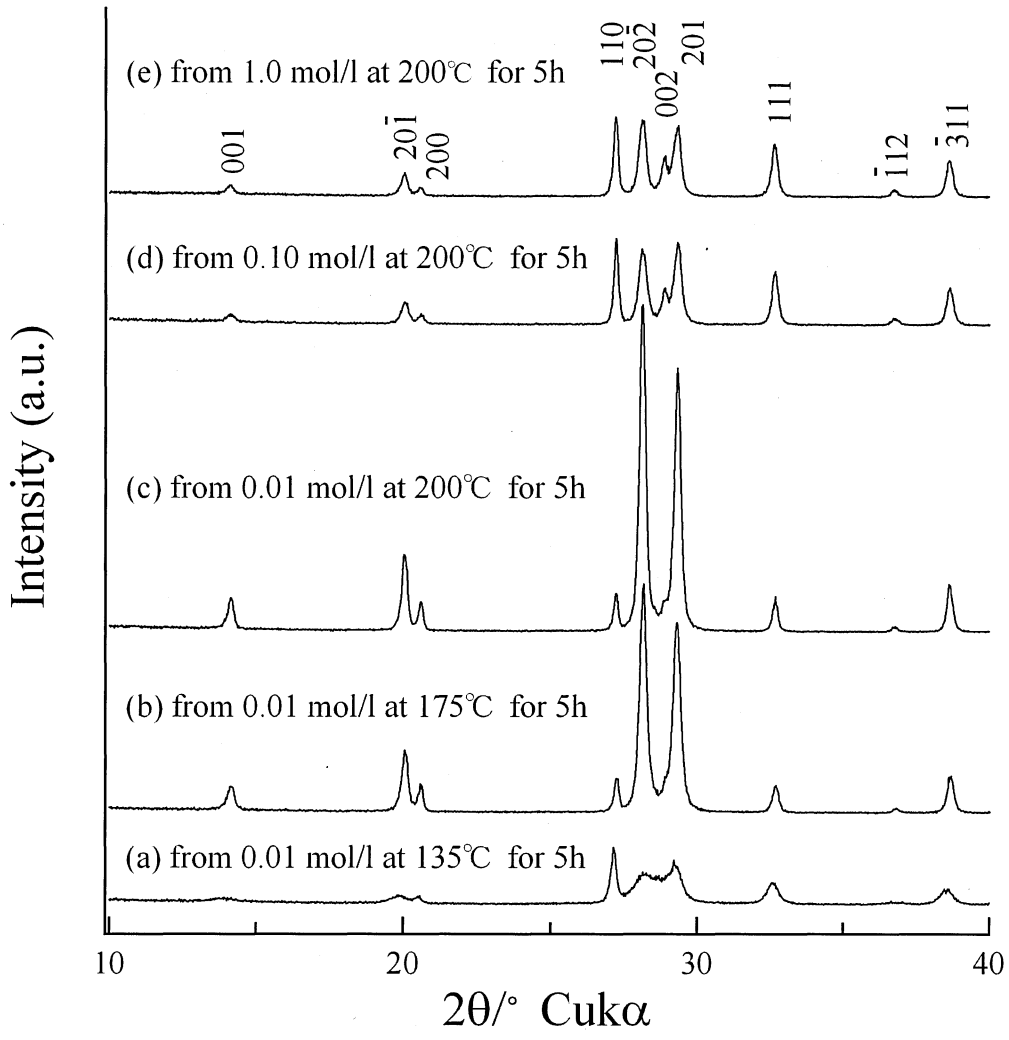

Fig. 2-3 XRD patterns of precipitates obtained under autogenous hydrothermal condition.

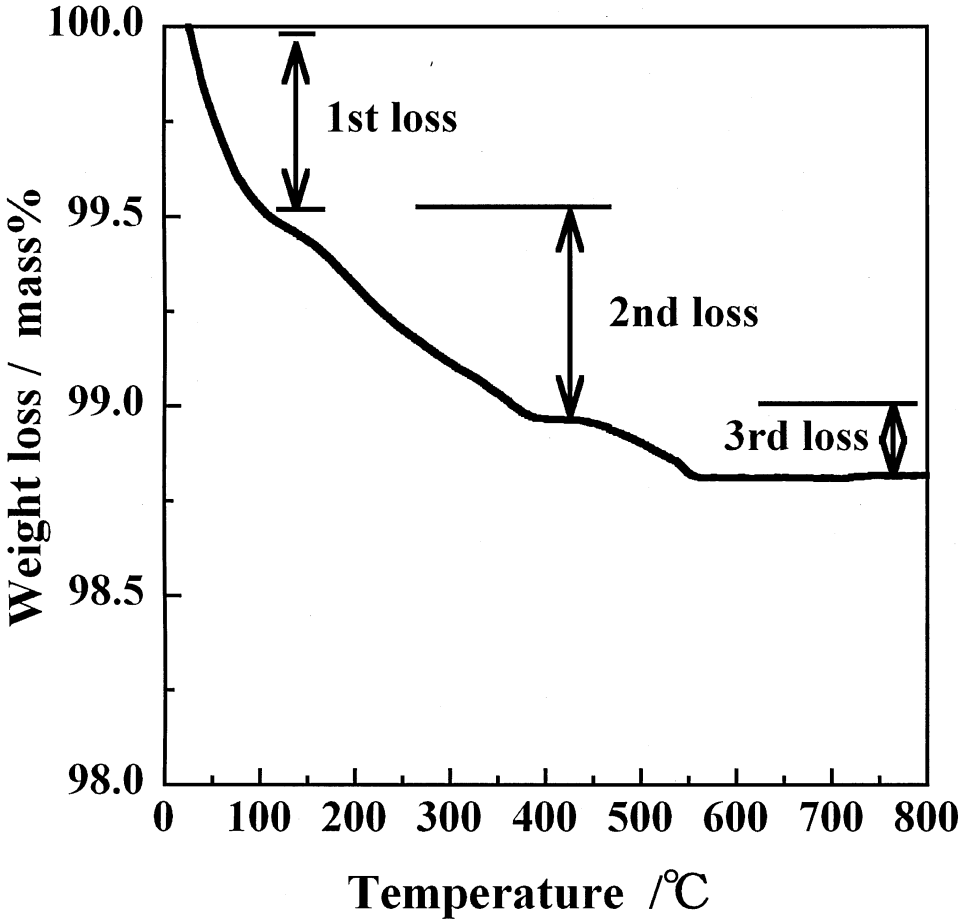

Fig. 2-4 TG curve of crystalline MnV_2O_6 powders obtained at 200 °C for 5h from the starting solution with metal concentration of 0.1 mol/L.

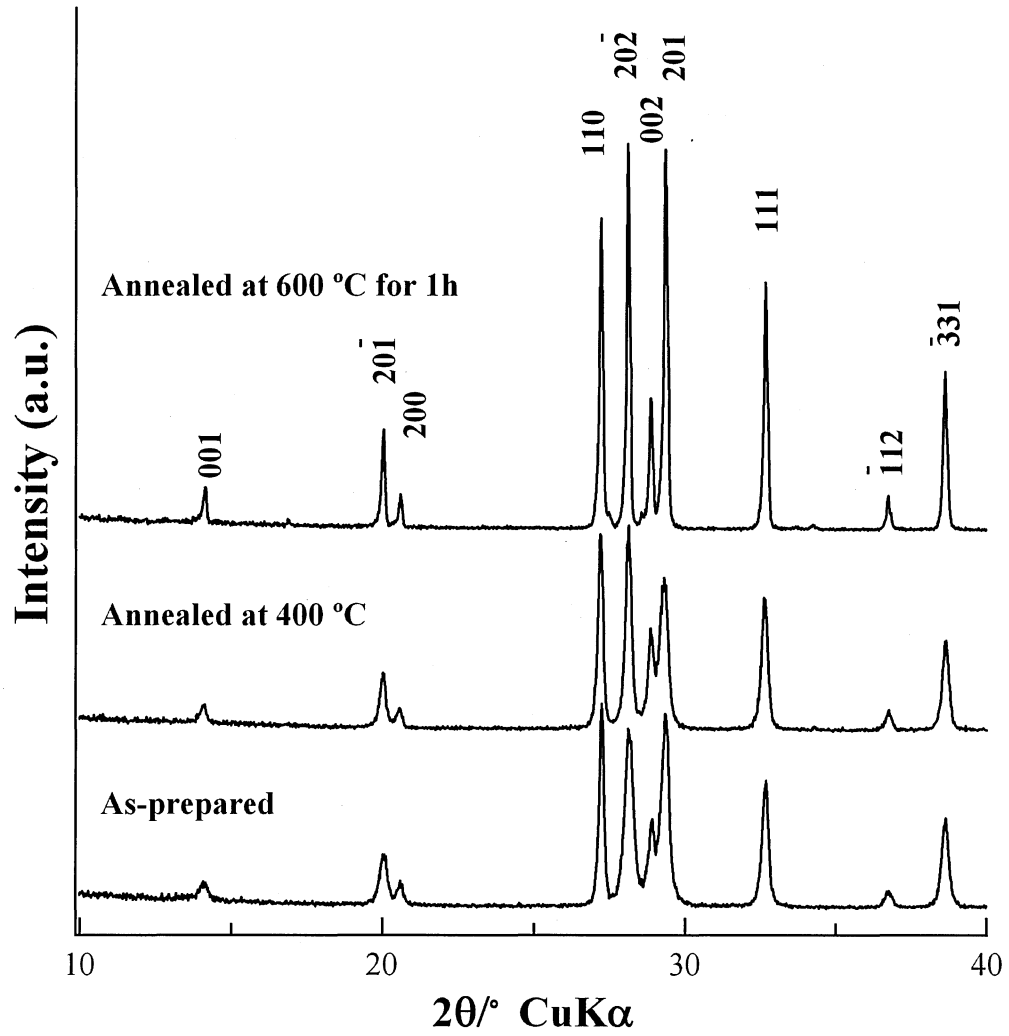

Fig. 2-5 XRD pattern of MnV_2O_6 powders as-prepared and annealed.

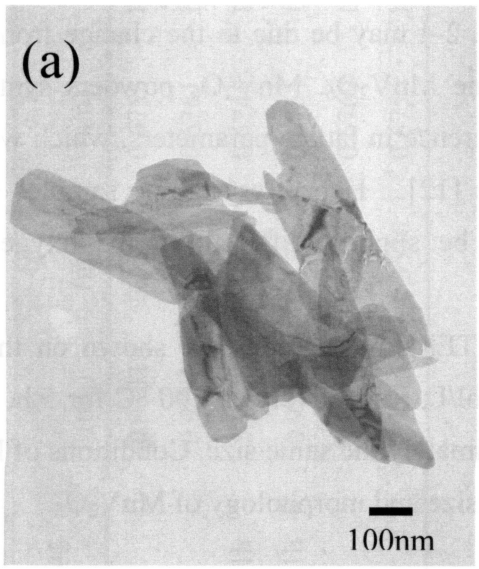

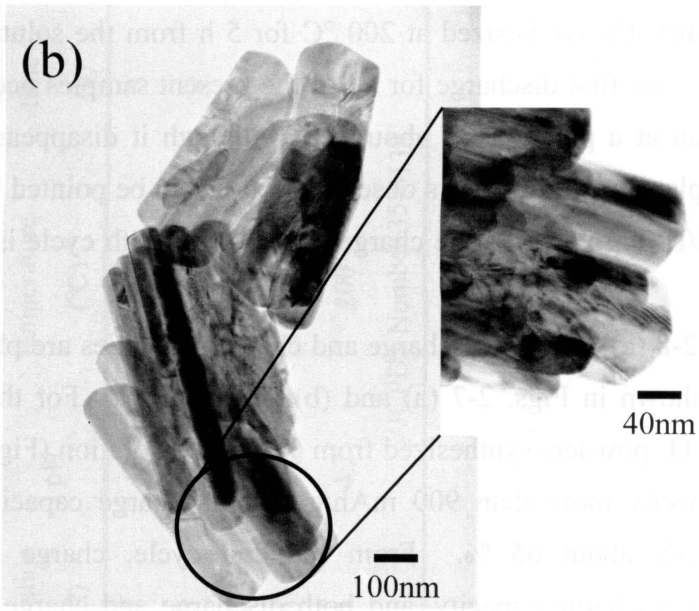

Fig. 2-6 TEM micrographs of the crystalline MnV_2O_6 powders obtained at 200 °C for 5h. (a) From the concentration of 0.01 mol/L and (b) 0.1 mol/L.

Lattice parameters measured on the samples synthesized under various conditions are summarized in Table 2-1. The sample annealed at 600 °C has the same lattice parameters as those in JCPDS card (No.35-139). However, the lattice parameters for all other samples, as-prepared and annealed up to 400 °C, are different from the JCPDS values; a_0 is much smaller and c_0 is a little larger, though b_0 and angle β are almost the same. Based on these results, the weight loss at 3rd step in Fig. 2-4 may be due to the change from non-stoichimetric compound $MnV_2O_{6+\delta}$ to stoichimetric one MnV_2O_6. MnV_2O_6 powders synthesized by polymer gellation method showed the same difference in lattice parameters, which was attributed to slightly excess oxygen content in the sample [12]. Hence, crystalline samples synthesized under autogenous hydrothermal condition may be slightly different in the oxygen content from stoichimetric compound MnV_2O_6.

In Fig. 2-6 (a) and (b), TEM micrographs are shown on the powders obtained from the solutions with 0.01 and 0.1 mol/L, respectively, at 200 °C for 5 h. Each particle looks rod-like, but rather thin and has approximately the same size. Conditions of hydrothermal synthesis did not give marked effect on particle size and morphology of MnV_2O_6.

b) Anodic performance of MnV_2O_6 powders

In Figs. 2-7 (a) and (b), discharge and charge curves at 1st and 10th cycle are shown on the powders of MnV_2O_6 synthesized at 200 °C for 5 h from the solutions with 0.01 and 0.1 mol/L, respectively. The first discharge for all of the present samples occurred in two steps, showing a distinct plateau at a potential of about 0.8 V, though it disappeared in 2nd cycle. On charge curves, faint plateaux were always observed. It has to be pointed that on the sample synthesized from 0.1 mol/L (Fig. 2-7 (b)) the charge capacity for 10th cycle is much larger than that for the first cycle.

In Figs. 2-8 (a) and (b), discharge and charge capacities are plotted against cycle number on the samples shown in Figs. 2-7 (a) and (b), respectively. For the first cycle of discharge and charge, MnV_2O_6 powders synthesized from 0.01mol/L solution (Fig. 2-8 (a)) show relatively large discharge capacity more than 900 mAh/g, but its charge capacity is 600 mAh/g, Coulombic efficiency being about 65 %. From the 2nd cycle, charge capacity decreases markedly, approaches to discharge capacity, and both discharge and charge capacities decrease gradually with cycling, Coulombic efficiency being kept more than 95 %. All samples synthesized from dilute solutions as 0.01 mol/L showed the same discharges in charge capacity *i.e.*, gradual decrease with cycle. Similar capacity changes were reported on the samples synthesized through gellation [12]. On the other hand, samples prepared from solution with the concentration of more than 0.1 mol/L showed the abrupt increase in both discharge and charge capacities after

Table 2-1 Lattice parameters of the samples synthesized.

Synthesis condition					lattice parameter			
concentration (mol/l)	pH	temperature (℃)	time (h)	annealing	a_0 (nm)	b_0 (nm)	c_0 (nm)	β (°)
0.01	4.0	200	5	---	0.9303	0.3536	0.6758	112.66
0.10	4.0	200	5	---	0.9299	0.3536	0.6761	112.45
0.10	4.0	200	5	400℃, 1h	0.9308	0.3532	0.6745	112.47
0.10	4.0	200	5	600℃, 1h	0.9313	0.3535	0.6754	112.66
1.00	4.2	200	5	---	0.9302	0.3537	0.6769	112.55
JCPDS Number 35-0139					0.9315	0.3536	0.6754	112.66

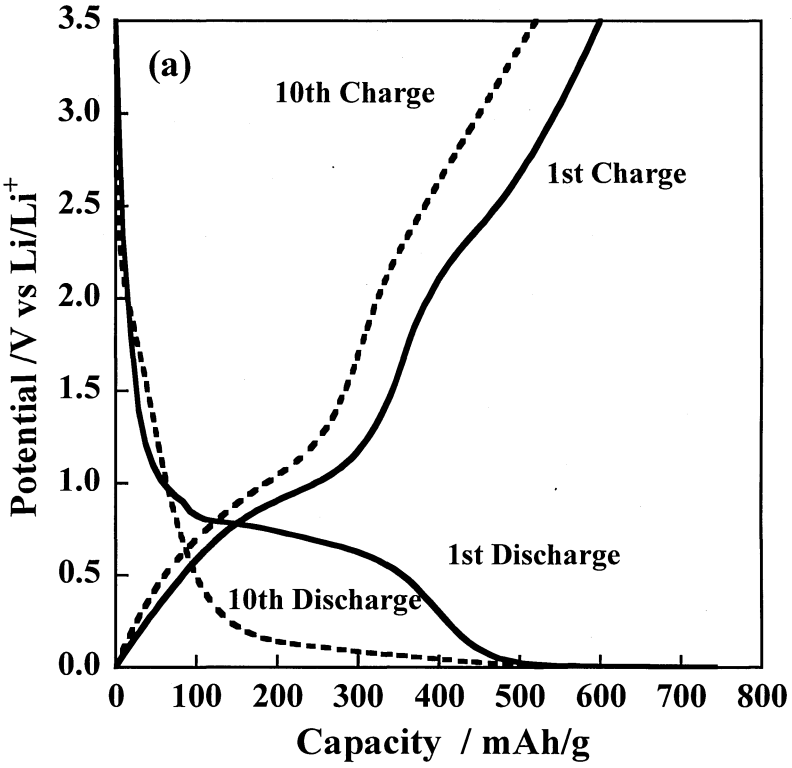

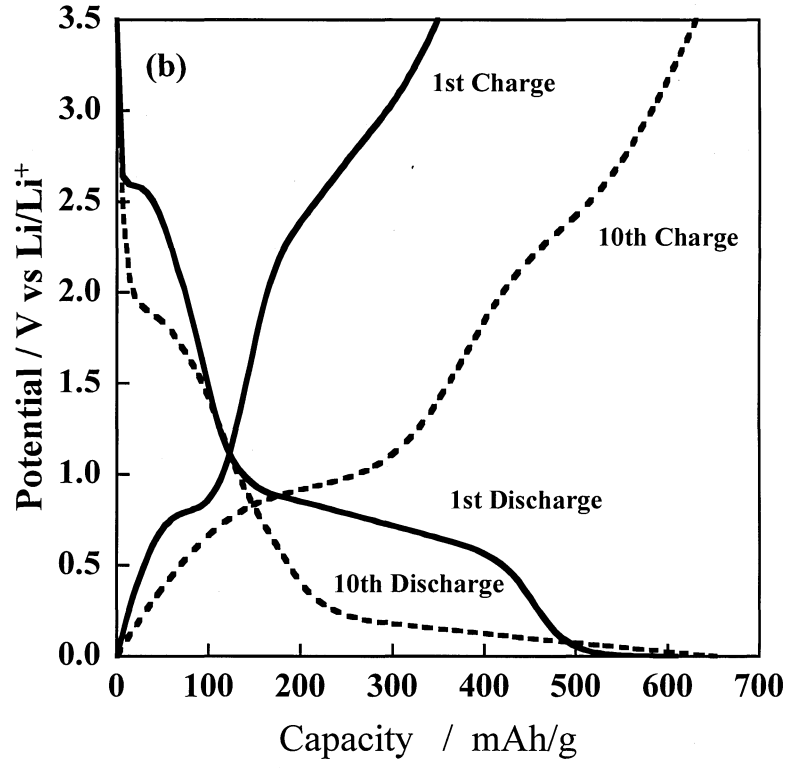

Fig.2-7 Discharge and charge curves with cycling on the MnV_2O_6 powder obtained under autogenous hydrothermal condition at 200 °C for 5 h. (a) From the concentration of 0.01mol/L and (b) 0.1 mol/L.

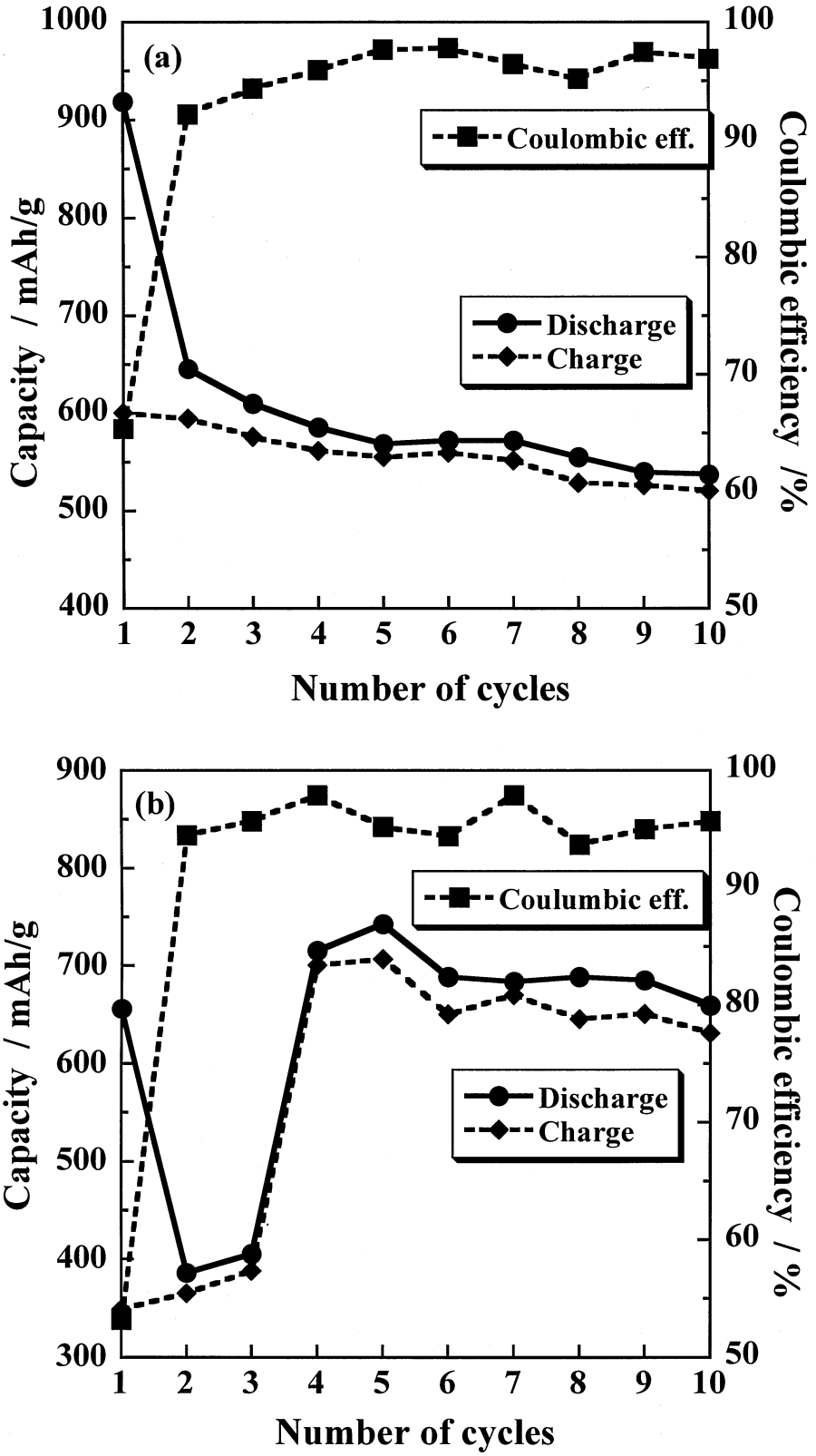

Fig.2-8 Cycling behavior of the samples obtained at 200 °C for 5h.
(a) From the concentration of 0.01 mol/L and (b) 0.1 mol/L.

3rd-4th cycle, as shown in Figs. 2-7 (b) and 2-8 (b). It has to be pointed out that charge capacities from 4th cycle in Fig. 2-8 (b) are much higher than charge capacity at 1st cycle and Coulombic efficiency is kept more than 90 %. From the comparison with the structural characterization shown in Figs. 2-3~2-6, this interesting cycling performance of Fig. 2-8 (a) is reasonably supposed to be due to the structure of sample powders. All samples, which were represented by strong 110 line in XRD pattern, showed this cycling performance, abrupt increase in discharge and charge capacities after either 3rd or 4th cycle. The samples annealed at 600 °C, however, showed gradual decrease in charge capacity with cycle, similar to Fig. 2-8 (a), even though the original ones were synthesized from 0.1 mol/L solution.

In Table 2-2, the discharge and charge capacities and Coulombic efficiency for 1st and 10th cycles are summarized. The samples obtained from 0.01 mol/L solution showed a gradual decrease in discharge and charge capacities, as the change shown in Fig. 2-8(a). However, the charge and discharge capacities even at 10th cycle are higher than that observed on graphite anode (its theoretical capacity is 372 mAh/g.). At 1st cycle, the samples synthesized at 200 °C gave high discharge and charge capacities, and better Coulombic efficiency than those synthesized at 135 °C, but almost the same capacities after 10th cycle. Residence time at 200 °C during synthesis seemed not to affect the anodic performance. On the other hand, the samples obtained from solutions with more than 0.1 mol/L showed a characteristic increase in capacity after certain cycle, as the change in Fig. 2-8 (b). The charge and discharge capacity in 1st cycle is not high, being similar or even lower than the samples obtained from 0.01 mol/L at 200 °C, but those at 10th cycle are much higher, as high as 600～700 mAh/g. These characteristics are lost by annealing at more than 600 °C, its discharge and charge profiles becoming similar to that in Fig. 2-8 (a) and capacities at 10th cycle decreasing below 200 mAh/g. A similar change occurs for the samples obtained from 0.01 mol/L annealed at 600 °C.

Fig. 2-9 shows XRD patterns of the anode after discharge and charge cycles. Even after the first discharge, starting crystalline structure of MnV_2O_6 changed drastically to amorphous state, faint peaks observed being not due to crystalline MnV_2O_6. After the first discharge and charge cycle, crystalline peaks disappeared completely. This amorphous state of the anode materials are kept during following discharge and charge cycles, as shown on the anode after 10th cycles. This change to amorphous state was reported in other paper [12] and supposed to be due to Li insertion into crystalline MnV_2O_6.

Table 2-2 Synthesis conditions and anodic performance on the MnV_2O_6 powders.
(current density: 60 mA/g, voltage range: 0.0-3.5V)

Synthesis Condition					1st cycle		10th cycle		Charge capacity change with cycle
concentration (mol/l)	pH	temperature (℃)	time (h)	annealing	Discharge//Charge capacity (mAh/g)	Coulombic efficiency (%)	Discharge//Charge capacity (mAh/g)	Coulombic efficiency (%)	
0.01	4.0	135	5	---	496 // 235	47.4	446 // 417	93.5	D
0.01	4.0	175	5	---	759 // 423	55.8	610 // 595	97.7	D
0.01	4.0	200	5	---	919 // 601	65.3	538 // 521	96.8	D
0.01	4.0	200	5	600℃, 1h	898 // 425	47.3	185 // 180	97.3	D
0.01	4.0	200	0.5	---	813 // 462	56.8	467 // 439	94.0	D
0.01	4.0	200	10	---	736 // 422	57.4	484 // 468	96.8	D
0.10	4.0	200	5	---	656 // 349	53.2	658 // 631	95.9	I
0.10	4.0	200	5	600℃, 1h	965 // 582	60.4	192 // 185	96.0	D
0.50	4.1	200	5		719 // 439	61.1	712 // 688	96.6	I
1.00	4.2	200	5	---	809 // 528	65.4	588 // 552	96.6	I

D : gradual decrease with cycle, see Fig. 2-8 (a) I : abrupt increase after 3rd or 4th cycle, see Fig. 2-8 (b)

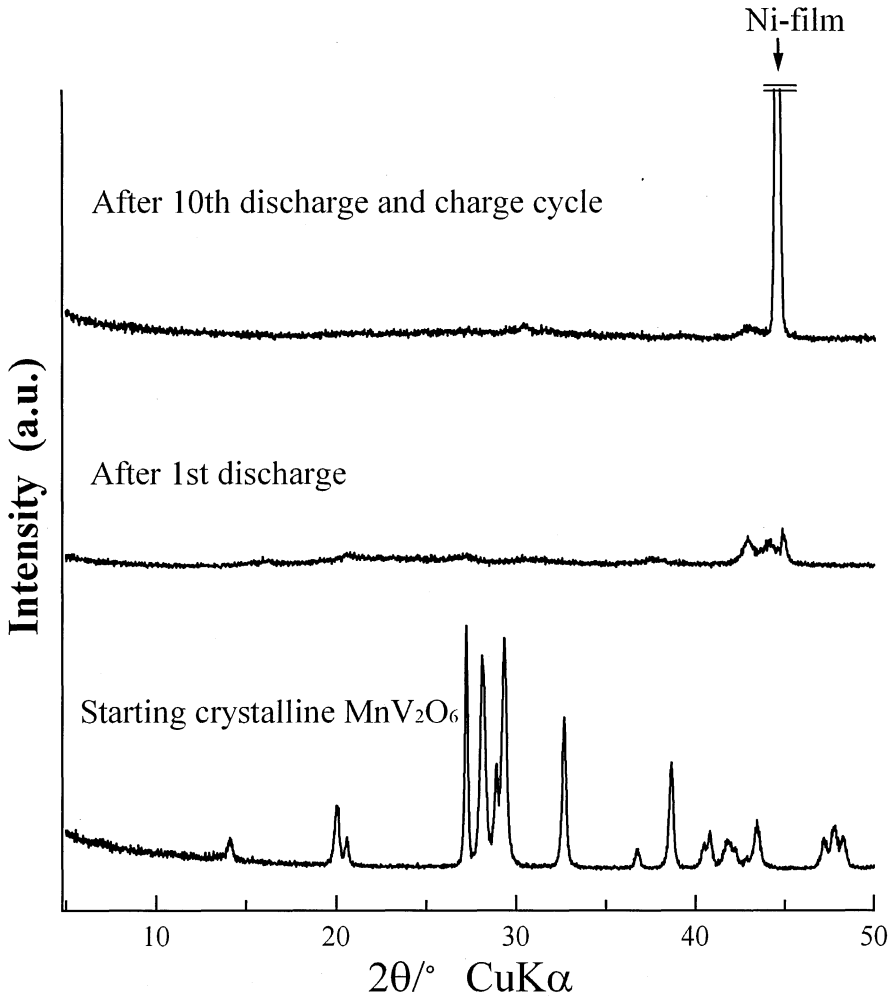

Fig.2-9 XRD patterns after discharge and charge cycle on the starting powders obtained 200 °C for 5 h from the concentration of 0.1 mol/L.

2-3-2 Synthesis of anhydrous MnV_2O_6 powders by coprecipitation

a) MnV_2O_6 powders synthesized

Fig. 2-10 shows the X-ray powder diffraction patterns of the precipitates prepared at 90 °C for 5 h from the solutions with different metal concentrations of 0.01, 0.1 and 0.9 mol/L (Process I). In clear solution with 0.01 mol/L concentration, the formation of the precipitates with dark red color started at a temperature of around 60 °C. The powder patterns of the precipitates formed from 0.01 and 0.1 mol/L solutions are different from that obtained in 0.9 mol/L solution. These two kinds of powder patterns were difficult to be indexed by manganese vanadate. However, the precipitates thus obtained were supposed to be a mixture of various hydrous compounds $MnV_2O_6 \cdot nH_2O$ with different n values, because crystalline $MnV_2O_6 \cdot nH_2O$ (n = 1~4) were reported to be synthesized from a similar condition [19] and also the present precipitates changed to anhydrous manganese vanadate above 150 °C, as will be shown below.

In Fig. 2-11, the changes in powder pattern with annealing at high temperatures are shown on the precipitates obtained from 0.01 mol/L solution. For the precipitates obtained from clear solutions, such as 0.01 mol/L solution, anhydrous manganese vanadate was obtained in a single phase already after 200 °C annealing, even though the crystallinity of the powder was poor. After 700 °C annealing, manganese vanadate with high crystallinity was obtained. From the precipitates obtained 0.9 mol/L solution in Fig. 2-11, anhydrous MnV_2O_6 was obtained by annealing at 700 °C for 5 h, even though the as-prepared precipitates gave a powder pattern from those different from other dilute solutions.

The precipitates synthesized by mixing aqueous solutions (Process I) were supposed to be hydrous manganese vanadate and required to anneal above 200 °C to change them to anhydrous manganese vanadate. It has to be pointed out, however, that the anhydrous manganese vanadate prepared through this process shows always the powder pattern with weak 110 peak, though a strong 110 peak is an important indication for the characteristic anode performance of manganese vanadate as shown in the previous section 2-3-1.

Dark brown precipitates were generated instantly by adding $Mn(CH_3COO)_2$ particles into aqueous suspension of V_2O_5 kept at 95 °C under refluxing. The yield of the precipitates was more than 97 %. In Fig. 2-12(a) and (b), X-ray powder diffraction patterns of the precipitates obtained at 95 °C for 24 and 72 h aging from 0.1 mol/L solution, respectively, together with those of annealed ones. The powder patterns of the as-prepared precipitates reveal the formation of anhydrous manganese vanadate. In 400 °C-annealed samples prepared from the precipitates after 24 h aging, however, V_2O_5 appears in addition to anhydrous manganese vanadate, which is reasonably supposed to come from a part of undissolved V_2O_5 particles. But no V_2O_5 was detected in the precipitate after long time aging, more than 72 h, and annealing at 400 °C.

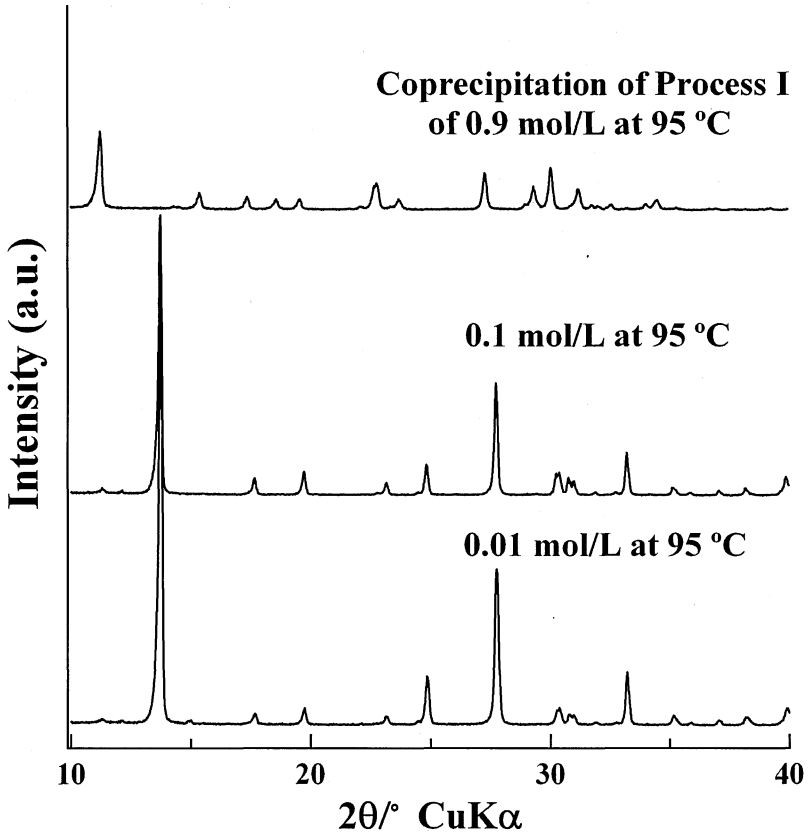

Fig. 2-10 XRD patterns of the precipitates obtained from different concentrations at 90 °C for 5 h (Process I).

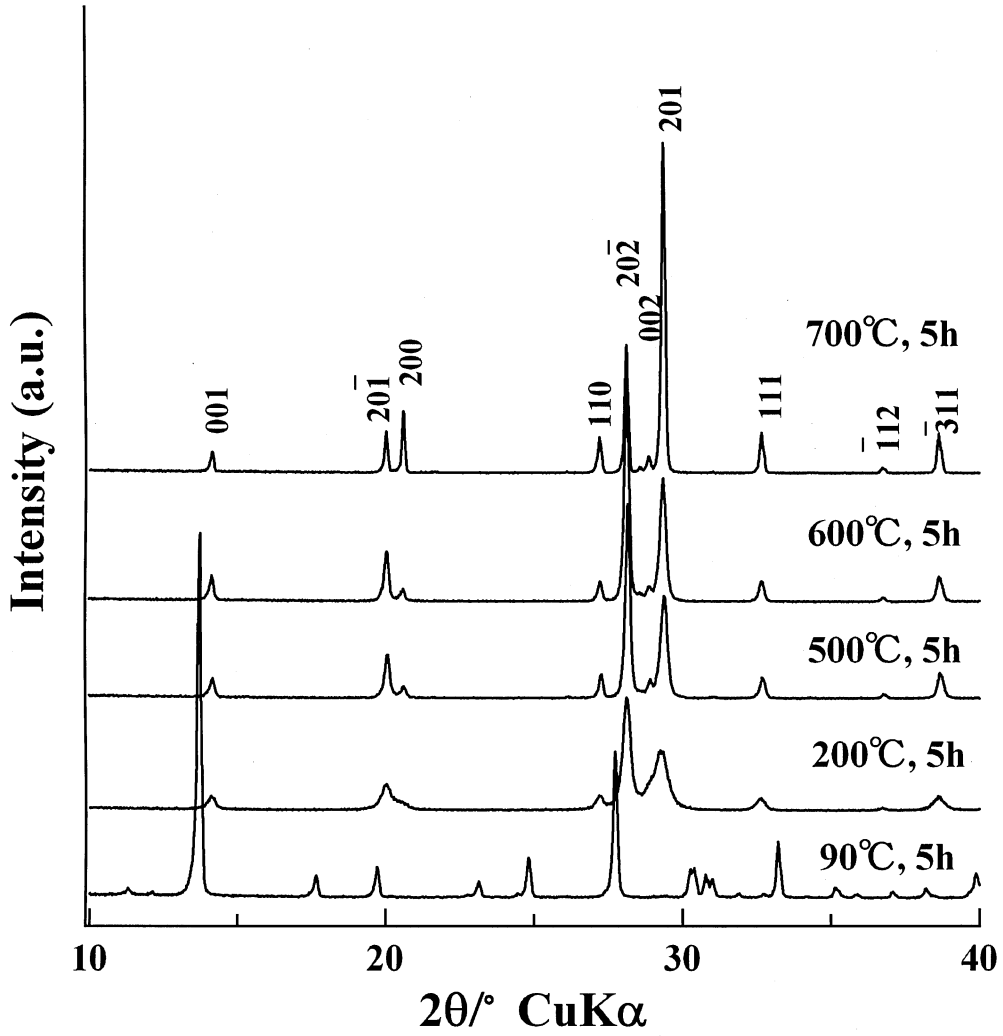

Fig. 2-11 Change in XRD pattern with annealing temperature for the precipitates obtained from 0.01 mol/L solution (Process I).

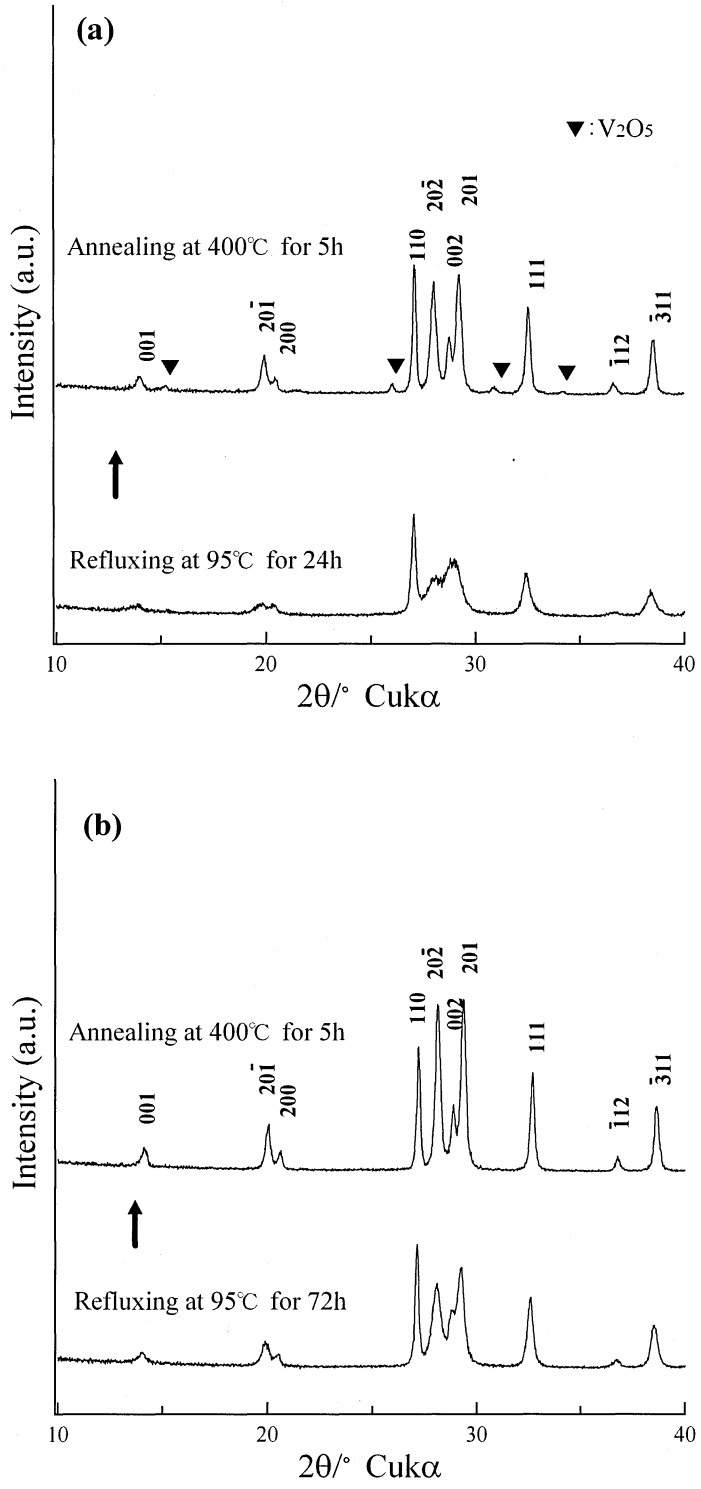

Fig. 2-12 XRD patterns of the as-precipitated samples prepared by mixing of V_2O_5 with $Mn(CH_3COO)_2$ in water medium (Process II) with the nominal concentration of 0.1 mol/L at 95 °C and of those annealed at 400 °C for 5 h in air. (a) The sample aged for 24 h and (b) for 72 h.

Here, it is worthwhile to point out that the present precipitates, even as-prepared ones, show relatively strong 110 peak in their powder patterns, as shown in Fig 2-12(a) and (b). Therefore, the Process II, *i.e.*, direct addition of $Mn(CH_3COO)_2$ particles into V_2O_5 suspension at 95 °C, was found to be effective to synthesize anhydrous manganese vanadate crystals, which show strong 110 peak in their powder patterns, but to need a long time aging, more than 72h, in order to complete the reaction of Mn^{2+} ions in the solution with undissolved V_2O_5 solid particles. The powder patterns observed on these samples are the same as those for the anhydrous manganese vanadate obtained under hydrothermal condition in the previous section 2-3-1.

In Fig. 2-13, TEM photographs are shown on the precipitates obtained by different conditions. For the precipitates obtained at 95 °C from 0.01 mol/L solution, the particles are very fine but lack of uniformity in their morphology, and their edges are round (Fig. 2-12 (a)). By annealing them to 150 °C, all particles change to rod-like and become very large size, which are reasonably suppose to be anhydrous manganese vanadate. However, all particles obtained through 95 °C, which were anhydrous crystals in as-precipitated state, showed rod-like morphology and homogeneity in size, as shown in Fig. 2-13 (c) and (d). In the precipitates obtained by 24 h aging, small round particles were observed, which are confirmed to be vanadium compound (i.e., V_2O_5) by EDS, in addition to rod-like particles (Fig. 2-13(c)). Rod-like particles in the precipitates obtained through Process II seemed much thinner than those through Process I coupled with high temperature annealing. Particle morphology observed on the samples obtained through Process II was very similar to that obtained under autogenous hydrothermal condition in previous section 2-3-1.

In Fig. 2-14, TG curves are compared for the as-precipitated samples obtained through Process I and II. TG curve observed on the precipitates obtained through Process II with 168h aging shows a weight change in three steps, though total weight loss is only a little more than 2 mass% (Fig. 2-12 (b)). This TG curve is almost the same as that on manganese vanadate obtained under hydrothermal condition. Therefore, the mechanism for the weight loss was supposed to be the same as before, adsorbed water release in the 1st step, evaporation of water film on the surface in the 2nd step and excess oxygen departure in the 3rd step (section 2-3-1). On the other hand, the precipitates obtained through Process I show 4 steps in weight decrease and total weight loss of about 6.5 %. The TG curves observed suggested that the precipitates obtained through the present process were manganese vanadate with excess oxygen $MnV_2O_{6+\delta}$.

Lattice parameters measured on the samples synthesized through Process II are summarized in Table 2-3. The samples aged for more than 72 h and those annealed at 400 °C have the same lattice parameters as those in JCPDS card (No.35-139).

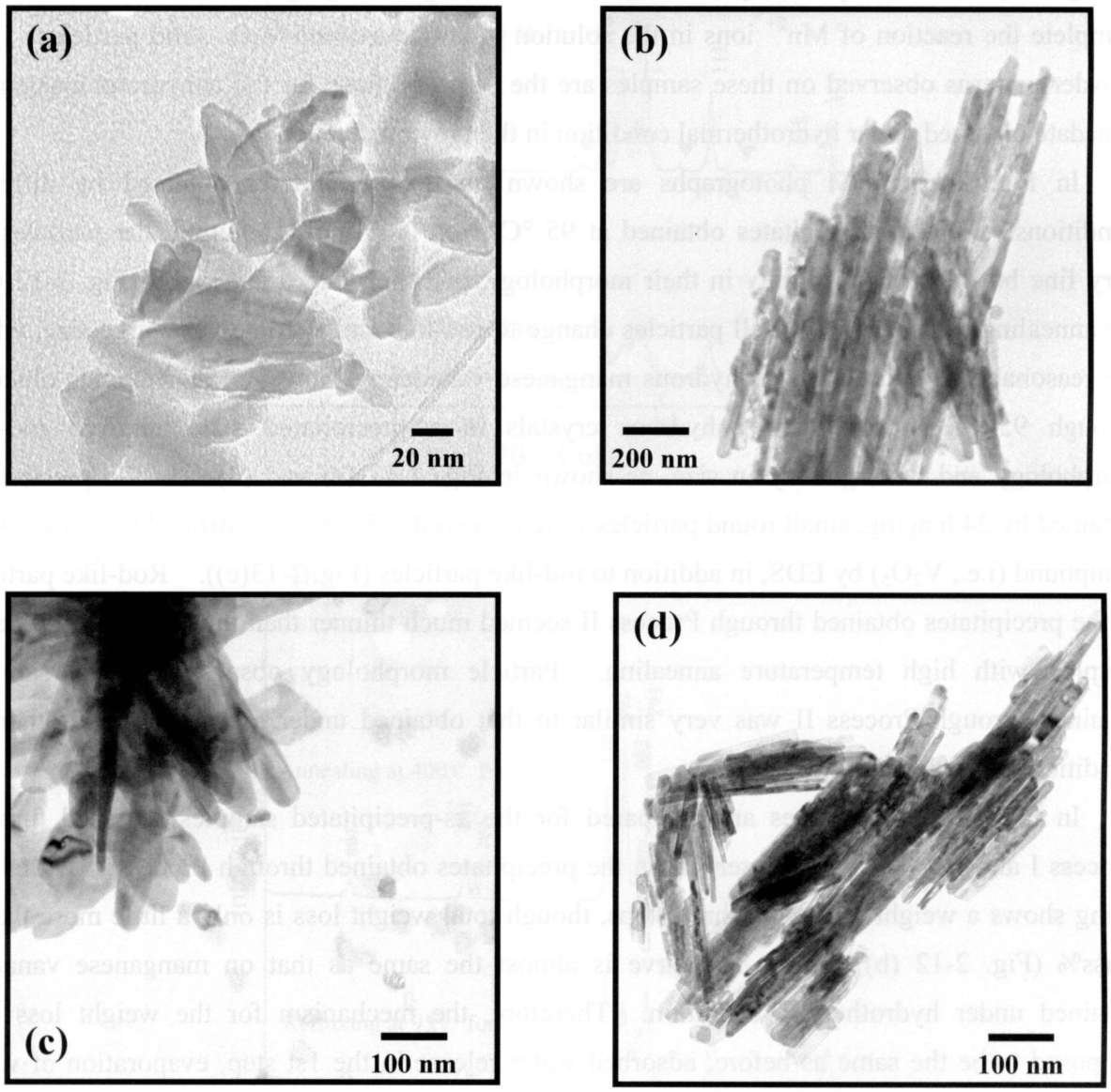

Fig. 2-13 TEM photographs of the samples. (a) As-precipitated sample obtained through Process I at 90 °C for 5 h with 0.01 mol/L, (b) the annealed at 150 °C for 1 h, and the precipitates obtained through Process II at 95 °C, (c) aging for 24 h and (d) for 168 h.

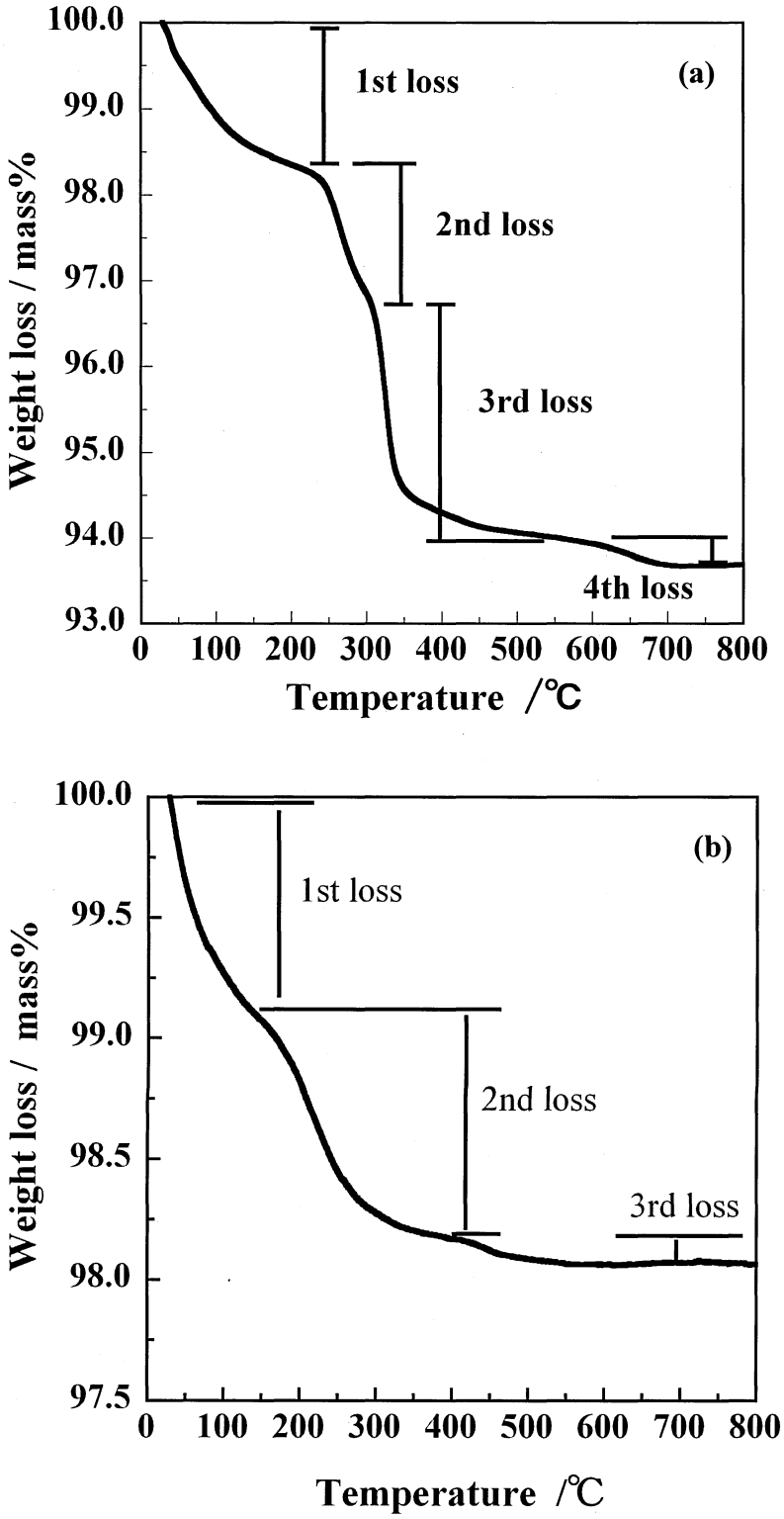

Fig. 2-14 TG curves of the precipitates obtained through Process I at 90 °C (a) and through Process II at 95 °C with 72 h aging (b).

Table 2-3 Lattice parameters of the samples synthesized through Process II under refluxing.

Synthesis through Process II					Lattice parameters of MnV_2O_6 phase			
concentration (mol/L)	temperature (℃)	time (h)	annealing	phases existed	a_0 (nm)	b_0 (nm)	c_0 (nm)	β (°)
0.10	90	24	---	MnV_2O_6	0.9337	0.3547	0.6710	112.02
0.10	90	24	400℃, 5h	$MnV_2O_6 + V_2O_5$	0.9313	0.3536	0.6757	112.66
0.10	90	72	---	MnV_2O_6	0.9310	0.3532	0.6731	112.70
0.10	90	168	---	MnV_2O_6	0.9309	0.3532	0.6730	112.77
0.10	90	168	400℃, 5h	MnV_2O_6	0.9316	0.3534	0.6752	112.67
ICDD Number 35-0139					0.9315	0.3536	0.6754	112.66

But lattice parameters for as-prepared powders with 24 h aging are different from those in JCPDS; a_0 and c_0 being much smaller, though b_0 and angle β are almost the same after annealing at 400 °C.

b) Anodic performance of MnV_2O_6 powders

For anhydrous manganese vanadate prepared through Process I with annealing at 150 °C for 5 h, discharge and charge capacities with Columbic efficiency are plotted against cycle number in Fig. 2-15. In the first cycle, discharge capacity is as high as 1100 mAh/g. However, charge capacity in the first cycle is 550 mAh/g, then Coulombic efficiency being about 50%. During the cycling after the first, both discharge and charge capacities become around 600 mAh/g with a fluctuation between 550 and 650 mAh/g and, as a consequence, Coulombic efficiency being also scattered in a range of 90 ~ 105 %.

In Fig. 2-16 (a), discharge and charge curves are shown on the sample obtained through Process II with 24 h aging, which was a mixture of anhydrous manganese vanadate with a small amount of amorphous V_2O_5. The first discharge curve shows clearly a wide plateau at 0.7 V. From the 2nd cycle, this plateau disappeared. In this figure, it has to be noted that the discharge capacity for the 10th cycle is much larger than that for the first cycle. Both discharge and charge capacities increase with cycling and then gradually decrease after the 5 or 6th cycle, as cyclic performance of this sample is shown in Fig. 2-16 (b). The Coulombic efficiency is rather low as 87 %. For these experimental results relatively low discharge and charge capacities and low Coulombic efficiency, the presence of a small amount of unreacted V_2O_5 in the sample was assumed to be responsible, because the cathodic behavior of a small amount of V_2O_5 might partly cancel out the anodic capacity of manganese vanadate.

In Fig. 2-17 (a), discharge and charge curves are shown on the sample of a single phase anhydrous manganese vanadate obtained through Process II with 72 h aging. The first discharge curve also shows a plateau at 0.7 V. The discharge capacity for the 50th cycle is much larger than the 1st. cycle. Characteristic property of cyclic performance, the increases in discharge and charge capacities with the cycle, which is the same as that observed on manganese vanadate powder synthesized under autogenous hydrothermal condition in the previous section 2-3-1, is clearly observed, as shown in Fig. 2-17 (b). Though the discharge capacity significantly reduced in the 2nd cycle, both discharge and charge capacities gradually increased with cycling up to 50th. Beyond 25th cycle, discharge and charge capacities became larger than the discharge capacity for the 1st cycle (620 mAh/g). With cycling, both capacities tended to saturate at about 700 mAh/g. Columbic efficiency reached approximately 100 % after first few cycles. All anhydrous manganese vanadate powders prepared through Process II with ageing for more than 72 h showed

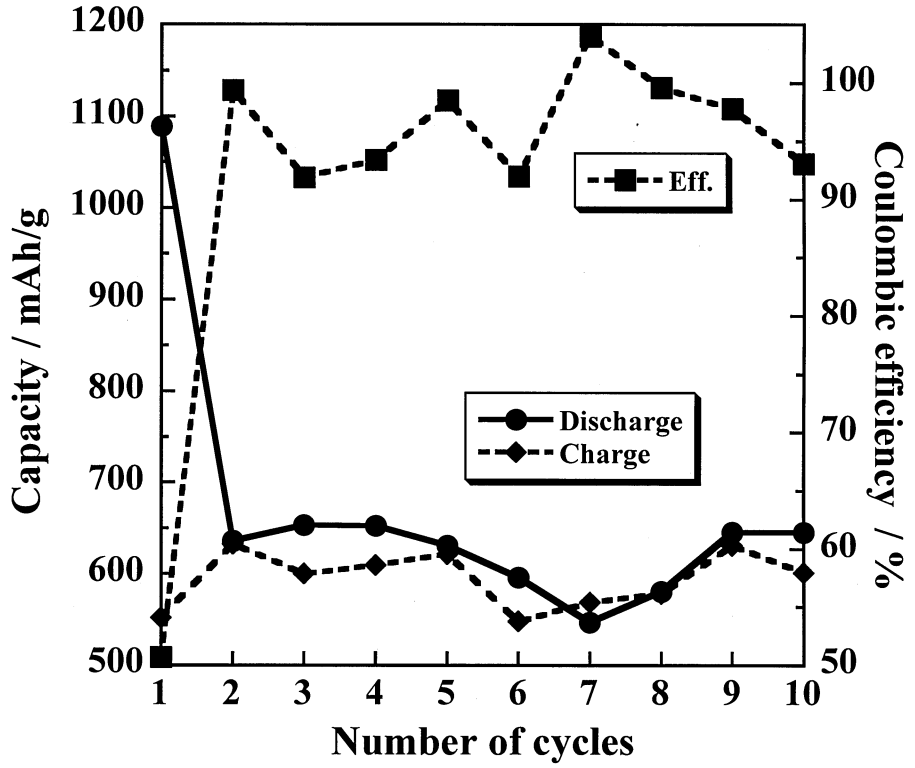

Fig. 2-15 Cyclic performance of the sample obtained through Process I from 0.01 mol/L solution at 90 °C and annealed at 150 °C for 5 h.

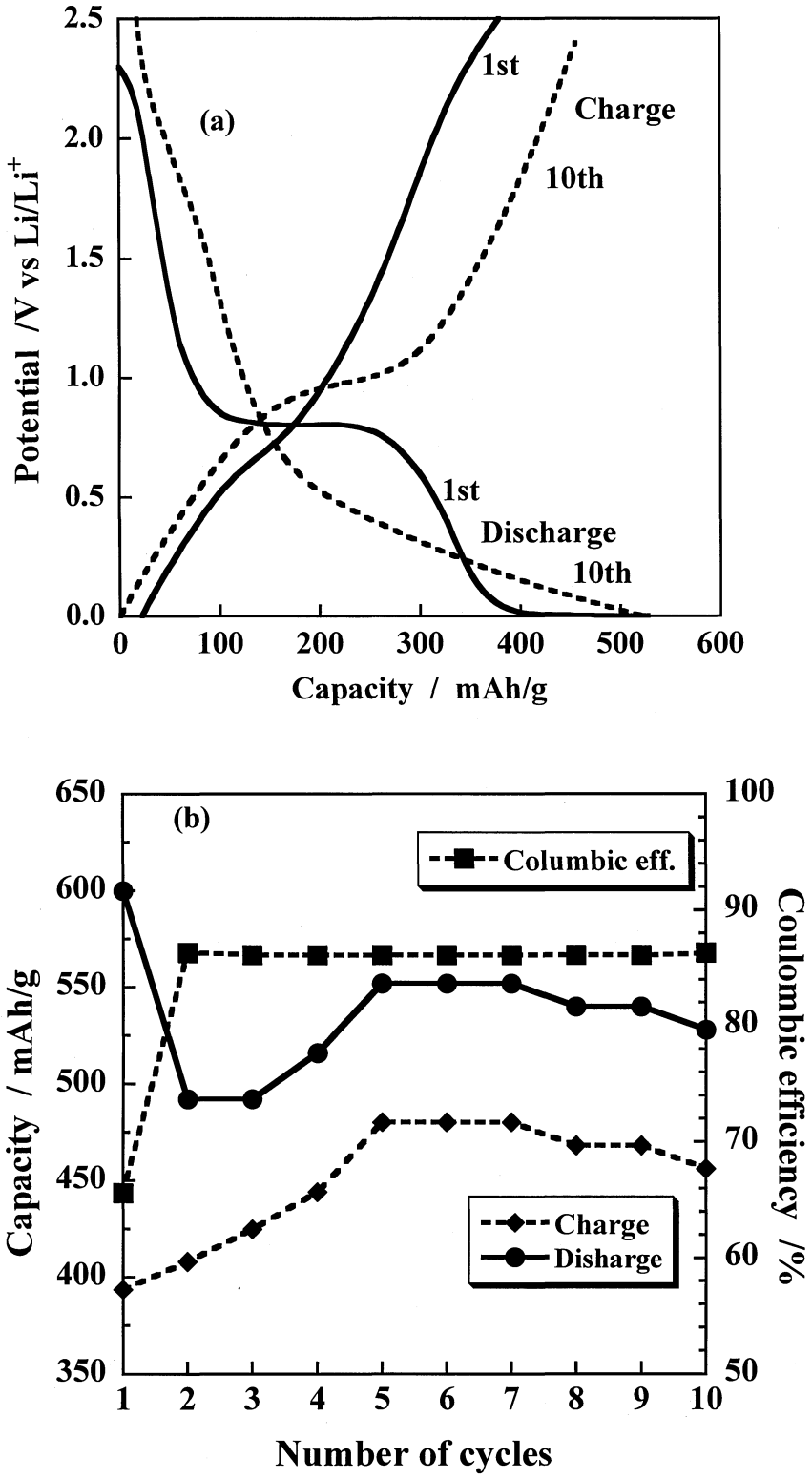

Fig. 2-16 (a) Discharge and charge curves and (b) cyclic performance on the sample obtained through Process II at 95 °C with 24 h aging, which was composed of anhydrous $MnV_2O_{6+\delta}$ with a small amount of amorphous V_2O_5.

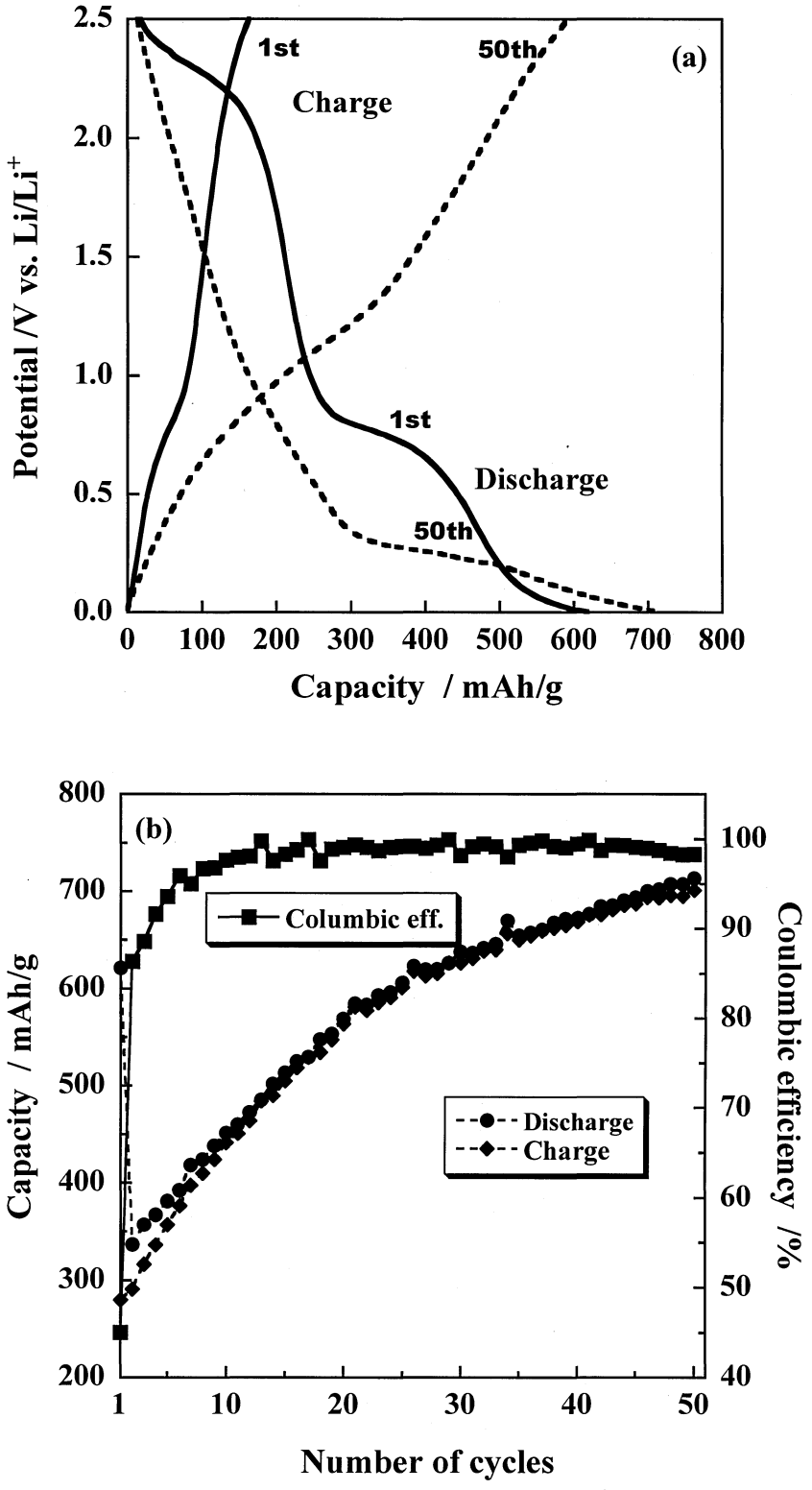

Fig. 2-17 (a) Discharge and charge curves and (b) cyclic performance on the sample of a single phase anhydrous MnV_2O_6 prepared through Process II at 95 °C with 72 h aging.

the same characteristics in discharge and charge performance with large values in capacities and Columbic efficiency close to 100 %. These powders always consisted of crystal with rod-like morphology and showed XRD patterns with sharp and strong 110 diffraction line.

2-3-3 Change in oxidation state on MnV_2O_6 anode during discharge/charge process

The electrochemical reaction in the test cell, where MnV_2O_6 was used as anode material with lithium metal as cathode can be written as follows;

$$\text{Anode: } xLi \underset{\text{charge}}{\overset{\text{Discharge}}{\rightleftarrows}} xLi^+ + xe^-$$

$$\text{Cathode (practical: anode-electrode): } MnV_2O_6 + xLi^+ \underset{\text{Charge}}{\overset{\text{Discharge}}{\rightleftarrows}} Li_xMnV_2O_6$$

$$\text{Cell reaction: } xLi^+ + MnV_2O_6 \underset{\text{Charge}}{\overset{\text{Discharge}}{\rightleftarrows}} Li_xMnV_2O_6$$

The changes in structure from crystalline state to amorphous one and in marked morphology change from rod-like particles to small round ones were observed even after 1st charging process, as shown in Section 2-3-1 and in Fig. 2-9. Amorphanization of anode MnV_2O_6 was also reported in the paper [12]. The diffraction peaks for brannerite structure were broadened and weakened. It was difficult to identify the peaks, even after 1st cycle and they disappeared completely after 10th cycle, as shown in Fig. 2-9. In the TEM photograph, the particles with irregular shapes were observed, as shown in Fig. 2-18, which were supposed to be in amorphous state because of no diffraction spots in electron diffraction pattern shown as an inserted figure in Fig. 2-18. The presence of both manganese and vanadium ions in the round particles formed after charging process was confirmed by EDS analysis under TEM.

On four powders which were discharged down to 0.7 and 0.0 V and also re-charged up to 0.7 and 2.5 V on the course of 1st discharge-charge cycle, the spectra of XAFS and XPS were measured using the films which were picked out from test cell of lithium ion rechargeable battery, which contained carbon black and binder PVDF, and compared with those observed on the as-synthesized powder, without any electrochemical treatment. XAFS spectra at around k-absorption edge of vanadium were shown in Figs. 2-19(a) for the sample powders on the way of discharging, together with those for the references, *i.e.*, V_2O_4 and V_2O_5 in which vanadium ions states of vanadium ions were 4+ and 5+, respectively, and in Fig. 2-19(b) for the sample powders on the way to charging. In Fig. 2-20, XPS spectra for vanadium are compared among four sample powders.

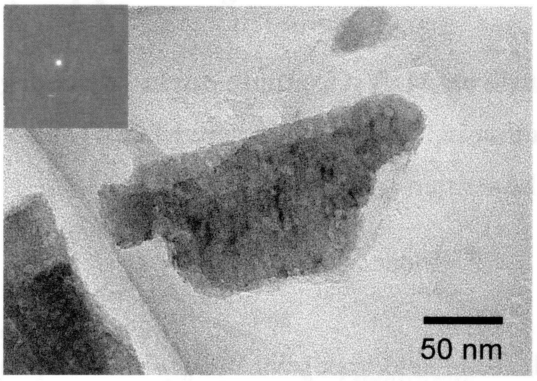

Fig. 2-18 Transmission electron microscope images of manganese vanadate synthesized at 200 °C after 1st discharge process.

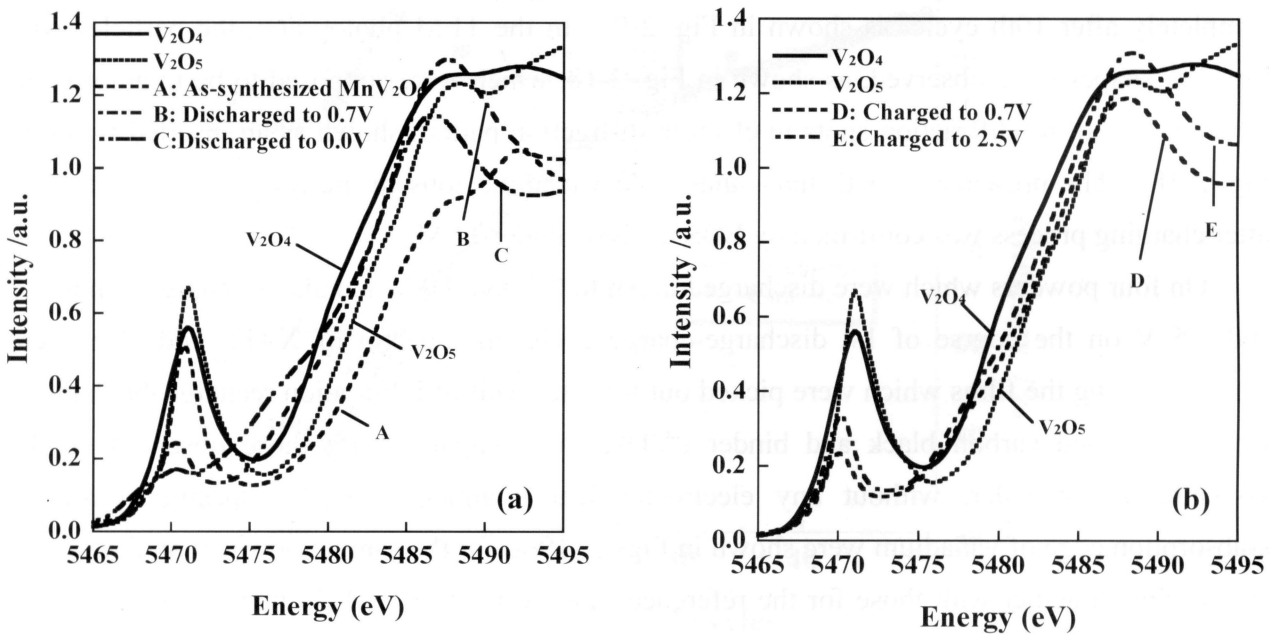

Fig.2-19 V K-edge XAFS spectra of manganese vanadate powders.

a) The powders as-synthesized and discharged down to 0.7 and 0.0 V, with the references V_2O_4 and V_2O_5, and b) the powders charged up to 0.7 and 2.5 V.

From the comparison of the shapes of absorption edge in XAFS spectra, especially based on the absorption edge energy, the starting manganese vanadate was found to contain V^{5+}. On the other hand, the powders on the way of discharging (discharged down to 0.7 and 0.0 V) were reasonably supposed to contain V^{4+}, in addition to $V5^{+}$. The content of reduced ion V^{4+} was higher in the latter case than in the former (Fig. 2-19(a)). The powders on charging have a high concentration of V^{5+} even before complete charge (charged up to 0.7 V), as shown in Fig. 2-19(b).

In XPS spectra in Fig. 2-20(a) for as-prepared MnV_2O_6, the peak for vanadium $V2p_{3/2}$ is located at the binding energy of 521.8 eV, which reveals the presence of V^{5+}. On the other hand, the XPS spectra observed on the samples on the way of discharging and charging are broadened, probably due to the fact that XPS measurements on these powders are performed on the films picked out from the test cell and so the film contain carbon black and binder PVDF. Irrespective of the broadening due to film forming, the peaks of $V2p_{3/2}$ observed on the powders discharged down to 0.7 and 0.0 V are very broad, as shown in Fig. 2-20(a). On these peaks, therefore, peak separation technique was applied, as shown the result on the powder discharged down to 0.7 V, which was reasonably supposed to consist of two peaks at the binding energy of 70.8 and 69.0 eV, which correspond to V^{5+} and V^{4+}, respectively, as shown in Fig. 2-20(b). After charged up to 2.5 V, the peak $V2p_{3/2}$ was sharpened back, but not as sharp as the as-synthesized one because of film forming, and its binding energy returned back to 70.8 eV, suggesting the presence of V^{5+}.

XPS spectra of Mn, $Mn2p_{3/2}$ and $Mn2p_{1/2}$ measured on the as-synthesized crystalline MnV_2O_6 shows the presence of Mn^{2+} (Fig. 2-21). The samples on the way of discharge-charge process gave very broad XPS spectra with marked noises, as shown on the sample discharged down to 0.7 V in Fig. 2-21(b). It was difficult to discuss on the oxidation state of manganese ions on these samples.

From XAFS and XPS analyses, oxidation state of vanadium ions in manganese vanadate was supposed to change from 5+ in as-synthesized powder to 4+ in the powder discharged down to 0.0 V, and by charging it returned from 4+ to 5+. It had to be pointed out that the reduction of vanadium ion from 5+ to 4+ seemed not to be completed by the first discharge process, but its oxidation state with 4+, which was formed by the previous reduction process, seemed to be re-oxidized to 5+ on the following charge process completely.

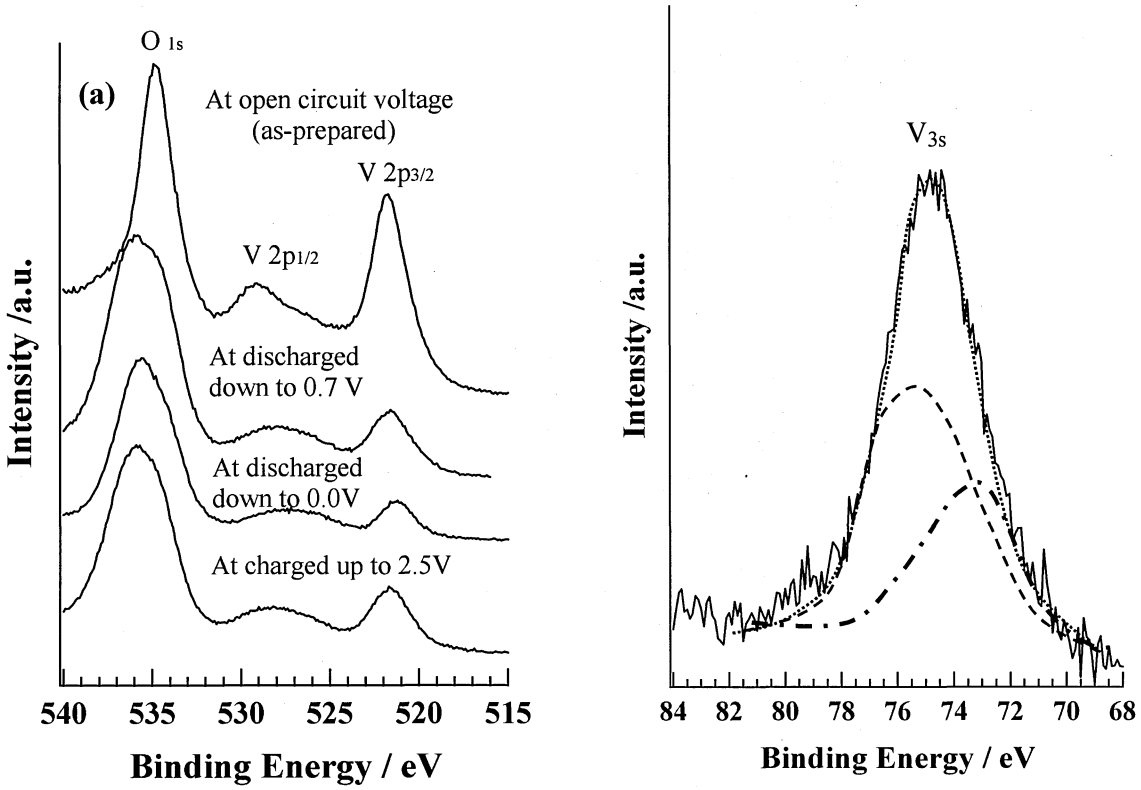

Fig. 2-20 XPS spectra of (a) V2pO1s and (b) V3s in manganese vanadate powders synthesized at 200 °C, discharged down to 0.7 and 0.0 V and charged up to 2.5 V in lithium ion rechargeable battery.

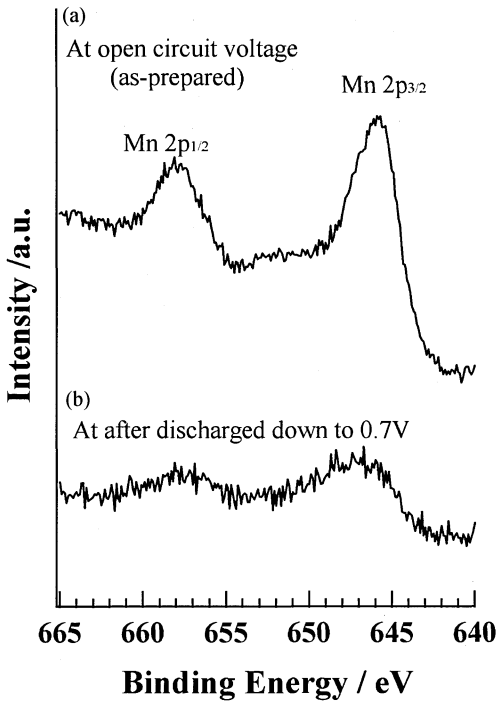

Fig. 2-21 XPS spectra of Mn2p for manganese vanadate powder as-synthesized and discharged down to 0.7 V.

2-3-4 Renewal of the synthesis of manganese vanadate powder and its anodic performance

The results of the analysis of oxidation state of vanadium ions in manganese vanadate powders, in addition to the fact that both XAFS and XPS analyses gave the information on the surface of the film, can be assumed that lithium insertion into manganese vanadate crystals is slow process. This assumption seems to agree with the experimental facts that manganese vanadate electrode shows very high irreversible capacity and that the powder synthesized at 200 ^{o}C few discharge-charge cycle to reach stable capacity.

The powder of crystalline manganese vanadate was synthesized once again under hydrothermal condition, at a lower temperature for a shorter time than the case described before (Section 2.1), *i.e.*, at 135 ^{o}C for 1h, other conditions being kept the same as before. XRD pattern and TEM image of the powder thus synthesized are shown in Fig. 2-22(a) and 2-22(b), respectively. XRD pattern of the powder (Fig. 2-22(a)) shows a strong 110 diffraction peak, as before (Fig. 2-3(a) in Section 2-3-1) and particle morphology is rod-like, but much thinner than before (compare to Fig. 2-6).

On the film formed from the powder newly synthesized, discharge-charge cycles were performed, in exactly the same procedure as before. Cyclic performance obtained is shown in Fig. 2-23. Discharge capacity at the 1st cycle is not so high, but charge capacity is relatively high (about 700 mAh/g), in other words, irreversible capacity is relatively small and Coulombic efficiency is relatively high, in comparison with the previous powder (Fig. 2-8(b) in Section 2-3-1). Also it has to be pointed out that discharge and charge capacities decrease slightly and quickly saturate by cycling. The capacity leveled off is 600 mAh/g.

The results on newly synthesized powder proved that the assumption derived from the results of XAFS and XPS, *i.e.*, thinner crystals of manganese vanadate is desirable, is the case. In order to get high anodic performance of manganese vanadate, therefore, low temperature synthesis is required.

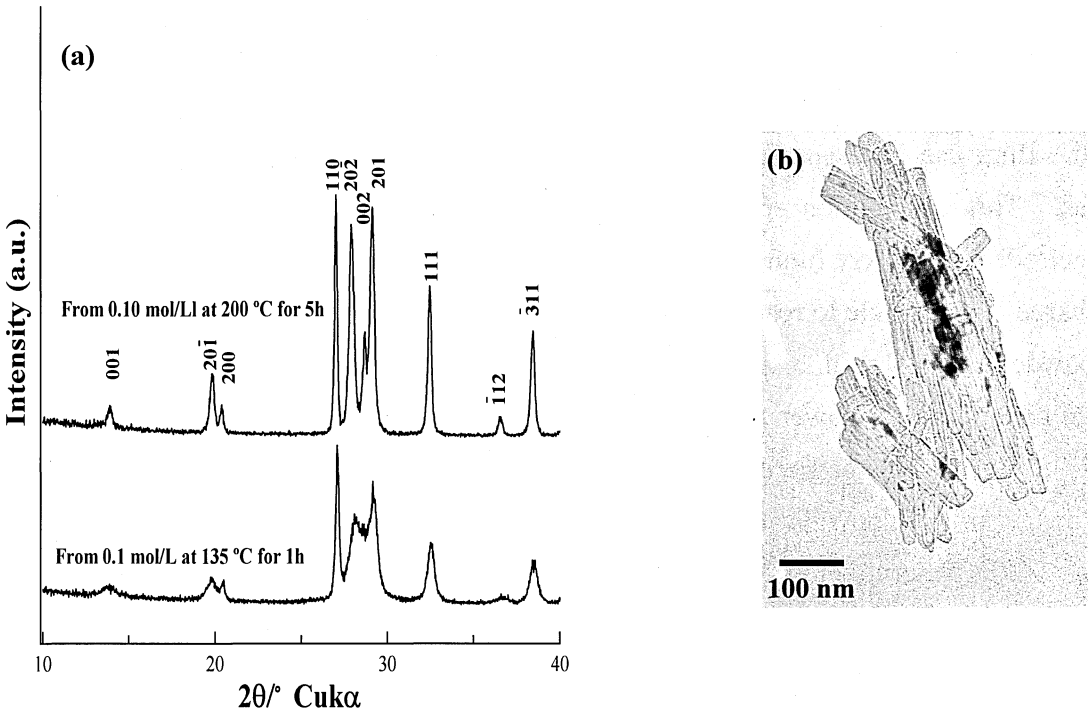

Fig. 2-22 Manganese vanadate powder synthesized at 135 °C
a) XRD pattern and b) TEM image.

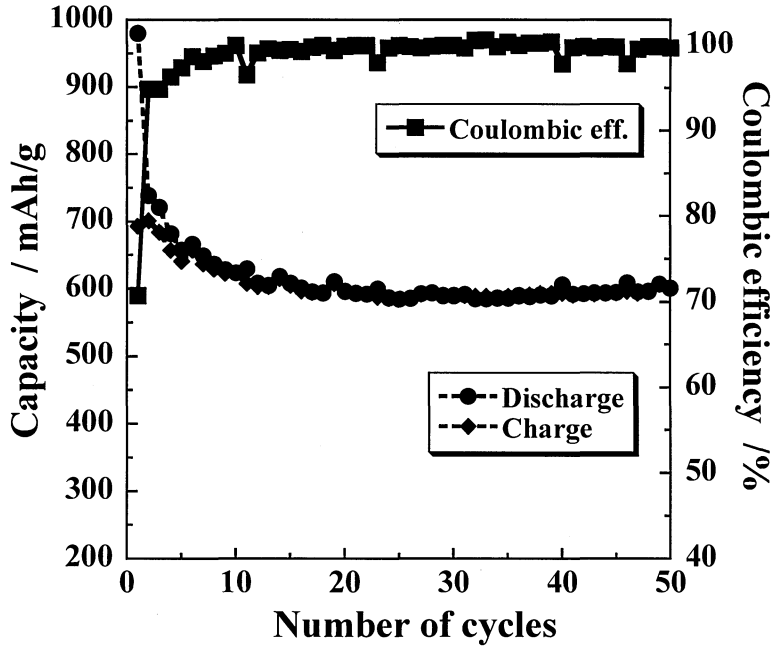

Fig. 2-23 Cyclic performance of manganese vanadate powder synthesized at 135 °C.

2-4 Summary

Crystalline anhydrous MnV_2O_6 powders were directly synthesized by mixing V_2O_5 with $Mn(CH_3COO)_2$ in water medium below 200 °C. This synthesis process was much simpler and lower temperature than those reported before. Anhydrous MnV_2O_6 powders obtained were homogenous in morphology and size of their particles, but relatively long aging time, more than 72h, was needed through coprecipitation process in order to obtain single phase.

Anodic performance of the powders thus obtained showed relatively high discharge and charge capacity for Li ion rechargeable batteries. Both discharge and charge capacities often 1st cycle of discharge and charge were 300~400 mAh/g in the beginning of cycle, but both of them increased with cycling, more than 600 mAh/g, and Coulombic efficiency became almost 100%. The requirements to show this interesting cycling performance, *i.e.*, strong 110 diffraction line in the powder pattern and rod-like particles morphology, were confirmed.

The oxidation state of vanadium in MnV_2O_6 during discharging, V^{5+} was found to change gradually to V^{4+}, but it returned back completely to V^{5+} on charge process. By taking into account of the fact that oxidation state changed gradually from the surface of MnV_2O_6 crystals, their thinner particles with rod-like morphology were synthesized at 135 °C, and much better anodic performance was achieved, much smaller irreversible capacity as about 300 mAh/g, stable reversible capacity as 600 mAh/g, and 100 % Coulombic efficiency.

Reference

1. T.Ohzuku, A.Ueda, M. Nagayama, Y. Iwakoshi and H. Komori, *Electrochim. Acta* **38** (1993).1159.
2. K. Sawai, A. Ueda, M. Nagayama, Y. Iwakoshi and H. Komori, *Denki Kagaku* **61** (1993) 715.
3. R.J.Gumow and M.M.Thackeray, *J. Electrochem. Soc.* **140** (1993) 3365.
4. J. M. Taraswn and D. Guyomard, *Solid State Ionics* **69** (1994) 293.
5. T. Tsumura, A Simizu and M. Inagaki, *Solid State Ionics* **90** (1996) 197.
6. T. Tsumura and M. Inagaki, *Solid state Ionics* **104** (1997) 183.
7. T. Tsumura, M. Inagaki and K. Yanagisawa, Trans. *Mater. Res. Soc. Jpn* **23** (1998) 48.
8. J. R. Dahn, A. K. Sleegh, H. Shi, B. M. Way, W, J, Weydanz, J.N. Reimers, Q, Zhong, U. von Sacken,Lithium Batteries, G. Pistoia, *editor, Elsevier* (1993) 1-44.
9. T. Takeda, R.Takahata, Y. J. Kim, K. Koshiba, K. Ishii, T. Kasai and M. Endo. *Tanso* **196** (2001) 14.
10. Y.Piffard, F.Leroux, D Guyomard, J-L.Mansot and M.Tournoux, *J.Power Sources* **68**

(1997) 698.
11. F.Leroux, Y.Piffard, G.Ourvard, J-L.Mansot and D.Guyomard, *Chem.. Master* **11** (1999) 2948.
12. S.-S.Kim, Hiromasa Ikuta, Masataka Wakihara, *Solid State Ionics* **139** (2001) 57.
13. V.L.Zolotavin, V.N.Bulygina and I.Ya.Bezukov, *Russ.J.Inorg.Chem.* **15** (1970) 222.
14. M. Hirano, E. Kato, *J.Am.Ceram.Soc.* **82** [3] (1999) 786.
15. M. Hirano, *J.Mater.Chem.* **10** [2] (2000) 469.
16. M. Hirano, M. Imai, M. Inagaki, *J.Mater Chem.* **10** [2] (2000) 473.
17. M. Hirano, M. Imai, M. Inagaki, *J.Am Ceram.Soc.* **83** [4] (2000) 977.
18. M.Rozman, M.Drofenik, *J.Am.Ceram.Soc,* **78** [9] (1995) 2454.

Chapter 3

Preparation of carbon-coated metallic tin powders and their anode performance for lithium ion rechargeable batteries

3-1 Introduction

The development in lithium ion rechargeable batteries has helped to make various modern electronic devices lighter and smaller. Now their higher power, better performance and longer life are strongly desired. Commercial batteries have been developed by selecting suitable electrode materials, either $LiCoO_2$ or $LiMn_2O_4$ for the cathode and graphite for the anode, where the intercalation and deintercalation processes of lithium ions were known to be fundamental electrochemical reactions [1-4].

For the anode, various types of carbon materials were used, a wide range of carbon materials from low-temperature-treated carbons with amorphous structure to well-crystallized natural graphite [5], surface modified carbons [6] and carbon nanotubes [7]. Instead of carbon materials, metal oxides and metal alloys also have been investigated; for example, MnV_2O_6 possessing brannerite-type structure [8, 9], silicon-carbon alloy [10] and carbon materials mixed with tin [11, 12]. Although the electric capacity of these materials is high, it also has some problems, such as cycle performance and stability. Tin, Sn, was one of the materials which attracted attention. Sn has a large theoretical capacity of 990 mAh/g, but it shows marked volume expansion when it is alloyed with lithium in the electrode of lithium ion rechargeable batteries. In order to prevent volume expansion, various preparing and dispersing methods of fine Sn particles were tried [11-14].

Carbon coating through a simple process, *i.e.,* heat treatment of a mechanical mixture of a ceramic powder with a carbon precursor in inert atmosphere, has been successfully applied on various ceramics, such as different aluminum oxides, magnesium oxide, titanium oxide, various iron oxides, nickel oxide, natural graphite, ceramic tiles, etc., and also aluminum plate of which surface was electrochemically oxidized [15-25]. The particles of oxides of typical elements, Al and Mg, were covered by thin carbon layers and kept in separated particles, no aggregation, if the mixing ratio of carbon precursor was selected appropriately [15]. In the cases of transition

elements, Fe and Ni, their oxides were reduced to metals through the interaction with coated carbon, resulting in carbon-coated metal particles, and graphite crystals were formed at a temperature of 900-1100 °C by the catalytic action of transition metals formed [18,19]. Carbon-coated TiO_2 having anatase type structure was prepared through this process and found to have various advantages as photocatalysts, suppression of the phase transformation to rutile, high adsorptivity, high crystallinity of anatase phase which was found to be advantageous for water purification, etc. [20-23]. Partial reduction of substrate TiO_2 to Ti_4O_7 was also observed [24]. Carbon coating of natural graphite flakes was found to improve the anodic performance in lithium ion rechargeable batteries [25]. Most of carbons thus coated on ceramic particles were found to be porous, which was confirmed by dissolving out MgO substrate with diluted sulfuric acid [26, 27].

In this chapter, the carbon-coated Sn particles were prepared from the mixture of tin oxide with poly(vinyl alcohol) by the same procedure as carbon coating described above, in order to study their performance in lithium ion batteries. The coexistence of MgO particles during carbonization was found to be essential in order to disperse metallic Sn particles as fine particles. The loading of these carbon-coated Sn particles onto graphite flakes was also carried out in order to increase the capacitance in lithium ion batteries.

3-2 Experimental

3-2-1 Preparation of carbon-coated Sn powders

As ceramic powders as carbon coating substrate, mixtures of SnO_2 and MgO were used. SnO_2 powder (reagent grade) had the particle size of about 200 nm, and MgO powder (reagent grade) had the particle size of about 100 nm and the BET surface area of 3 m^2/g. Carbon precursors used in the present study were poly(vinyl alcohol) (PVA) and natural graphite. These four powders, SnO_2, MgO, PVA and graphite, were mechanically mixed in an agate mortar in different ratios and then heated in a flow of argon at a temperature of 700 ~ 900 °C for 1 h. Heating rate to the programmed temperature was 5 °C/min and a flow rate of Ar gas was 60 mL/min.

After heat treatment, black powders were always obtained. During this heat treatment, SnO_2 was found to be reduced to metal, but no change was observed in MgO. Therefore, metallic Sn and MgO particles were supposed to be coated by carbon, as in our previous papers used anatase and MgO ceramic substrates [18,23]. From the carbon-coated Sn/MgO powders thus prepared, MgO was dissolved out by using 1 mol/L HCl and carbon-coated Sn powders were obtained. The samples obtained were examined by X-ray powder diffraction (XRD) with CuKα

radiation. Morphology of the particles was observed under field-emission-type scanning electron microscope (FE-SEM) with the acceleration voltage of 1.0 kV and transmission electron microscope with the acceleration voltage of 200 kV (TEM). The content of carbon coated was determined from the ignition loss of the sample heated at 800 °C for 1 h in air in a TGA apparatus.

3-2-2 Anodic performance of carbon-coated Sn powders

The electrode to determine anodic performance was prepared by mixing the sample powder with acetylene black as an electrical conductor and polyvinylidene difluoride (PVDF) as a binder in a mass ratio of 80:10:10, and pasting on a thin film of Ni. Li metal was used as counter electrode and the reference electrode. The electrolyte solution was the mixture of ethylene carbonate (EC) and diethyl carbonate (DEC) in equal volume ratio, in which 1 mol/L $LiPF_6$ was dissolved. The electrochemical performance was measured in the potential range of 0.0 - 2.0 V with a current density of 50 mA/g at room temperature in a glove box filled with high purity He. Discharge and charge cycles were performed up to 20th. Discharge and charge capacities were determined as the electric quantities discharged and charged at the potential range between 0.0 and 2.0 V.

3-3 Results and discussion

3-3-1 Carbon-coated Sn powders synthesized

Tin oxide, SnO_2, was found to be reduced to metallic tin, Sn, by heating with PVA above 800 °C, as shown in Fig. 3-1(a). Tin metal was melted under these temperatures and agglomerated to large particles, most of which were separated from carbon formed by the pyrolysis of PVA, as shown in Fig. 3-2(a), because the melting temperature of tin metal was about 230 °C. Sometimes, large particles of tin with metallic luster were observed even by naked eyes. Under the coexistence of MgO powder, however, carbon-coated tin was found to be successfully prepared without marked agglomeration by the heat treatment above 800 °C. The formation of metallic Sn was clearly shown in X-ray diffraction pattern after dissolving out of MgO(Fig. 3-1(b)) and small Sn particles were recognized in the pores left by MgO after its dissolution under SEM (Fig. 3-2(b)). Before dissolution of MgO by HCl, only metallic Sn and MgO were detected after 800 °C treatment (Fig. 3-1(a)), but after dissolution broad peaks for SnO_2 and also a peak for SnO were observed, suggesting that the reduction of SnO_2 was not yet completed by the heat treatment at 800 °C for 1 h. On the samples heated up to 900 °C, no SnO and SnO_2 were detected even after washing by HCl.

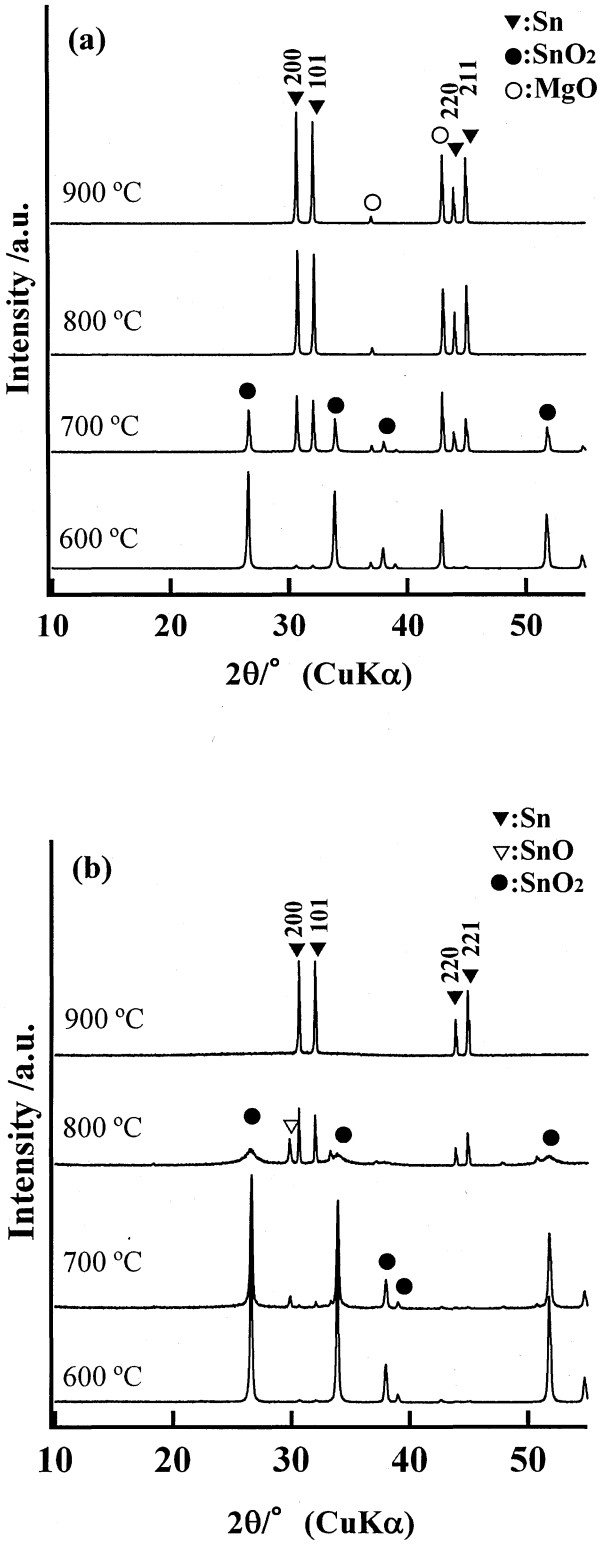

Fig. 3-1 Changes in X-ray diffraction pattern of the powder mixture of PVA and SnO_2 in mass ratio of 50 and 50 with heat treatment temperature in Ar flow before (a) and after (b) washing out of MgO.

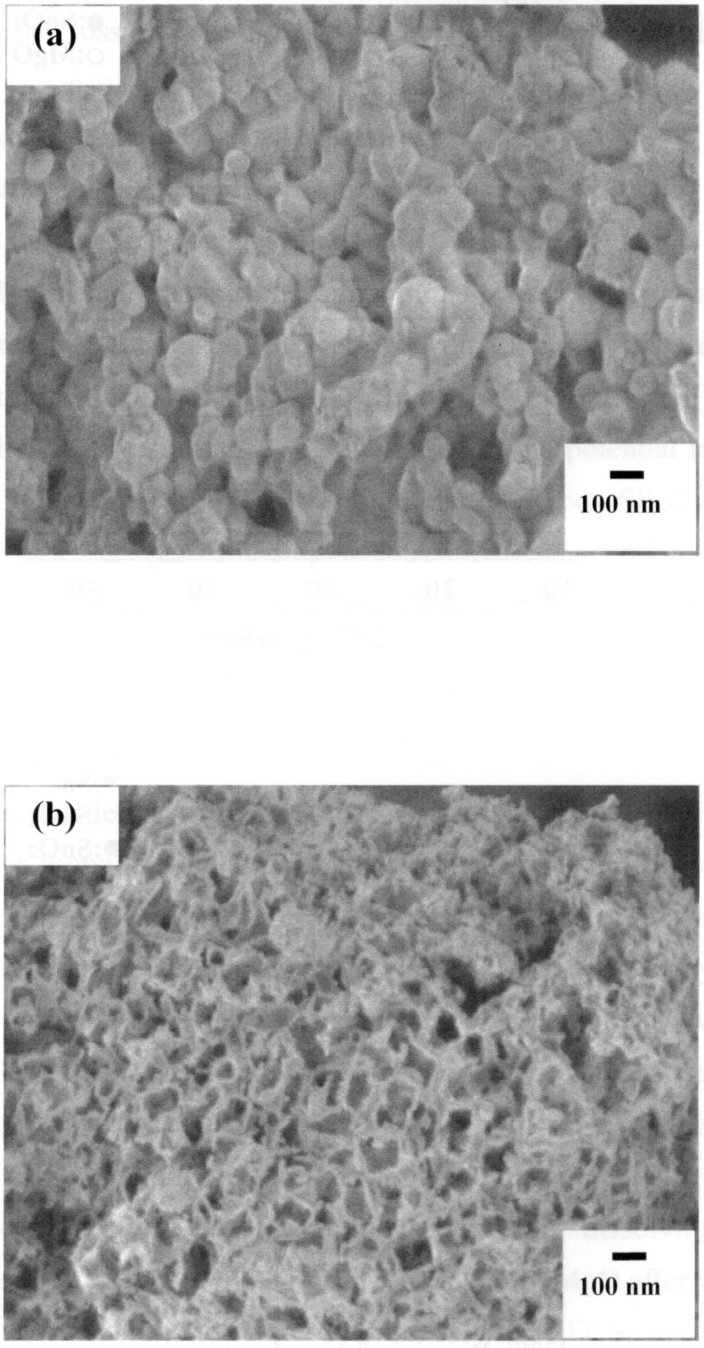

Fig. 3-2 SEM images of the products heated at 900 °C with or without MgO coexistence. a) Heat treated without and b) with MgO.

These powders obtained after carbonization of PVA were perfectly black, both silver metallic particles of Sn and white particles of MgO being not observed. From SEM images like Fig. 3-2(a), the thickness of carbon shells, which left by MgO particles after its dissolution [27], was supposed to be few nanometers, but it was difficult to be determined accurately.

When the powders obtained above 800 °C was washed by either sulfuric or acetic acid in order to dissolve out of MgO, a part of metallic tin was found to be oxidized to either SnO or SnO_2. However, MgO was able to dissolve out with 1 mol/L HCl without any oxidation of metallic tin, as shown in Fig. 3-1(b).

In order to demonstrate the effectiveness of mixing of MgO, XRD patterns of carbon-coated Sn powders are shown in Fig. 3-3, which were prepared from the mixtures with different PVA/MgO/SnO_2 ratios at 900 °C, by keeping the ratio of PVA to total oxides (MgO+SnO_2) constant and then MgO in the carbonized samples was dissolved out by diluted HCl. TEM images of Sn particles in three samples used in Fig. 3 are shown in Fig. 3-4 (a) to 3-4(c).

Only metallic tin can be identified and its diffraction peaks are sharpened with decreasing MgO/SnO_2 ratio, as shown by enlarged 220 line around 45 ° in 2θ in Fig. 3. The crystallite size determined from the line broadening of 220 line in XRD pattern was 150, 45 and 35 nm with changing PVA/MgO/SnO_2 ratio of 10/2/8, 10/5/5 and 10/8/2, respectively. The particle sizes of Sn observed in TEM images in Fig. 3-4 (a) to 3-4(c) for these three samples agree roughly with those determined from XRD. In these three samples prepared from PVA/MgO/SnO2 of 10/2/8, 10/5/5 and 10/8/2, the content of metallic Sn was 96, 80 and 75 mass%, respectively.

The present results showed that, by the coexistence of MgO with SnO_2, carbon-coated Sn powders could be prepared, avoiding the agglomeration of molten Sn metal, at a temperature above 800 °C. MgO particles were assumed to play a following role during high temperature treatment; molten Sn formed by the reduction of SnO_2 through the reaction with coated carbon was kept on the surface of MgO particles due to its wettability, which made difficult for molten Sn to flow and coagulate with each other. Without MgO, molten Sn could be easily coagulated with each other to large particles because of its poor-wettability to carbon. In chapter 4, MgO particles were experimentally shown to be covered by carbon formed from PVA at high temperatures. When relative amount of MgO to SnO_2 was small, such as MgO/SnO_2=2/8, MgO surface might not be enough to keep molten metallic tin formed, and as a consequence molten tin tended to coagulate into large particles. On the other hand, when ratio was MgO/SnO_2=8/2, small metallic tin particles were obtained because molten tin was quickly wetted on MgO surface and hindered its agglomeration.

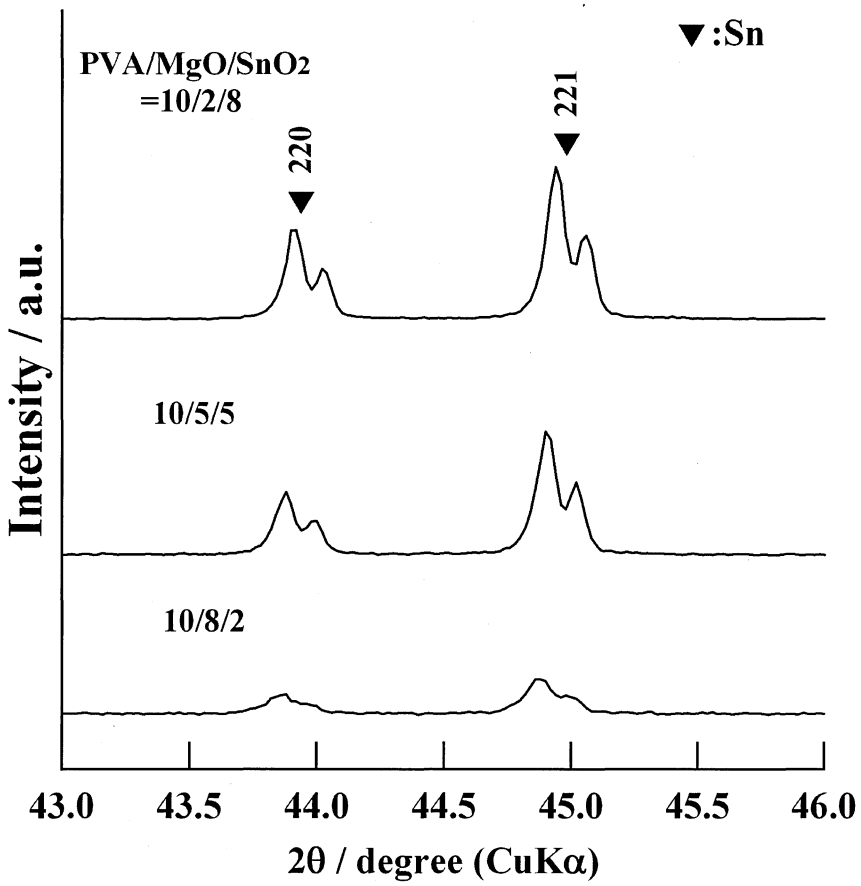

Fig.3-3 XRD patterns of powder the mixture of MgO and SnO_2 in various mass ratios on constant PVA amount with heat treatment at 900 °C in Ar flow after washing out of MgO.

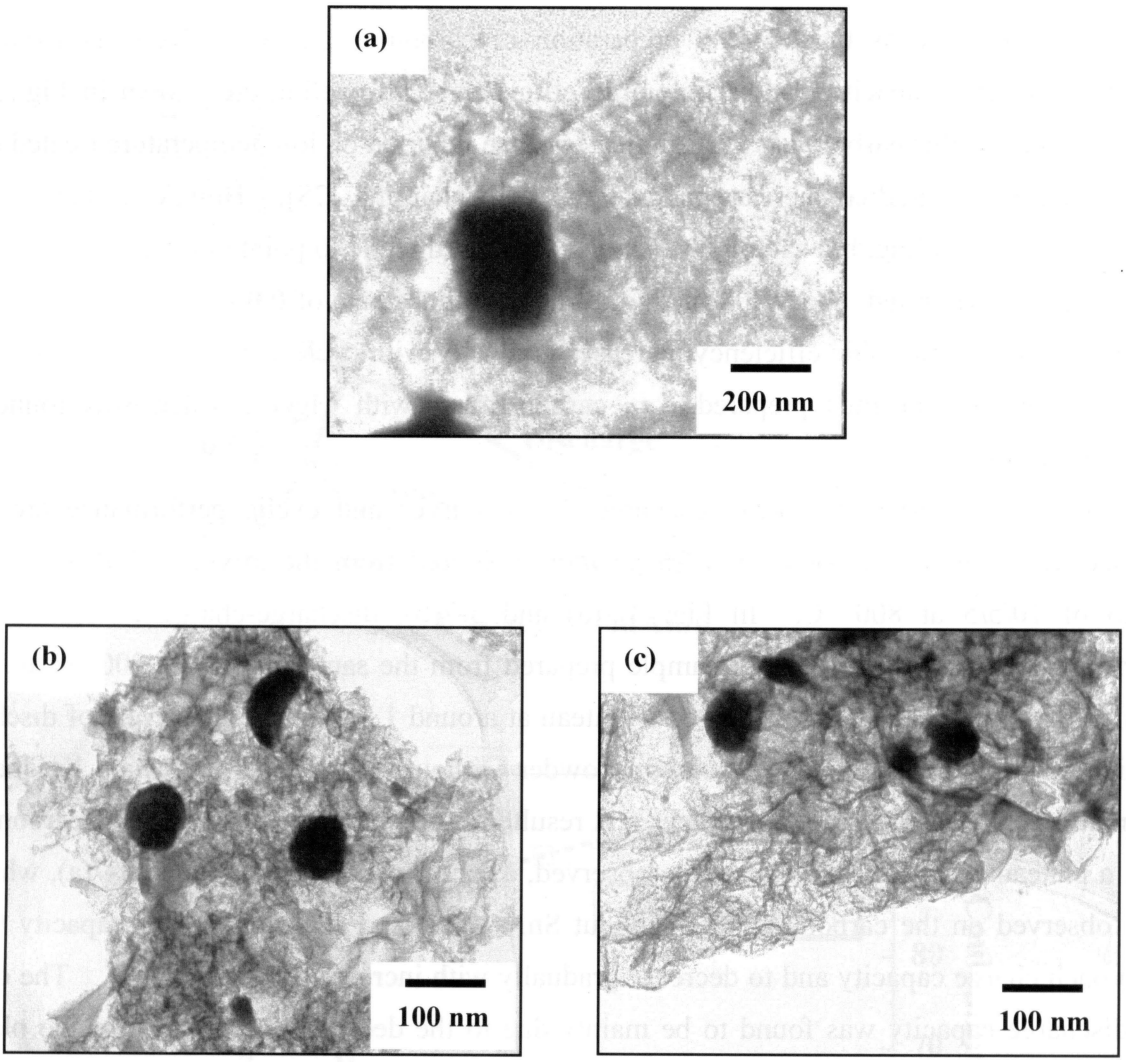

Fig. 3-4 TEM images of carbon-coated metallic Sn particles with mixture of PVA/MgO/SnO_2=10/2/8 (a), 10/5/5(b) and 10/8/2(c).

3-3-2 Anodic performance of carbon-coated Sn powders

In Fig. 3-5(a), discharge-charge curves for 1st and 10th cycles are shown on the carbon prepared from the mixture of PVA with MgO in the ratio of 10/5 at 900 °C, the procedure being exact by the same as that for the preparation of carbon-coated Sn. Cyclic performance in discharge-charge capacities and Coulombic efficiency with cycling are shown in Fig. 3-5 (b). Performance of this carbon was very similar to those reported on low-temperature treated carbons in other reports, gradual increase in potential with charging [28]. However, charge capacity decreases with cycling, but saturates quickly. It is worthwhile to point out that it gives relatively high capacity saturated, about 300 mAh/g in the potential range of 0.0 - 2.0 V, about 200 mAh/g in 0.0-1.0 V. Coulombic efficiency increases gradually with cycle and reaches only about 95 %. The carbon powder thus prepared, *i.e.*, carbonization with MgO powder, was found to be microporous [27].

In Figs. 3-6(a) and 3-6(b), discharge-charge curves and cyclic performance are shown, respectively, for the carbon-coated Sn powders prepared from the mixture of PVA/MgO/SnO_2 ratio of 10/5/5 at 800 °C. In Fig. 3-7(a) and 3-7(b), discharge-charge curves and cyclic performance, respectively, on the sample prepared from the same mixture at 900 °C are shown. All carbon-coated Sn samples showed a plateau at around 1.0 V in the first cycle of discharging, which was also observed on the carbon powder without Sn and was known to be due to the formation of solid/electrolyte interfaces and resulted in irreversible capacity. For carbon-coated Sn, a plateau at around 0.5 V was also observed, as shown in Figs. 3-6(a) and 3-7(a), which was not observed on the carbon samples without Sn. After 2nd cycle, discharge capacity tends to approach charge capacity and to decrease gradually with increasing cycle number. The decrease in discharge capacity was found to be mainly due to the decrease in capacity for the plateau at around 0.5 V, as shown by the charge curves of 1st and 10th cycle in Figs. 3-6(a) and 3-7(a). Coulombic efficiency for two samples of carbon-coated Sn increases rapidly at 2nd cycle and then gradually with increasing cycle number, tending to saturate to about 97 % (Figs. 3-6(a) and 3-7(a)). High irreversible capacity and low Coulombic efficiency at the first discharge-charge cycle on the sample prepared at 800 °C (Fig. 3-6)may be due to small amount of SnO_2 or SnO remained, as shown in Fig. 3-1(b), due to incomplete reduction of SnO_2. The sample prepared at 900 °C had much smaller irreversible capacity than that at 800 °C, about 550 mAh/g for the former and about 1000 mAh/g for the latter (Figs. 3-7(b) and 3-6(b)).

The comparison among the discharge-charge performances between carbon and carbon-coated Sn powders prepared in the same procedure shows that the carbon-coated Sn gives higher capacity saturated, though it takes more cycling to reach the saturation; about 500 mAh/g for carbon-coated Sn with the total Sn content of 75 mass%, but about 300 mAh/g for the carbon

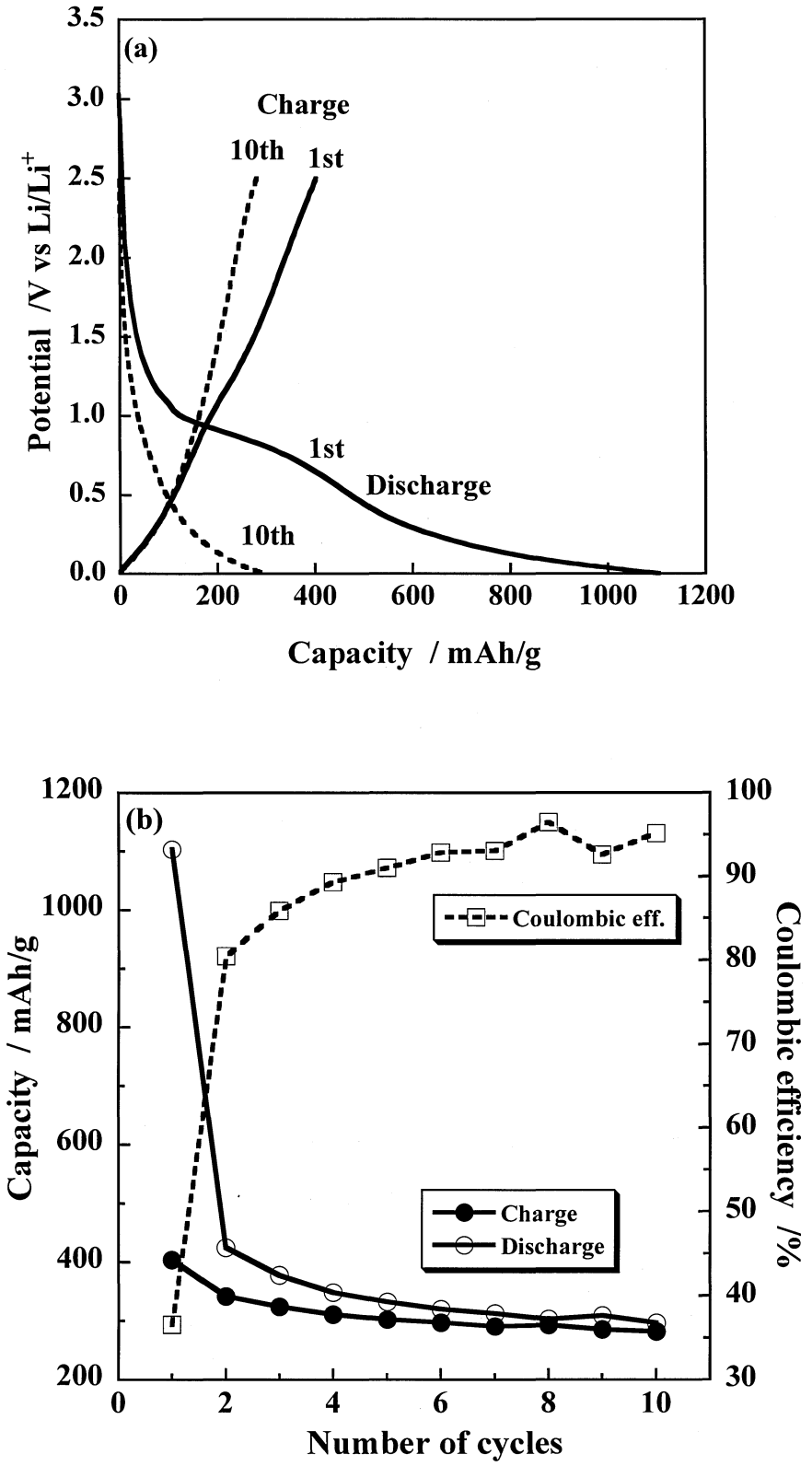

Fig. 3-5 Discharge and charge curves (a) and cyclic performance (b) for the carbon powder prepared from the mixture of PVA/MgO in 10/5 mass ratio at 900 °C.

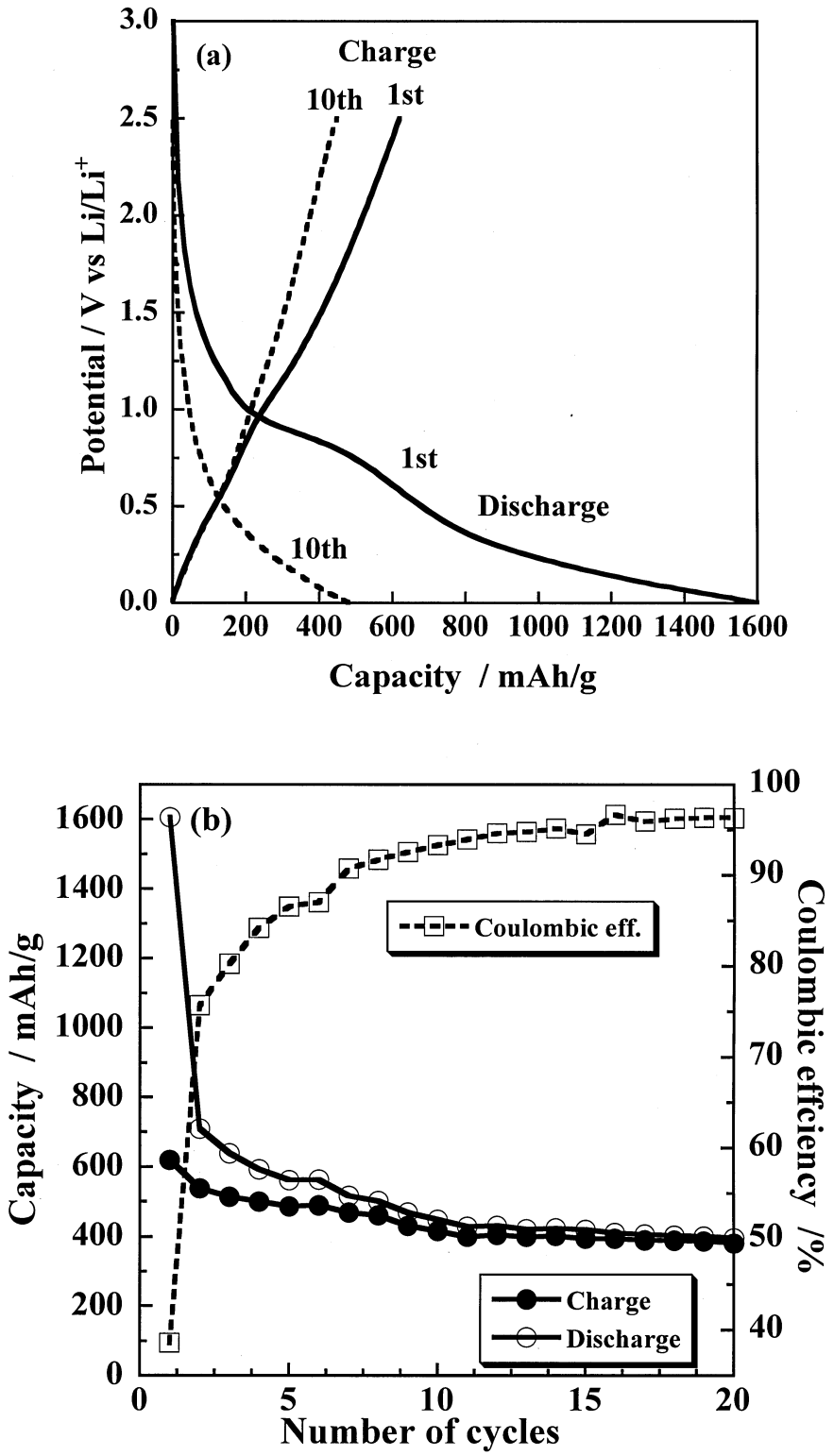

Fig. 3-6 Discharge and charge curves (a) and cyclic performance (b) for the powder of carbon-coated Sn prepared from the mixture of PVA/MgO/SnO_2 in 10/5/5 mass ratio at 800 °C.

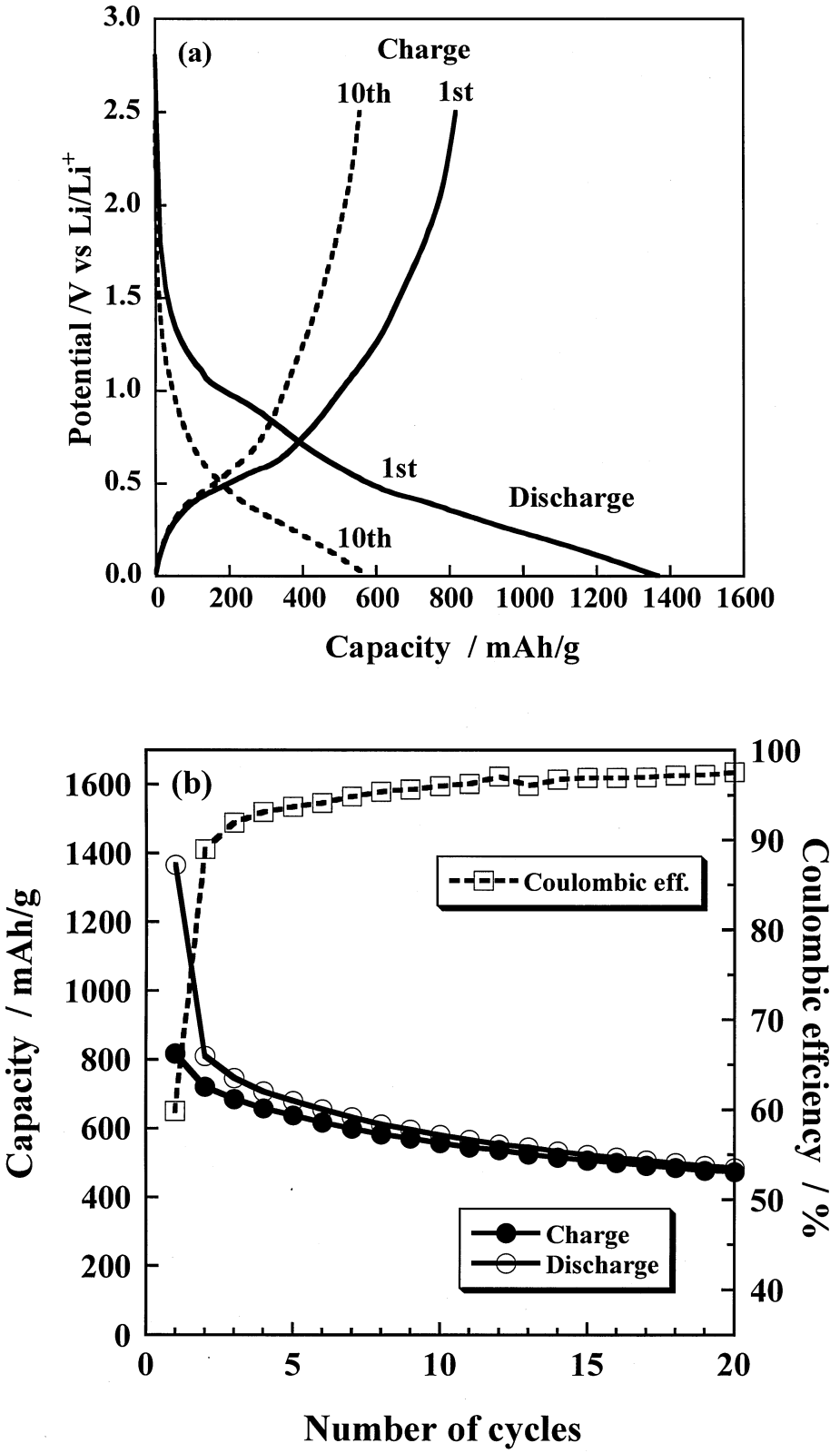

Fig.3-7 Discharge and charge curves (a) and cyclic performance (b) for the powder of carbon-coated Sn prepared from the mixture of PVA/MgO/SnO_2 in 10/5/5 mass ratio at 900 °C.

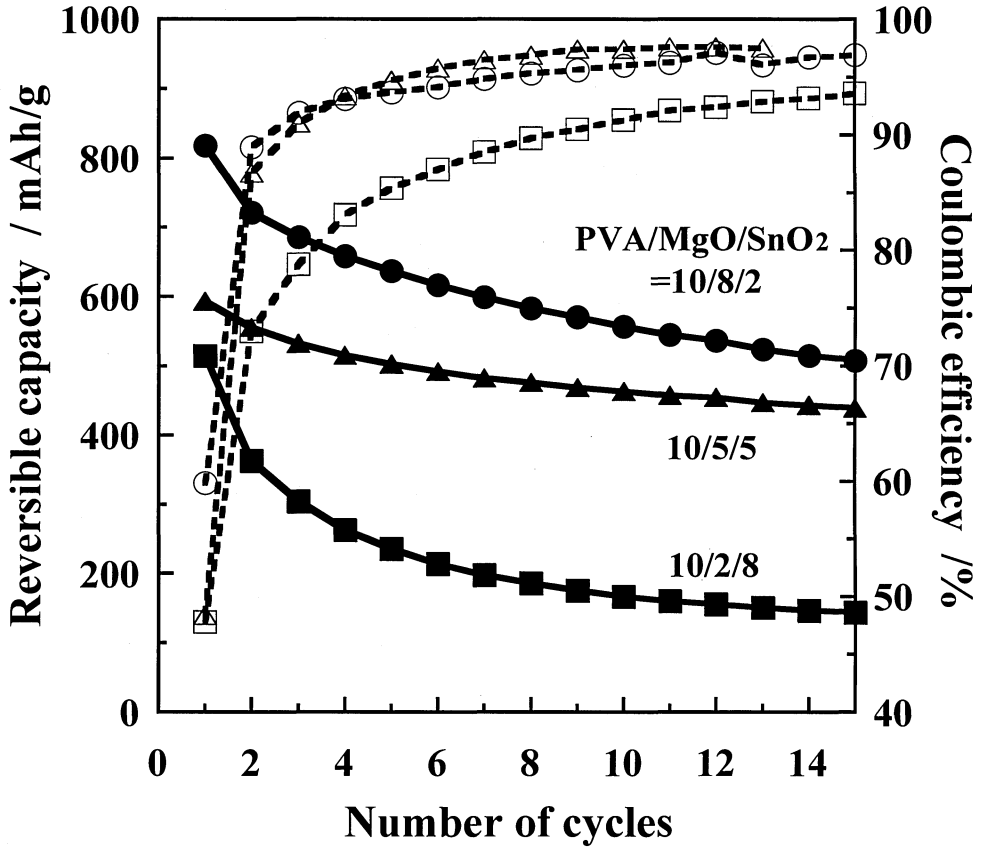

Fig. 3-8 Changes of charge capacity and Coulombic efficiency with cycling for the carbon powders prepared from the mixture of PVA/MgO/SnO in 10/2/8, 10/5/5 and 10/8/2 mass ratio at 900 °C.

without Sn. It has to be pointed out here that the cyclic performance observed on the present carbon-coated Sn powders did not show any marked degradation, as reported in tin metal anode [14]. This high performance of carbon-coated Sn powders was supposed to be due to the presence of open spaces neighboring to metallic Sn in carbon shell, which was formed by dissolving out of MgO particles. These spaces are assumed to absorb a large volume expansion due to alloying of Li into Sn metal during discharging.

In Fig. 3-8, cyclic performance is shown for the carbon-coated Sn powders prepared from the mixtures of three different PVA/MgO/SnO ratios, of which XRD patterns and TEM images of tin particles were shown in Figs. 3-3 and 3-4, respectively. This result shows that it is important to disperse fine particles of metallic Sn to get high capacity and high Coulombic efficiency, the sample prepared with PVAMgO/SnO_2 of 10/2/8 giving much small capacity and Coulombic efficiency than that with 10/8/2. The sample prepared with PVA/MgO/SnO_2 of 10/5/5 has a little smaller capacity but more stable with cycling and a little higher Coulombic efficiency than that with 10/8/2.

3-3-3 Graphite flakes loaded by carbon-coated Sn powders

Loading of carbon-coated Sn onto graphite flakes (carbon-coated Sn/graphite) was performed by heating the powder mixtures of PVA, MgO, SnO_2 and natural graphite in the mixing ratio of 10/7/2/1 in mass. XRD pattern and its SEM image of the powder obtained after heat treatment at 900 ^{o}C and then dissolving out of MgO are shown in Fig. 3-9(a) and 3-9(b), respectively. In XRD pattern, diffraction peaks for metallic Sn are observed, though very weak, because 002 peak for graphite is so strong. SEM image, however, proves clearly the coexistence of carbon-coated Sn with graphite flakes.

In Figs.3-10(a) and 3-10(b), discharge-charge curves and cyclic performance, respectively, are compared for graphite with and without loading of carbon-coated Sn. On carbon-coated Sn/graphite sample, faint plateau at around 0.5 V is seen, in addition to the plateau at around 0.2 V due to graphite flakes. Although carbon-coated Sn/graphite gives Coulombic efficiency less than graphite, it gives about 1.5 times larger capacity than graphite. This proves that carbon-coated fine particles of metallic Sn have certain contribution to the increase in capacity.

3-4 Summary

Carbon-coated Sn powders were successfully prepared from the powder mixtures of thermoplastic precursor PVA, SnO_2 and MgO. The presence of MgO particles was found to be effective to avoid the agglomeration of molten Sn metal at high temperatures and also to leave open spaces neighboring to Sn metal particles in carbon shell which could absorb a large volume

expansion due to alloying of Li. Therefore, a high charge capacity and high discharge-charge cyclicability were successfully added to carbon electrode. The carbon-coated Sn was demonstrated to be able to load onto graphite flakes through a simple process; mechanical mixing of PVA, MgO and SnO_2 with graphite flakes, heating in inert atmosphere at 900 ^{o}C and then washing out of MgO using 1M HCl. The composites of carbon-coated Sn/graphite gave high discharge capacity and stable cyclic performance.

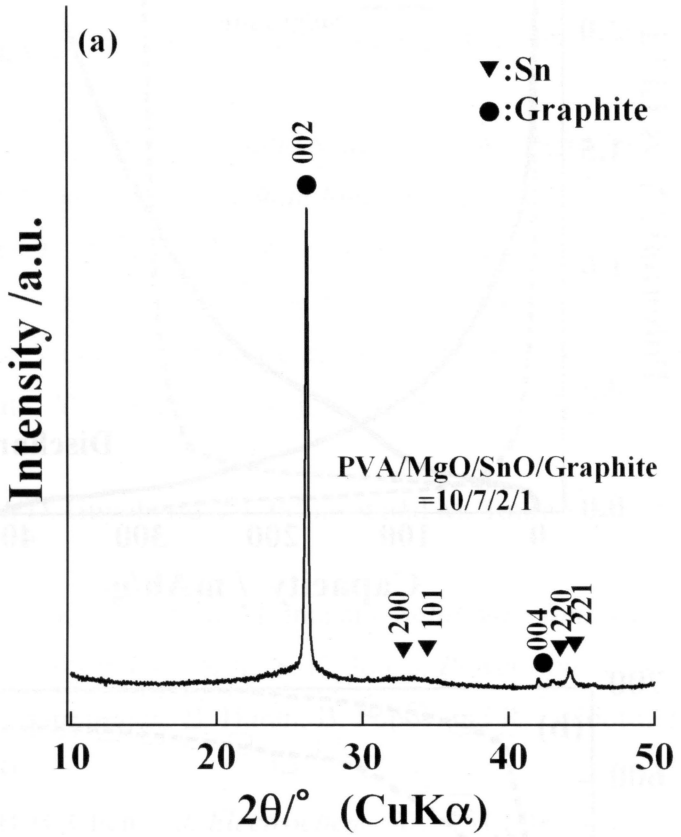

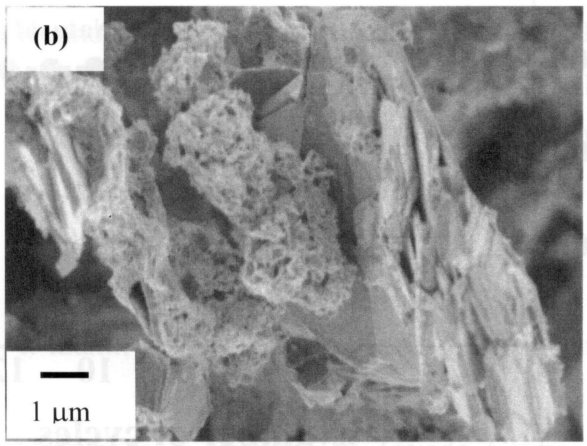

Fig. 3-9 XRD patter (a) and SEM image (b) of graphite loaded by carbon-coated Sn.

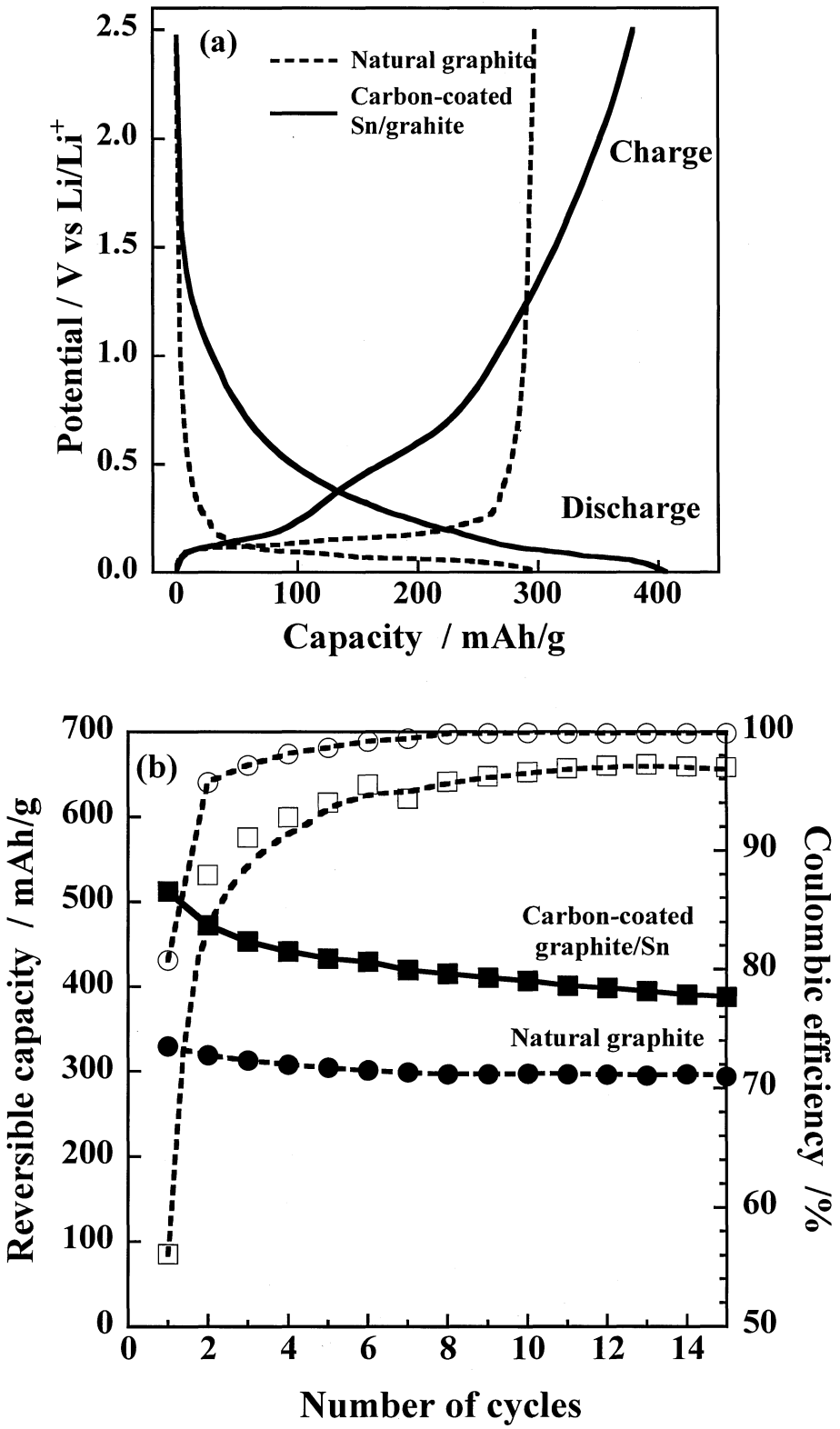

Fig. 3-10 Discharge and charge curves (a) and cyclic performance (b) for graphite with and without loading of carbon-coated Sn.

References

1. T. Ohzuku, A. Ueda, M. Nagayama, Y. Iwakoshi and H. Komori, *Electrochim. Acta* 38 (1993) 1159-1167.
2. K. Sawai, A. Ueda, M. Nagayama, Y. Iwakoshi and H. Komori, *Denki Kagaku* 61 (1993) 715-721.
3. T. Tsumura, A Simizu and M. Inagaki, *Solid State Ionics* 90 (1996) 197-200.
4. J. M. Taraswn and D. Guyomard, *Solid State Ionics* 69 (1994) 293-305.
5. J. R. Dahn, A. K. Sleegh, H. Shi, B. M. Way, W, J, Weydanz, J.N. Reimers, Q, Zhong, U. von Sacken, Lithium Batteries, G. Pistoia, *editor, Elsevier* (1993) 1-48.
6. H. Buqa, P. Golob, M. Winter, and J. O. Besenhard, *J. Power Sources* 97-98 (2001) 122
7. T. Takeda, R.Takahata, Y. J. Kim, K. Koshiba, K. Ishii, T. Kasai and M. Endo. *Tanso* 196 (2001) 14-20.
8 Y. Piffard, F. Leroux, D. Guyomard, J-L. Mansot and M. Tournoux, *J. Power Sources* **68** (1997) 698-703.
9 T. Morishita, K. Nomura, T. Inamasu, M. Inagaki, *Solid State Ionics* 176 (2005) 2235-2341
10 H. Jung, M. Park, Y-G. Yoon, G-B. Kim, S. K. Joo, *J. Power Sources* 115 (2003) 346-351.
11 B. Veeraraghevan, A. Durairajan, B. Haran, B. Popov and R. Guidotti, *J. Electrochem. Soc.* 149 (2002) A675-681
12 Y. Wang, J. Y. Lee, B-H. Chen, *J. Electrochem. Soc.* 151 (2004) A563-570
13 A. Ulus, Y. Resenberg, L. Burstein, D. Peled, *J. Electrochem. Soc.* 149 (2002) A635-643
14 A. Sivashanmugam, T. Kumar, N.Renganathan, S. Gopukumar, M. Wohlfathrt-Mehrens, J. Grarche, *J. Power Sources* 144 (2005) 197-203
15 M. Inagaki, H. Miura, H. Konno. *J. Europ. Ceram. Soc.* 18 (1998) 1011-1015.
16 H. Konno, H. Miura, K. Oyamada, M. Inagaki, *ATB Metallurgie.* 37 (1977) 149-152.
17 H. Konno, K. Oyamada, M. Inagaki, *J. Europ. Ceram. Soc.,* 20 (2000) 1391-1396.
18 M. Inagaki, Y. Okada, H. Miura, H. Konno. *Carbon* 37 (1998) 158-161.
19 M. Inagaki, K. Fujita, Y. takeuchi, K. Oshida, H. Iwata, H. Konno, *Carbon* 39 (2001) 921-929
20 T. Tsumura, N. Kojitani, I. Izumi, N. Iwashita, M. Toyoda, M. Inagaki, *J. Mater. Chem.* 12 (2002) 1391-1396.
21 M. Inagaki, Y. Hirose, T. Matsunaga, T. Tsumura, M. Toyoda. *Carbon* 41 (2003) 2619-2624.
22 B. Tryba, A. W. Morawski, T. Tsumura, M. Toyoda, M. Inagaki, *J. Photochem. Photobio. A:Chem.* 167 (2004) 127-135.
23 M. Inagaki, F. Kojin, B. Tryba, M. Toyoda, *Carbon* 43 (2005) 1652-1659.
24 T. Tsumura, Y. Hattori, K. Kaneko, M. Ingaki, M. Toyoda, *Desalination* 169 (2004) 269-275.

25 T. Tsumura, A. Katanosaka, I. Souma, T. Ono, Y. Aihara, J. Kuratomi, M. Inagaki, *Solid State Ionics* 135-137 (2000) 209-213.

26 M.Inagaki, S. Kobayashi, F. Kojin, N. Tanaka, T. Morishita, B. Tryba *Carbon* 42 (2004) 3153-3158.

27 T. Morishita, R. Suzuki, T. Nishikawa, T. Tsumura, M. Inagaki. 219 (2005) *TANSO* 226-231

28 F. Chevallier, S. Gautier, J.P. Salvetat, C. Clinard, J.N. Rouzaud, F. Beguin, E. Frackwiak, *J. Power Sources* 97/98 (2001) 143-145.

Chapter 4

Preparation of porous carbons from thermoplastic precursors without activation process and their performance for electrode materials of electric double layer capacitors

4-1 Intorduction

Various kinds of porous carbon materials are widely produced, and there can be used as adsorbents and catalytst supports, etc. [1]. The application of activated carbon and other carbonaceous materials with a high surface area to the electrode of electric double layer capacitor (EDLC) was recently studied by various authors [1-3].

In order to get a high surface area, activation process of carbon has usually been employed. Through this process various activated carbons have been prepared and various applications have been developed [1,4,5]. So far, activated carbons were produced mostly from thermosetting resins and after carbonization their pore structure was controlled by activation process. When thermoplastic resins are used, it was necessary to perform stabilization in order to change them to be thermosetting, even partly, before carbonization, and then subjected to carbonization and activation.

There have been reported various precursors and processes to prepare porous carbons without any activation process. Microporous and mesoporous carbons were prepared by using various templates, such as zeolites and silicas [6-8]. For these template processes, however, it was pointed out that the template had to be dissolved out by strong acids after carbonization and that large amount of production was not easy, although the pores with a specific size were easily obtained. By deflurorination of poly(tetrafluoroethylene) using alkali metals, mesoporous carbons were prepared [9.10]. Carbonization of organic aerogels was also reported to give mesoporous carbons [11-13].

We were developed a simple process to coat ceramic particles by carbon; the powder mixtures of thermoplastic resin, such as poly(vinyl chloride), poly(vinyl alcohol), etc., and ceramics were heat-treated at a high temperature in an inert atmosphere [14-16]. The carbon layer generated on the surface of a ceramic particle was found to be porous, by using MgO as substrate ceramics and dissolved it out by sulfuric acid [16]. This result suggested us a new

preparation process of porous carbons without any stabilization and activation processes even starting from thermoplastic precursors.

In the present chapter, porous carbons with high surface area were prepared from various combinations of carbon precursors and MgO precursors using two mixing methods, powder mixing and solution one. Pore structure of the carbons thus obtained was studied by N_2 adsorption. The porous carbons thus prepared were applied to the electrode for electric double layer capacitor and their capacitance was discussed in the relation to their pore structure.

4-2 Preparation of porous carbons

4-2-1 Experimental

Magnesium oxide MgO was selected as a substrate because of its chemical and thermal stability, no structural and compositional changes and no reaction with carbon, and easily dissolving to acidic aqueous solutions. As MgO precursors, MgO itself, magnesium acetate $Mg(CH_3COO)_2$, magnesium citrate $Mg_3(C_6H_5O_7)_2$ and magnesium gluconate $Mg(C_{11}H_{22}O_{14})$ were used. MgO powder (reagent grade) had the particle size of about 100 nm and the BET surface area was 3 m^2/g. Latter three precursors were water soluble and were confirmed to give nano-sized particles of MgO through pyrolysis. Carbon precursor used in this study was mostly poly(vinyl alcohol) (PVA), in addition hydroxy propyl cellulose (HPC) and poly(ethylene terephtalate) (PET) being also used. Mixing of two precursors, MgO and carbon precursors, was performed through following two processes, powder mixing and solution one. Two precursors were mixed mechanically in an agate mortar (powder mixing). Aqueous solution of MgO precursors (except MgO itself) was mixed with aqueous solution of carbon precursor of PVA and HPC (10 mass% concentration) in different ratios and then dried at 100 °C in air. Various mixing ratios in MgO precursor/carbon precursor from 2/8 to 8/2, which were calculated on the basis of the mass of MgO expected to be formed from the precursor and carbon precursors themselves. The mixtures thus prepared were heated at a temperature of 900 °C for 1 h in a flow of Ar.

After carbonization at 900 °C, the substrate MgO was dissolved out using 1 mol/L H_2SO_4 and carbon powders were isolated. The carbons obtained thus were characterized by XRD, SEM, TEM and N_2 gas adsorption at 77 K. The content of carbon coated was determined from the ignition loss of the sample by heating at 800 °C for 1 h in air in a thermogravimeter. Adsorption/desorption isotherms of N_2 gas measured at 77 K on the carbons isolated from MgO were analyzed by using different methods, BET, α_s and BJH, to obtain pore structure parameters.

4-2-2 Results

a) Carbonization process

Carbon coating on MgO was successfully carried out using carbon precursors of PVA, HPC and PET, because they are thermoplastic. The carbon-coated MgO was obtained as a powder with small size and perfectly black, white particles of MgO being not observed even under high magnification optical microscope.

Fig. 4-1 shows TG curves observed in Ar atmosphere for the mixtures of MgO and Mg acetate with PVA prepared by either powder mixing or solution one. Since MgO does not have any changes in mass and structure before 1000 °C, the changes in TG curve is due to PVA. Since plasticized PVA wetted to MgO and formed thin films on MgO particles, the evolution of decomposition gases from PVA occurred rapidly. In the case where MgO was used, plasticized PVA decomposed more quickly at a little lower temperature than PVA itself and then remaining parts of PVA pyrolyzed. In the case of the mixture of two precursors in solution, PVA was decomposed slightly faster than pure PVA. Magnesium acetate was pyrolyzed to give MgO before reaching 250 °C, which was confirmed by XRD on quenched sample from 250 °C, and formed nano-sized particles of MgO, as shown in Fig. 4-2(c) as TEM image. Since the pyrolysis of PVA occurs after the decomposition of Mg acetate, MgO particles were covered by plasticized PVA and their grain growth was inhibited. Above 500 °C, slight weight loss was observed in all cases, where carbonization proceeded. Plastic flow of plasticized PVA was strongly disturbed on MgO particles, and so PVA was carbonized as thin layer, evolving decomposition gases quickly.

In Fig. 4-2(a) and (b), TEM images are shown for the starting particles of MgO and after carbon-coating, respectively. Even after 900 °C treatment for carbon coating, MgO particles keep their sizes as the starting, about 100 nm. No grain growth was observed, which is reasonably supposed to be due to the fact that all MgO particles are covered by carbon. MgO particles formed from Mg acetate were very small sizes as about 5 nm even after 900 °C treatment, as shown in Fig. 4-2(c). Also from Mg citrate, nano-sized MgO particles were formed.

In Fig. 4-3, carbon yield in the mixtures with MgO powder was plotted against mixing ratio of MgO/carbon precursor for three different carbon precursors. Carbon yield depends strongly on precursors, as large as about 27 % in PET and about 8 % in PVA and HPC, but not on mixing ratio to MgO. Carbon yield of PVA, HPC and PET without mixing with MgO were 1, 2, and 8 mass%, respectively. Since the plastic flow of these thermoplastic precursors is strongly hindered by the presence of MgO particles, as discussed above, relatively high carbon yield, much higher than their carbonization without any constraint, is supposed to be obtained.

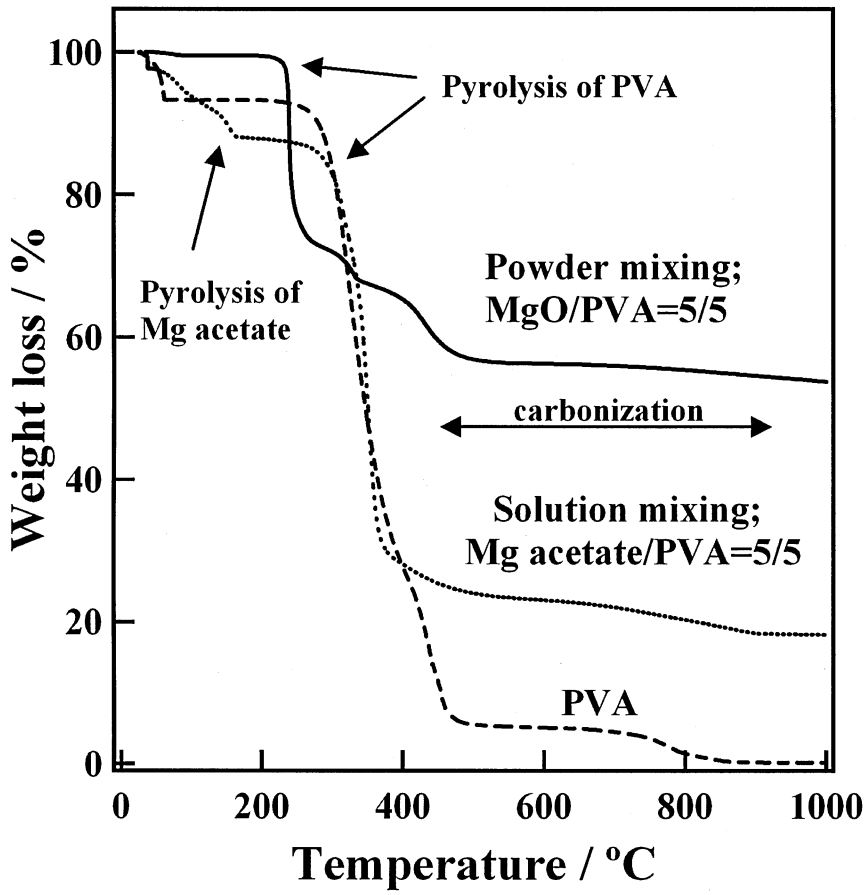

Fig. 4-1Thermogravimetric curves on the mixtures of MgO and Mg acetate with PVA in comparison with PVA itself.

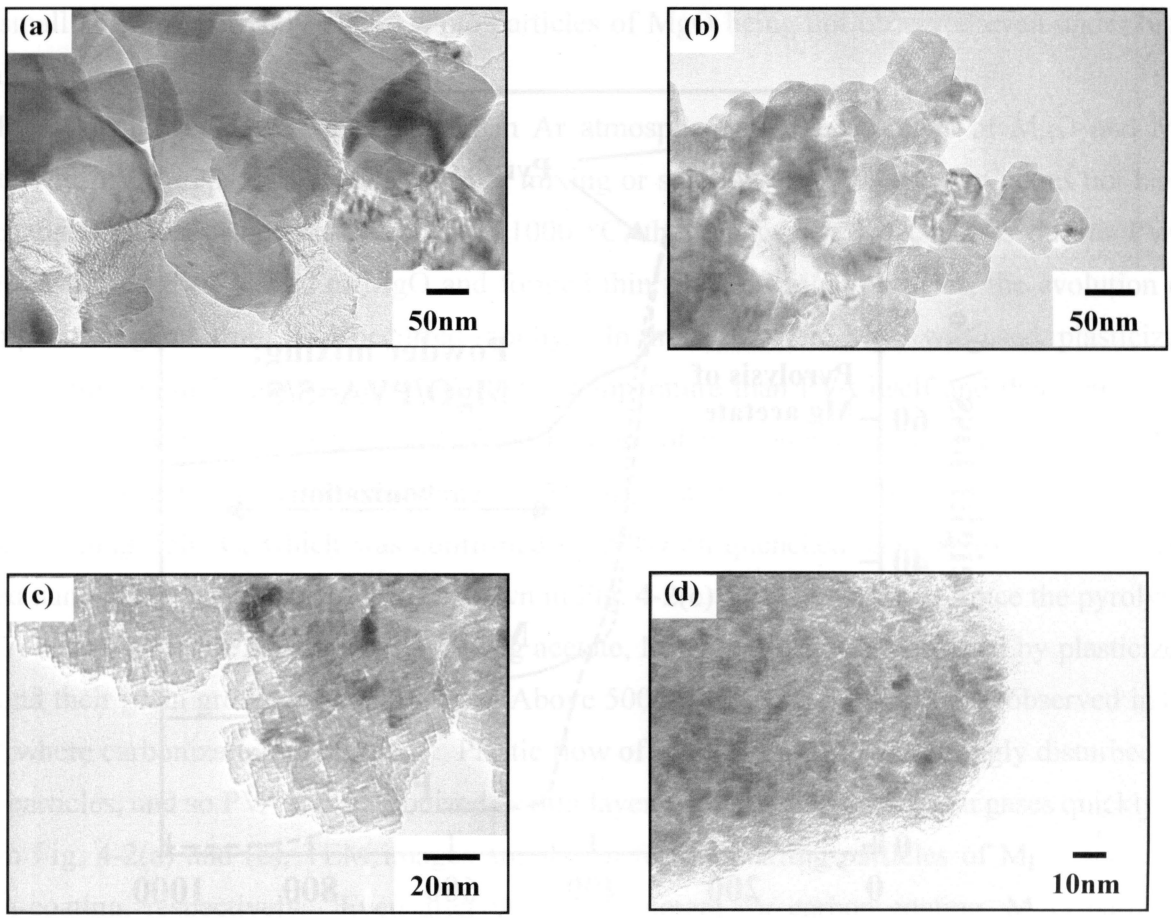

Fig. 4-2 TEM images of carbon-coated MgO particles derived from (a) MgO/PVA powder mixture, (b) Mg acetate/PVA powder mixture, (c) Mg acetate/PVA solution mixture, (d) Mg citrate/PVA powder mixture.

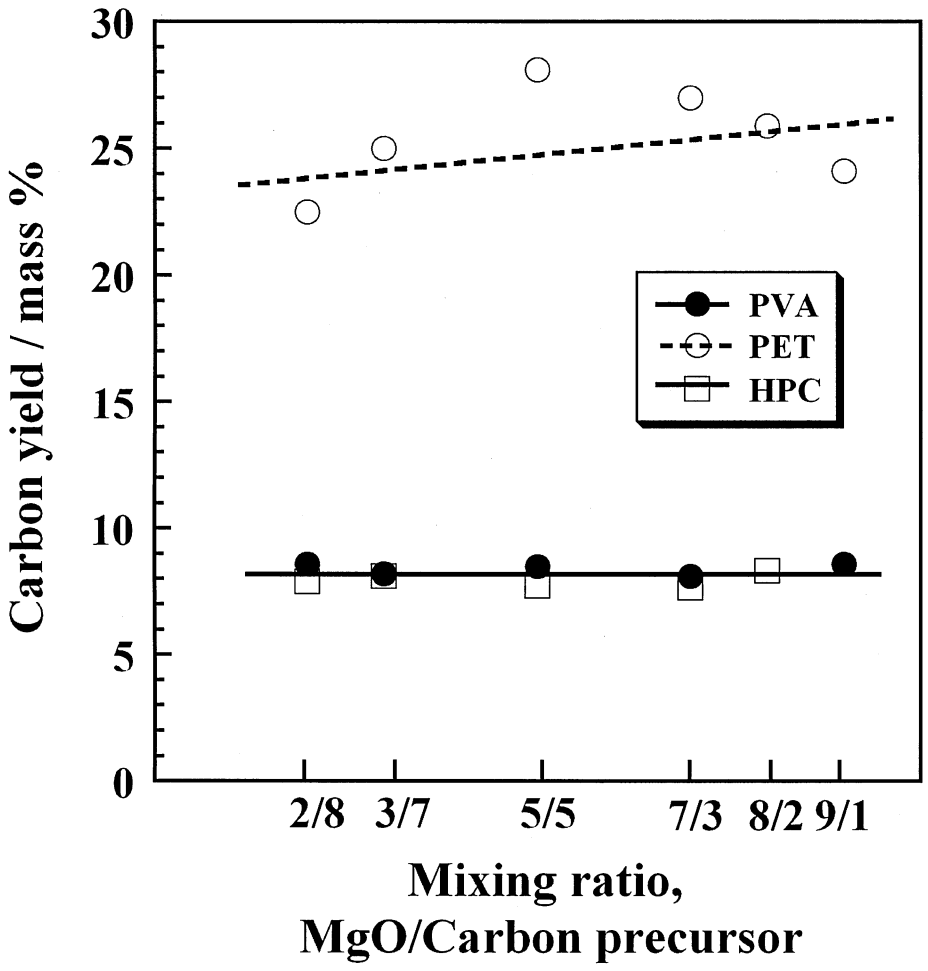

Fig. 4-3 Carbon yield in the mixtures with MgO powder was plotted against mixing ratio MgO/carbon precursor for three different carbon precursors

b) Pore structure

In Fig. 4-4(a), BET surface area is plotted against mixing ratio of MgO/carbon precursor for the carbons obtained from the mixtures of MgO with PVA, HPC and PET by powder mixing and dissolving out of MgO. BET surface area also depends strongly on carbon precursor and its mixing ratio with MgO. PVA and HPC show similar dependences on mixing ratio to MgO, showing a maximum at the ratio of 7/3, but the former gives much higher surface area than the latter. PET shows an increase in BET surface area with increasing mixing ratio, *i.e.*, decreasing the amount of PET to MgO. By taking into account of the fact that PET has higher carbon yield than PVA and HPC (Fig. 4-3), there is the most suitable mixing ratio of carbon precursors to MgO in order to get high surface area, for example 7/3 in the case of PVA.

In Fig. 4-4(b), the same plots are shown for the mixture of the Mg acetate with PVA prepared by powder and solution mixing. By changing from MgO with the particle size of about 100 nm to Mg acetate, BET surface area of the carbon obtained becomes much larger, particularly with solution mixing.

In Table 4-1, pore parameters obtained by α_s plot are summarized, where BET surface area is listed in order to show that it is corresponding to total surface area obtained by α_s plot, even though it is shown in Fig. 4-4. When PVA was used as carbon precursor with MgO (powder mixing), a large part of surface area was due to micropores, relatively larger micropore volume being obtained. When started the powder mixture of either HPC and PET with MgO, on the other hand, the carbons obtained gave relatively high external surface area, which was mainly due to the formation of mesopores. When Mg acetate was used with PVA in powder mixing, the resultant carbons gave higher external surface area than the powder mixture of MgO with PVA, the difference being mainly due to the increase in external surface area. In general, the solution mixing resulted in very high total surface area, much higher than powder mixing, of which the principal part was external surface area, very small microporous surface area.

In Fig. 4-5, the pore size distribution in mesopore region, which is determined by BJH method, is shown on three carbons obtained using different MgO precursors. The powder mixture of MgO and PVA did not give any mesopores, because MgO particles used had the size of about 100 nm, which left the large pores with almost the same size. From the mixture of Mg acetate with PVA prepared through solution mixing, on the other hand, relatively high population of mesopores with the size of 2 ~ 25 nm. The powder mixture of Mg citrate with PVA gave very sharp peak around 5 nm, because of the formation of very small particles of MgO from Mg citrate after pyrolysis.

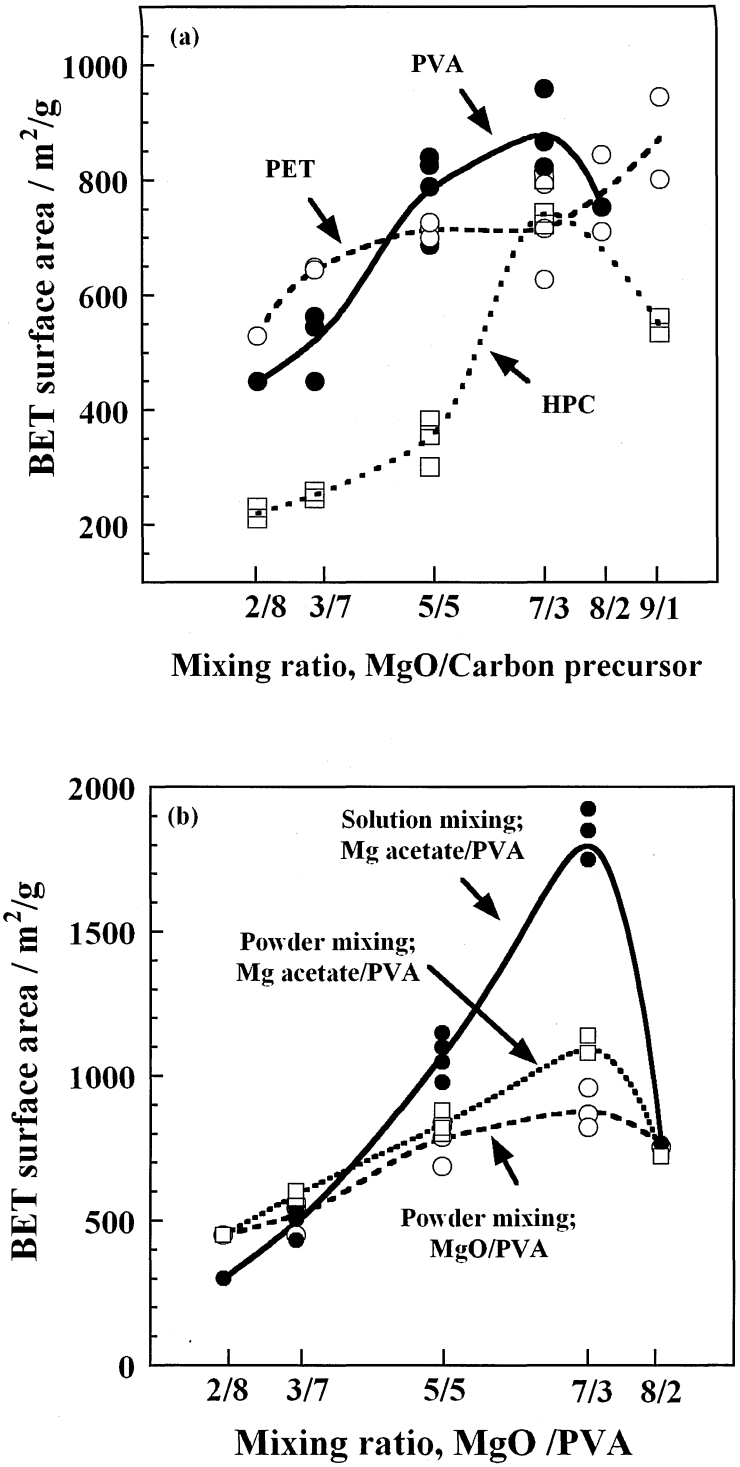

Fig. 4-4 Changes in BET surface area with mixing ratio on (a) powder mixtures of MgO with various carbon precursor and (b) different mixing method of Mg acetate or MgO with PVA.

Table 4-1 Pore parameters determined by BET and α_s plot on carbons prepared.

Mixing method	Mixing ratio	S_{BET} / m^2/g	α_s analysis			
			S_{total} / m^2/g	$S_{ext.}$ / m^2/g	S_{micro} / m^2/g	Micropore Volume / mL/g
Powder mixing	MgO/PVA=7/3	920	959	137	880	0.34
	MgO/HPC=7/3	741	723	621	102	0.06
	MgO/PET=9/1	940	936	894	42	0.01
	Mg acetate /PVA=7/3	1080	961	510	451	0.14
Solution mixing	Mg acetate /PVA=7/3	1800	1788	1701	87	0.10
	Mg acetate /PVA=5/5	980	966	901	65	0.04
	Mg acetate /PVA=2/8	289	312	286	26	0.01

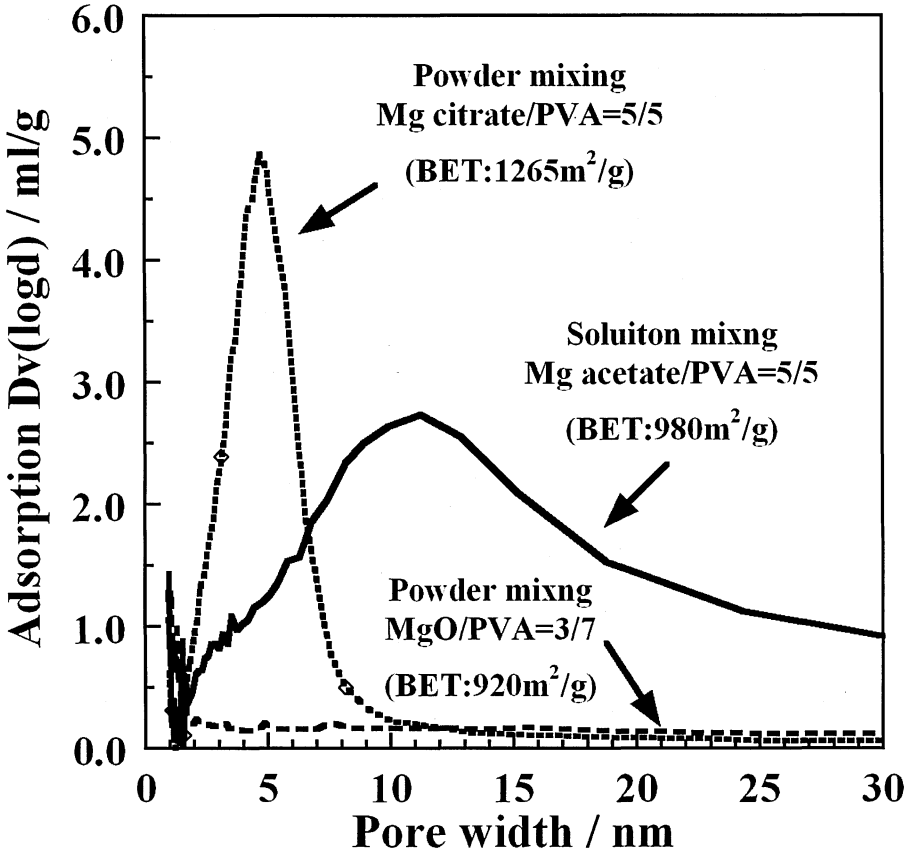

Fig. 4-5 Mesopore size distributions of different mixing methods of Mg acetate or MgO with PVA

A marked increase in mesopores volume when Mg precursors were used was found to be due to the formation of nano-sized MgO particles from the precursors. In Fig. 4-6(a) and (b), TEM and FE-SEM of the carbons obtained are shown, respectively. The size of MgO particles observed under TEM is almost the same as the pores observed under FE-SEM after dissolving out of MgO, in other words, nano-sized MgO left the pores with almost the same size in the carbon after its dissolution.

In conclusion, BET surface area of the carbons obtained through powder mixing, reaching to a very high value as 1000 m^2/g, even though any activation process was not applied. By mixing carbon precursor with MgO precursor through their solutions, much higher BET surface area and total surface area could be obtained, reaching to 1900 m^2/g. Main part of total surface area was due to external surface area, to which mesopores with almost the same size of the substrate MgO were responsible.

c) Estimation of BET surface area of carbon layer coated

Carbonization products of the mixtures of carbon precursors and ceramics powders, including the precursors for ceramics such as Mg acetate, were carbon-coated ceramic powders, i.e., composites of ceramic particles with carbon. In most cases, substrate ceramics were difficult to be dissolved out, but we would like to discuss about porosity of carbon layer coated on ceramic particles. Therefore, BET surface area of carbon layer was estimated from the apparent BET surface area measured and carbon content on the composite by assuming zero surface area for the substrate ceramics [16-18].

In the present work, carbons coated could be isolated from the substrate MgO and their pore structure was studied in detail. Therefore, BET surface area calculated from apparent BET surface area measured on carbon-coated MgO and its carbon content, $S_{calc.}$, under the assumption of zero surface area of MgO substrate was compared with BET surface area measured on carbon isolated from MgO by dissolution, $S_{dis.}$, in Fig. 4-7. Relatively good coincidence between $S_{calc.}$ and $S_{dis.}$ suggesting that, the estimation of BET surface area from apparent one measured on carbon-coated ceramics is valuable. On high surface area regions, the values of $S_{calc.}$ were slightly smaller than $S_{dis.}$, which is supposed to be due to the contribution of relatively larger mesopores and macrospores.

The corresponding between carbon content measured by burning off, $C_{burn.}$, and the amount of carbon recovered by dissolution of MgO, $C_{dis.}$, was also discussed, on the carbon-coated MgO prepared by using different carbon precursor in Fig. 4-8. Two values, $C_{burn.}$ and $C_{dis.}$, show a good coincidence, which indicates that the carbon coated on MgO is recovered almost 100 % by dissolution of MgO using diluted acid.

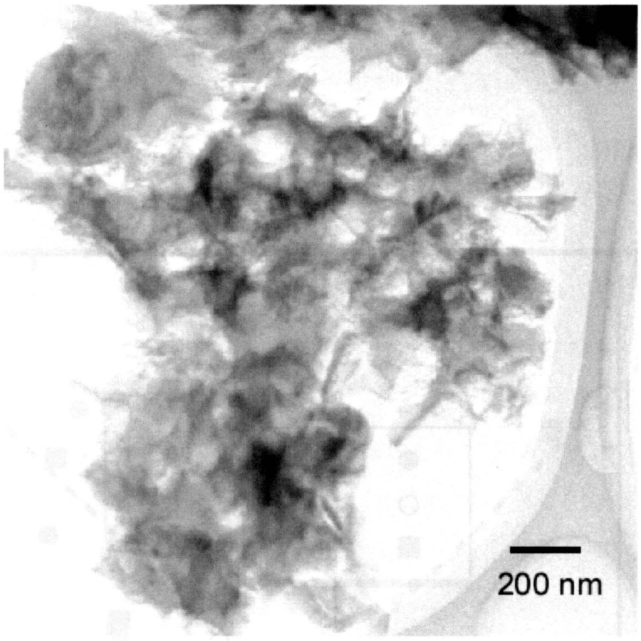

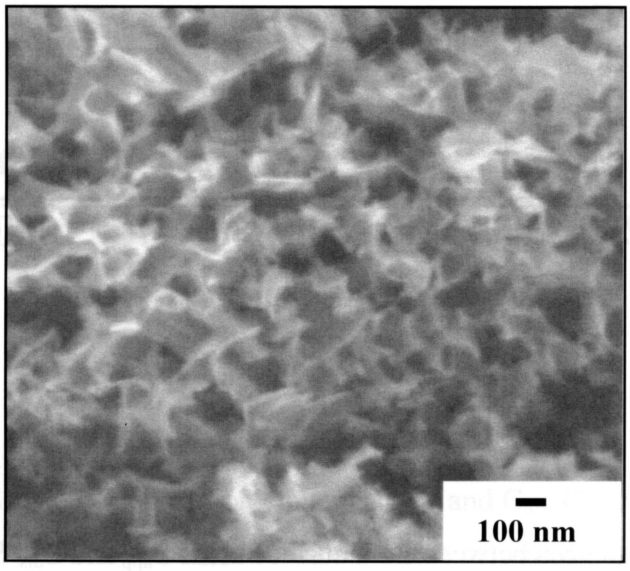

Fig. 4-6 TEM and FE-SEM images of the carbon obtained from powder mixture of MgO with PVA in the ratio of 5/5.

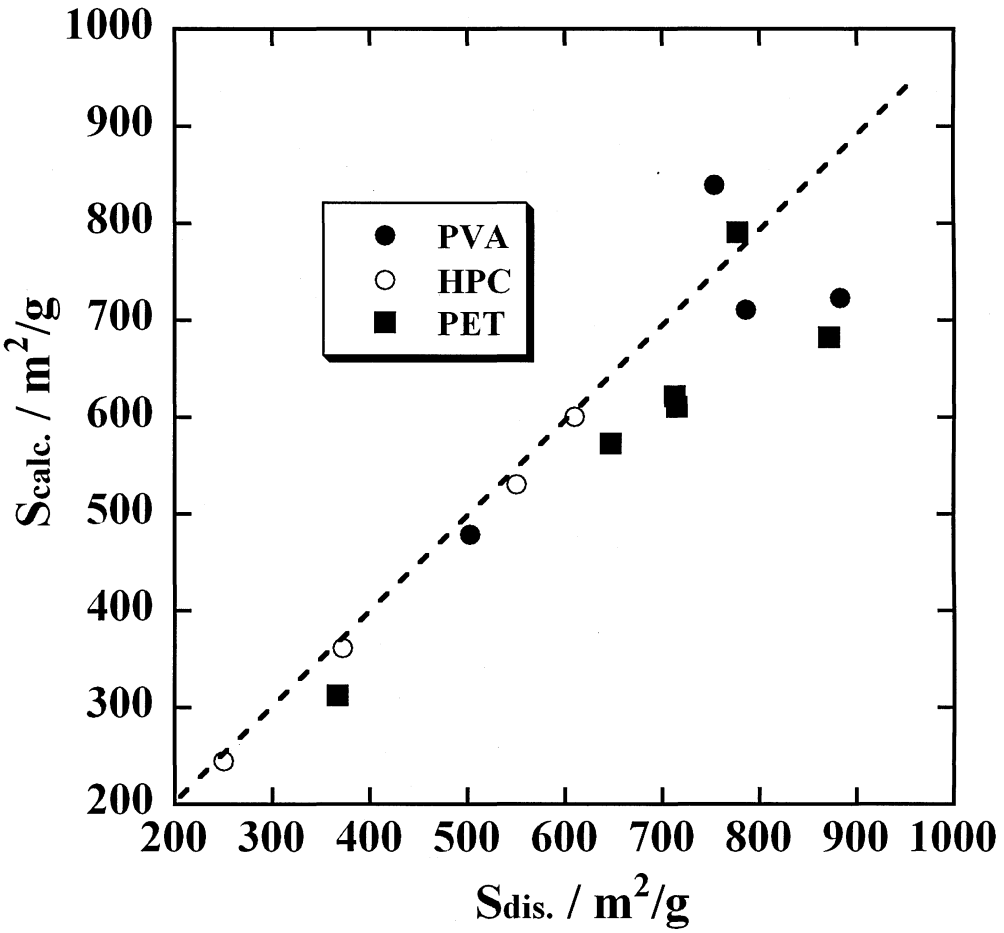

Fig. 4-7 Correspondences between BET surface areas $S_{app.}$and $S_{dis.}$ $S_{calc.}$: BET surface area calculated from apparent BET surface area $S_{app.}$ measured on carbon-coated MgO and C_{burn}, and $S_{dis.}$: BET surface area measured on carbon separated by MgO dissolution.

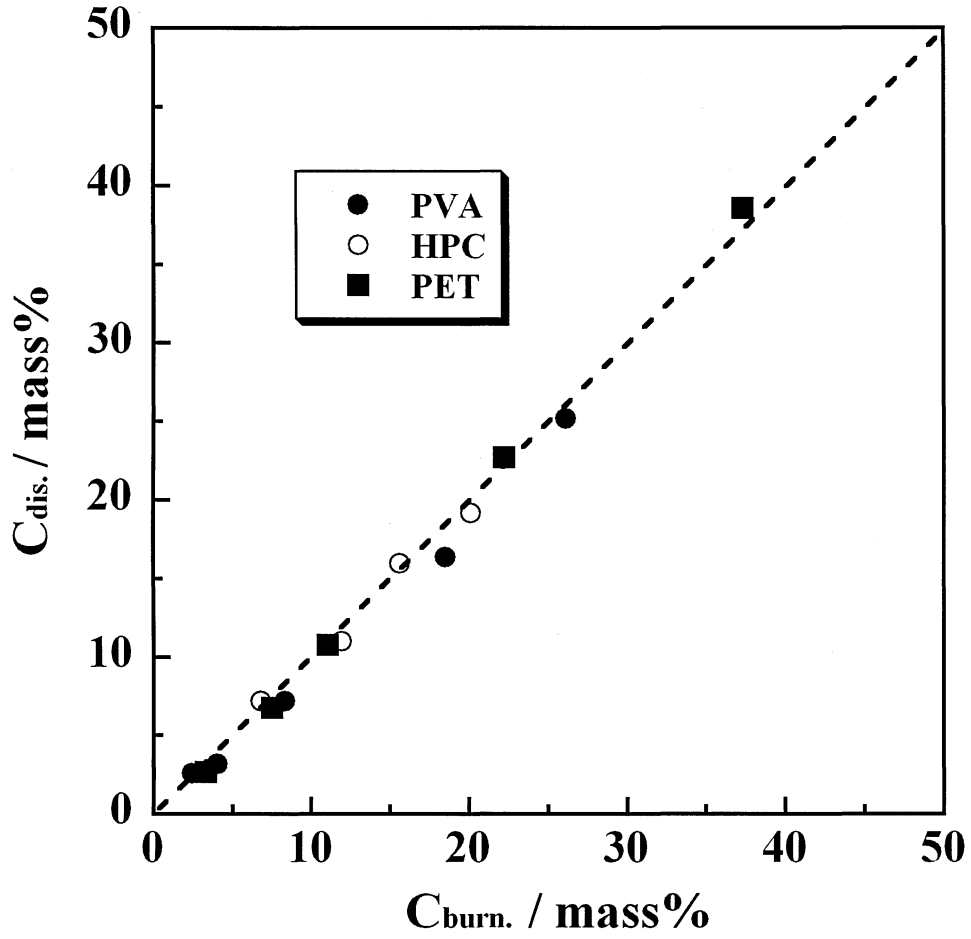

Fig. 4-8 Correspondences between carbon contents C_{burn} and $C_{dis.}$ C_{burn}: Carbon content determined by burning at 900 °C in air, $C_{dis.}$: Carbon content by dissolving MgO with 1 mol/L sulfuric acid.

4-3 Electrode performance for porous carbon synthesized

4-3-1 Experimental

For the determination of the performance of electric double layer capacitor (EDLC) for the carbons obtained, the electrode was prepared by mixing the carbon powders with acetylene black as an electrical conductor and PTFE as a binder in a mass ratio of 80:10:10, which were blended to be homogeneous by using n-methyl-2-pyrolydone as solvent. The mixture was pressed to get the films in approximate thickness of about 100 μm and then dried at 100 °C for 1 h under vacuum. Three-electrodes test cell was used with 1 mol/L H_2SO_4 as electrolyte, Ag^+/AgCl as a reference electrode and a platinum plate as a counter electrode. In Fig. 4-8, the construction of capacitor cell were illustrated. For these sample electrodes the measurement of cyclic voltamogram with a scanning rate of 1 mV/sec and the charge-discharge measurement with the potential window from 0.0 to 1.0 V were carried out at room temperature. The capacitance of the sample electrode was calculated from charge-discharge curves. The current density employed for the measurement of capacitance was 20 ~ 1000 mA/g.

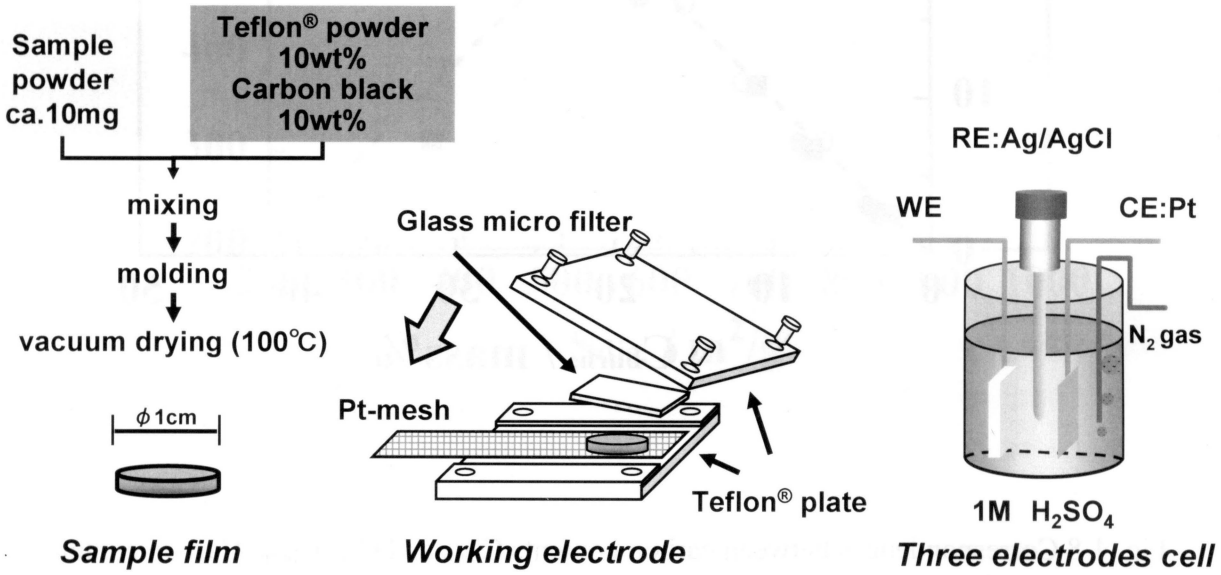

Fig. 4-9 Experimental of electrochemical measurement

4-3-2 Results

a) Electrode performance

In Fig. 4-10, CV curves observed on the carbons prepared by different mixing methods and different MgO precursors are shown. All carbon powders show box-shaped curves, that is, behavior of electric double layer construction and destruction on the carbon surface. Carbon powders prepared by solution mixing seem to give larger EDLC capacitance than those by powder mixing.

In Table 4-2, EDLC capacitances with the charging rates of 20 and 1000 mA/g together with microporous and mesoporous surface areas determined by BJH method are listed on the samples prepared. Carbon powders obtained showed relatively high EDLC capacitance, in comparison with the values reported on various activated carbons with high BET surface area. In either powder or solution mixing methods, carbon powders prepared from Mg acetate/PVA=7/3 mixture were maximum surface area and also maximum capacitance at 20 mA/g.

For the carbons prepared by two mixing methods, the dependence of EDLC capacitance on current density was shown in Fig. 4-11. Although carbon powders prepared by powder mixing gave high surface area and relatively large capacitance at small current density, as well as a commercially available activated carbon with high surface area, but its capacitance markedly decreased at high current density. On the carbon powders prepared by solution mixing, which contained a large amount of mesopores, on the other hand, capacitance at large current density didn't drop down, comparing with those at low current density; for Mg acetate/PVA =2/8, for example, 250 F/g with a current density of 20 mA/g and 210 F/g with 1000 mA/g.

b) Dependence of EDLC capacitance on pore structure

Capacitance in EDLC had been discussed in the relation to surface area, which seemed to be reasonable because of the formation of electric double layers on the surface of carbon electrodes. It was proposed an idea to differentiate the surface due to micropores and other larger pores, such as microporous and external surface areas, which have different contribution to EDLC capacitance [19,20]. Recently, it was pointed out that the contribution of microporous surface area to EDLC capacitance was much smaller than that of external surface area when non-aqueous electrolyte was used and their difference became larger for high rate charging than low one [21]. On the present samples, the same analysis was tried. The results supported this idea, but the difficulty was recognized, at what size of pores we have to differentiate two surfaces, microporous and external surfaces. The carbons obtained, particularly through solution mixing, were very high content of mesopres and only small amount of micropores, which gave us a difficulty to analyze α_s plot observed.

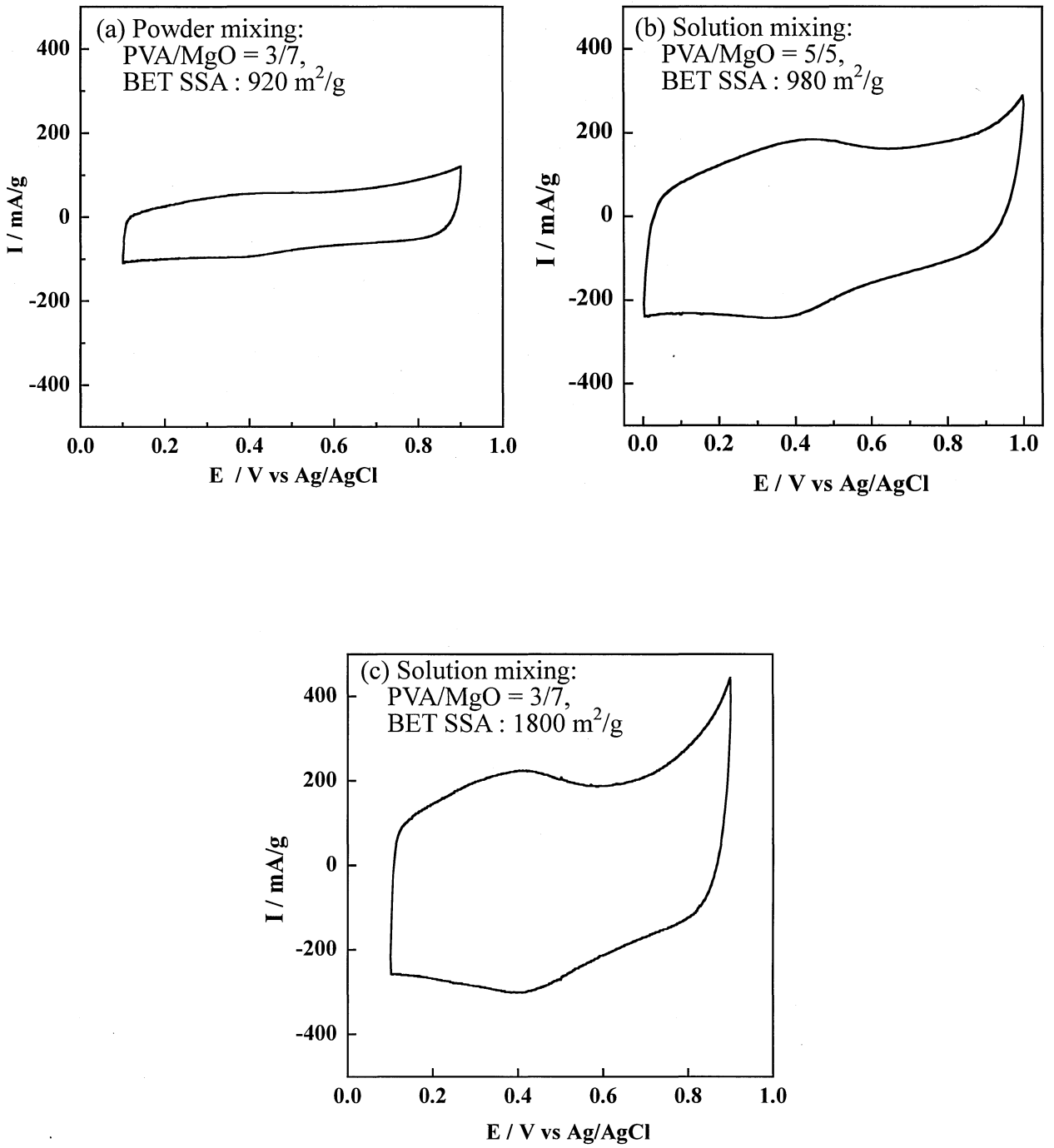

Fig. 4-10 Cyclic voltammogram curves of carbon obtained by different mixing method of Mg acetate or MgO with PVA

Table 4-2 EDLC capacitances at different charging rates and rate performance for the carbons obtained.

Mixing method	Mixing ratio	Pore volume / ml/g		S_{meso}/S_{total}	Capacitance / F/g		Rate performance
		micro	meso		20 mA/g	1000 mA/g	1000 mAg^{-1} /20mAg^{-1}
Powder mixing	MgO/PVA=7/3	0.22	0.11	0.17	151	34	22.5%
	MgO/PVA=2/8	0.11	0.13	0.21	65	28	43.1%
	Mg acetate /PVA=7/3	0.16	0.37	0.65	190	96	50.5%
	Mg citrate /PVA=5/5	0.11	1.60	0.76	296	144	48.6%
	Mg citrate /PVA=7/3	0.14	1.74	0.77	320	154	48.1%
Solution mixing	Mg acetate /PVA=7/3	0.12	2.10	0.78	347	198	57.1%
	Mg acetate /PVA=5/5	0.06	1.66	0.91	251	210	83.7%
	Mg acetate /PVA=2/8	0.01	0.48	0.85	89	68	76.4%

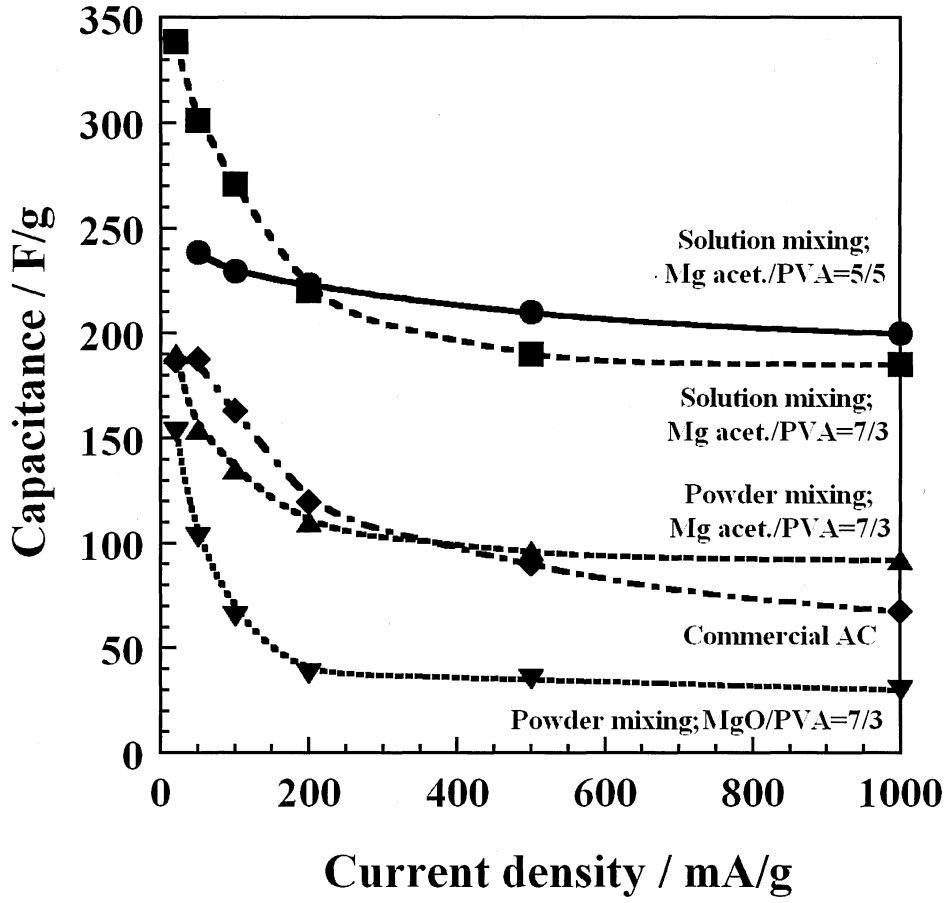

Fig. 4-11 Dependences of EDLC capacitance on current density for the carbons prepared by different mixing methods and a commercially available activated carbon.

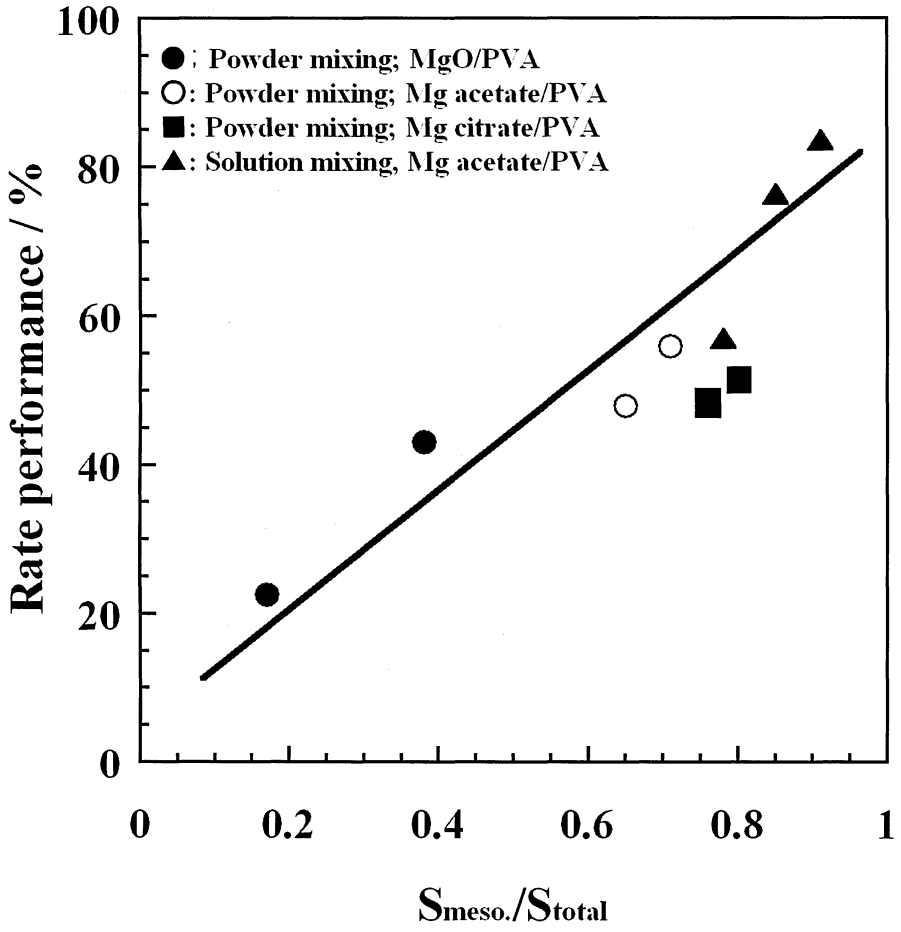

Fig. 4-12Dependence of rate performance $C_{at\ 1000\ mA/g}/C_{at\ 20\ mA/g}$ on mesoporous surface area $S_{meso.}$ relative to total surface area S_{total}.

The excellent rate performance, which was expressed by the ratio of the capacitance at the rate of 1000 mA/g to that at 20 mA/g, was supposed to be due to the high content of mesopores in carbons prepared by solution mixing method. In Fig. 4-12, rate performance showing by how much capacitance can be retained at 1000 mA/g is plotted against relative amount of mesoporous surface area to total surface area. With increasing ratio of mesopore, the parameter for rate performance increases linearly.

4-4 Discussion

4-4-1 Novel process for the preparation of porous carbons

By using thermoplastic resins as the precursors of carbon and magnesium salts, such as acetate, citrate, etc., as the precursors of the substrate ceramics, the powders of porous carbon were obtained, which were covered onto the substrate MgO particles and had very high surface area after the dissolution of the substrate MgO even though they did not pass through stabilization and activation processes.

In Fig. 4-13, 14 and Table 4-3, experimental procedure, BET surface area and yield of carbon obtained on recycling of MgO substrate are shown. It is possible to get carbons having high surface area repeatedly by cycling MgO, where only carbon precursor is supplied.

In Table 4-4, BET surface area was shown when other substrate materials, NaCl, $MgCO_3$, $Mg(OH)_2$ and CaO were used as substrate together with PVA. All substrates are easily removed after the carboniztion of PVA by using either water or diluted acid. Although NaCl with PVA gave very small surface area, relatively high surface area was obtained when $MgCO_3$, $Mg(OH)_2$ and CaO were used with PVA. Pyrolyzed carbonaceous products from thermoplastic resins were supposed to be unable to coat NaCl particles because of their poor compatibility. However, $MgCO_3$ and $Mg(OH)_2$ changed to MgO on the course of heating. These oxides, including CaO seemed to have good affinity with pyrolyzed products from PVA to be covered. This is the reason why the carbons isolated from these oxide substrates are porous. On the other hand, thermosetting resins, such as phenol, can not cover any substrate because they do not pass through fluid state during heat treatment to carbonization and so no porous carbons are obtained.

In Fig. 4-15, an expecting image was shown on carbon coating process on MgO particles and formation of porous carbon after dissolving MgO substrate. So far, the use of thermoplastic resins as carbon precursors was considered to be not suitable for the production of porous carbons, because they changed to viscous products by pyrolysis and shrink during carbonization process as illustrated in the upper part of Fig. 4-14. In the mixtures with ceramic particles, viscous pyrolyzed products from thermoplastic resins can coat ceramic substrate particles to form thin films, of which viscous flow seemed to be restrained on the ceramic particles. As a consequence,

the release of decomposition gases from thermoplastic resins became easier and their carbonization proceeded faster, resulting in the formation of porous carbons. For the ceramic substrate, MgO was particularly recommended because of the easiness of its dissolution.

Inhibition of the growth of MgO particles by carbon coating at high temperatures attributed to the increase in surface area and mesopore volume in the resultant carbons. Most of mesopores formed in the resultant carbons were supposed to be originated from the MgO particles, a good correspondence in size between MgO particles and mesopores formed (Section 4-4-2). The size of MgO particles generated by thermal decomposition of magnesium salts seemed to depend principally on the starting salt, suggesting the possibility to control the size and volume of mesopores by magnesium salts selected.

4-4-2 EDLC performance of porous carbons

Although carbon powders prepared through powder mixing process and possessed a high surface area gave a relatively large capacitance at small current densities as 20 and 50 mA/g, their capacitance decreased markedly at high current density as 1000 mA/g. On the carbon powders prepared through solution mixing process, on the other hand, the capacitance didn't drop down so much by increasing current density, from 50 to 1000 mA/g, as shown in Fig. 4-11.

In Fig. 4-16, an expecting image is illustrated for charge and discharge mechanism of micropore rich and mesopore rich carbons. On the wall of micropores, the formation of electric double layers for electrolyte ions is reasonably supposed to be not so easy, in other words, diffusion of ions into micropores to form electric double layers can not be done fast. Onto the wall of mesopores, on the other hand, electric double layers of electrolyte ions can be formed more quickly and, as a consequence, charge-discharge processes with high rate can be applied without a large loss in capacitance. A high rate performance observed, therefore, is supposed to be due to the high content of mesopores in carbons prepared through solution mixing process starting from magnesium salts as MgO precursor.

The present preparation method, *i.e.*, carbon coating process on ceramic particles, allows the production of carbons with desired pore size, which may be important to prepare the carbon electrode with pore size suitable for the electrolyte used in EDLCs. Fig. 4-17 shows one of examples of porous carbons possessing bimodal pore size distribution, large pore volumes at the sizes of about 2 and 10 nm, which are prepared by selecting two different magnesium salts. Its EDLC performance is shown in Fig. 4-18 as the dependence of capacitance on current density, by comparing with the micropore rich carbon. At a small current density as 50 mA/g, the capacitance value is not so much different for these two carbons. However, it decreases with increasing current density rapidly for micropore rich carbon, but not much decrease in capacitance

for bimodal mesopore rich carbon, rate performance calculated as a ratio of capacitance at 1000 mA/g to that at 50 mA/g being only 60 % for the former, but about 90 % for the latter.

The present results suggest us the importance of the presence of mesopores and the control of pore size distribution in electrode carbons for EDLCs. The carbon coating process using MgO as substrate is attractive for preparing porous carbons for EDLC electrode because the carbons with various pore sizes having a sharp size distribution were able to be produced easily and much economically, in comparison with other processes proposed. Also the same process is possible to be employed to prepare carbons for other applications, such as activated carbons for car canister and for removal of organic pollutants with large molecular sizes.

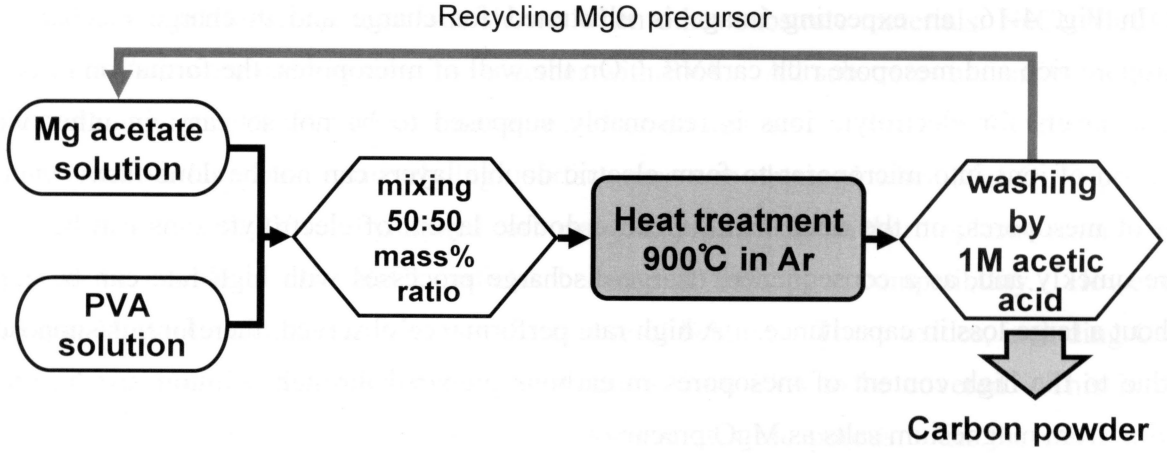

Fig. 4-13 Experimental procedure for recycling of MgO precursor.

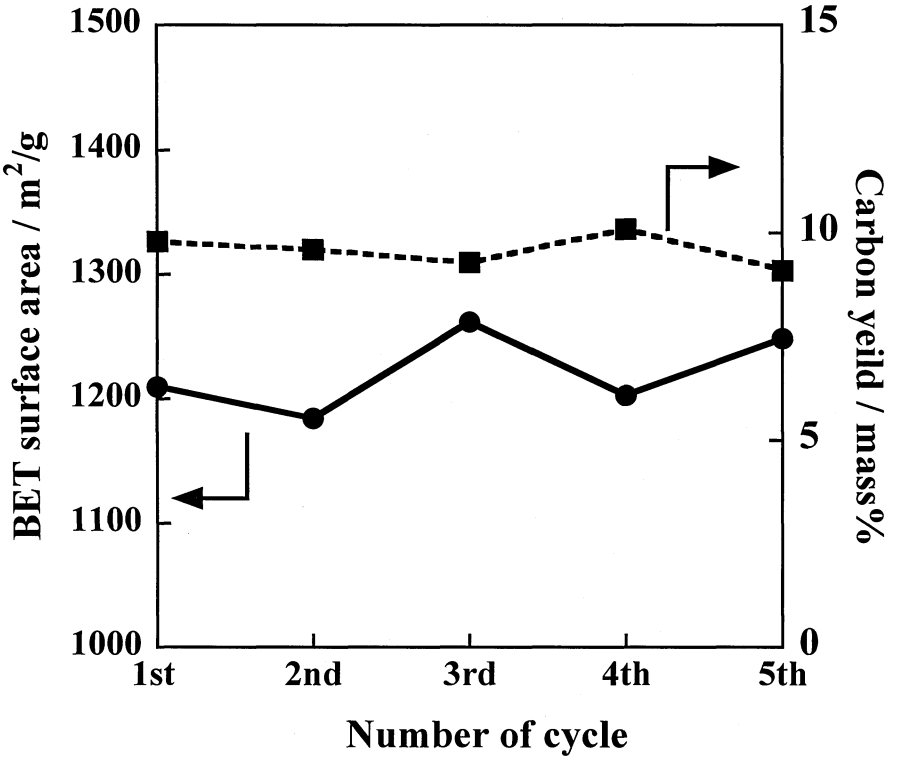

Fig. 4-14 Change in BET surface area and carbon yield of carbons obtained under recycling MgO precursor.

Table 4-3 BET surface area and carbon yield of carbons obtained under recycling MgO precursor.

Mixing method	Mixing ratio	cycle times	BET surface area m^2/g	Carbon yield mass %
Solution mixing	Mg acetate /PVA=7/3	1st	1210	9.8
		2nd	1185	9.6
		3rd	1262	9.3
		4th	1203	10.1
		5th	1249	9.1

Table 4-4 BET surface area by using different substrates and carbon precursors.

Carbon precursor	Prepared condition			BET surface area / m^2/g
	Substrate	Mixing ratio	HTT /°C, h	
PVA	NaCl	5/5	700, 1	16
	$MgCl_2$			45
	---	---	900, 1	83
	$MgCO_3$	5/5		1289
	$Mg(OH)_2$			990
	CaO			441
Phenol resin	---	---	900, 1	2
	MgO	5/5		8

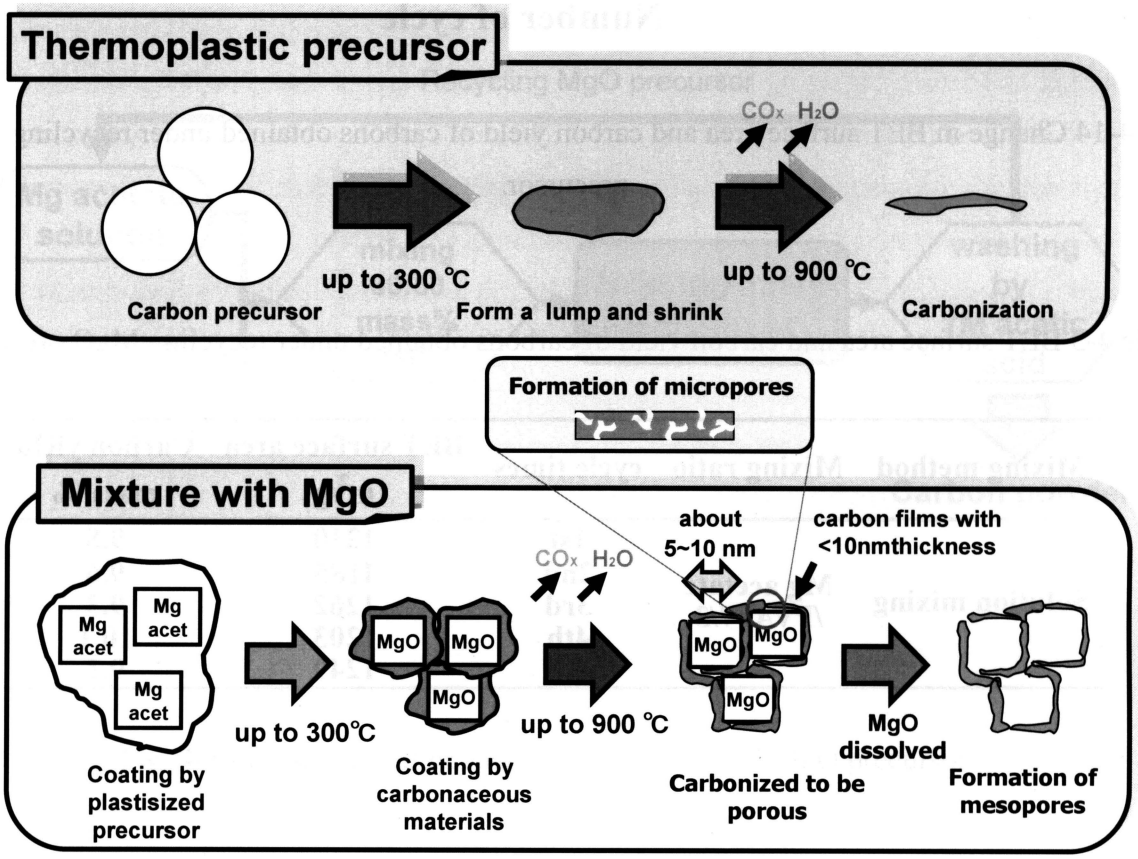

Fig. 4-15 Illustration of carbon coating process on ceramic particles and preparation of mesoporous carbons.

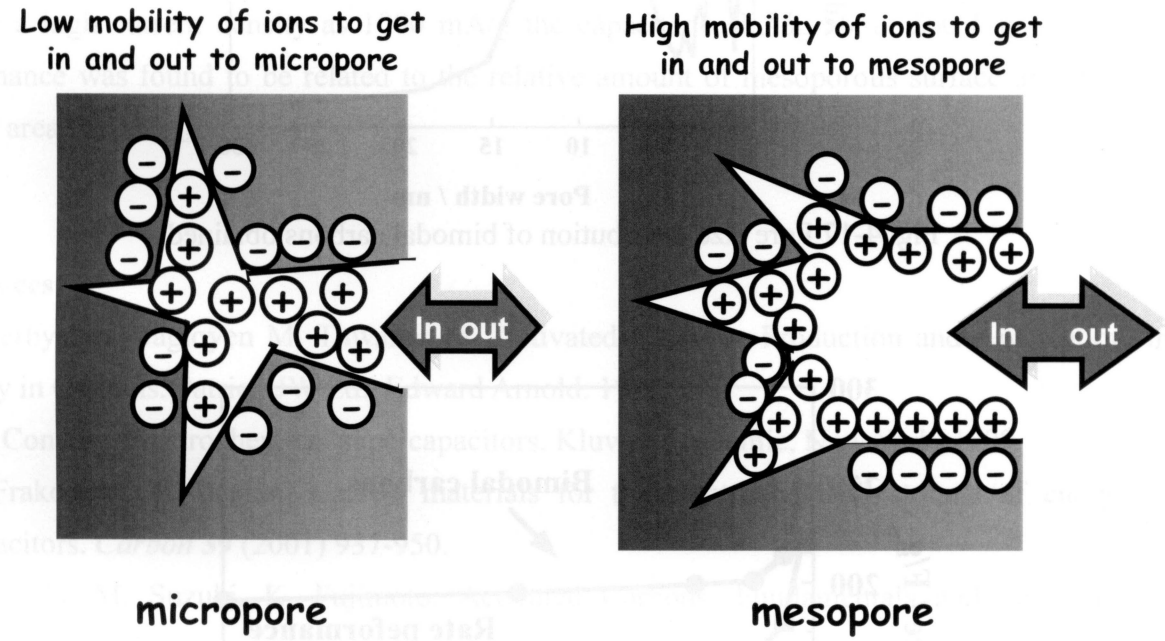

Fig. 4-16 Illustration of charge and discharge mobility of electrolyte ions in micropores and mesopores of carbon.

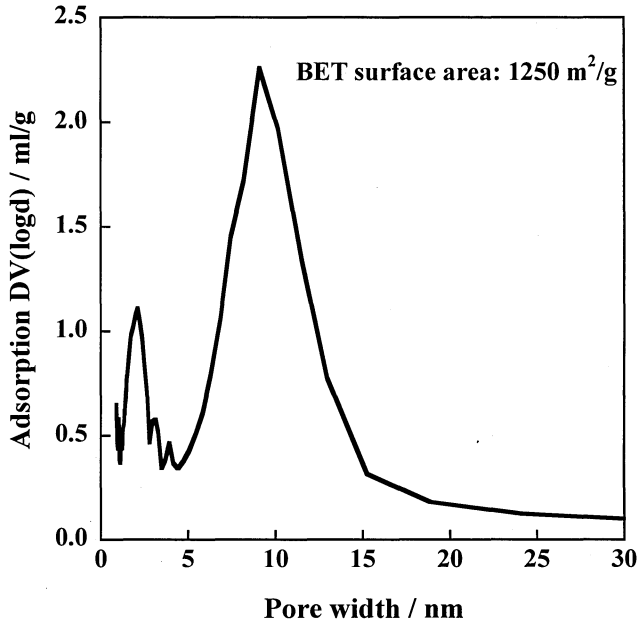

Fig. 4-17 Pore size distribution of bimodal carbons obtained.

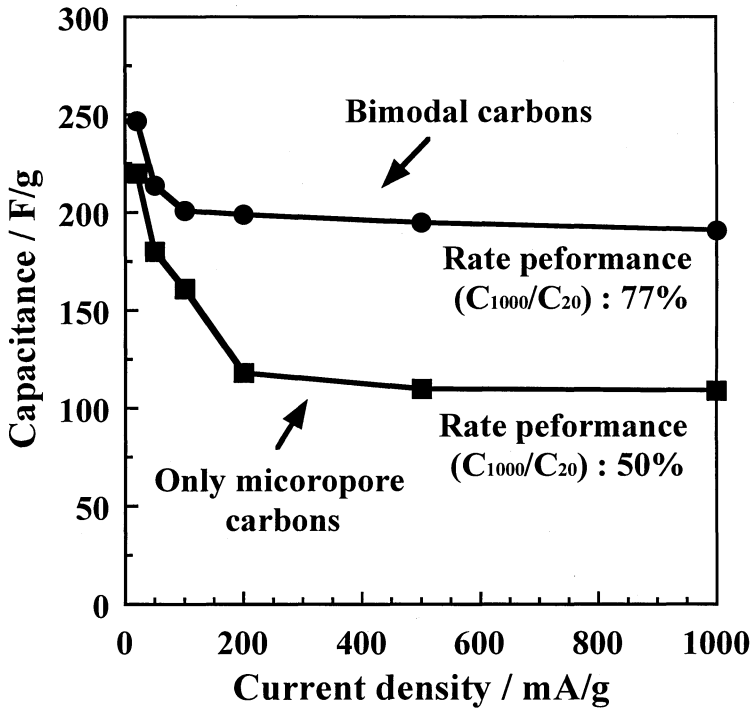

Fig. 4-18 Dependences of EDLC capacitance on current density for the bimodal carbons and carbons possessing only micropore.

4-5 Summary

Carbon coating on MgO was successfully carried out using the mixtures of thermoplastic precursors with MgO precursors prepared either powder or solution mixing. BET surface area of the carbons isolated from MgO by dissolving out was very high, such as 2000 m^2/g on the carbon prepared through solution mixing, even though any stabilization and activation processes were not applied. The carbons obtained through solution mixing were rich in mesopores, of which sizes were almost the same as MgO particles.

The EDLC capacitance of the samples obtained by the present method showed very large value, as 300 F/g. The carbons dominated in mesopores showed excellent rate performance, even at a high current density as 1000 mA/g the capacitance being about 200 F/g. This rate performance was found to be related to the relative amount of mesoporous surface area to total surface area $S_{meso.}/S_{total}$.

References

1. F. Derbyshire, Jagtoyen M, Thwaiter M. Activated Carbons -Production and Application, in Porosity in Carbons. Patrick JW Ed., Edward Arnold. 1995.
2. B.E. Conway. Electrochemical supercapacitors. Kluwer Academic, New York, 1999.
3. E. Frakowiak. F. Beguin. Carbon materials for the electrochemical storage of energy in capacitors. *Carbon* **39** (2001) 937-950.
4. Y.Sanada, M. Suzuki, K. Fujimoto. Activated Carbons. Fundamentals and Applications. Koudannsha, 1992.
5. M. Inagaki, Porous carbons, in New Carbons -Control of Structure and Functions. Elsevier, 2000.
6. T. Kyotani, E. Yasuda et al. (eds), Elsevier, Amsterdam, (2003) 109-127.
7. Z-G Shi, Y-Q Feng, Xu L, S-L Da. *Carbon* **41** (2003) 2668-70.
8. A.B. Fuertes, F. Pico, J. M. Rojo. *J. Mater. Sci.* **137** (2002) 907-10.
9 .S. Shiraishi, H. Kurihara, H. Tsubota, A. Oya, Y. Soneda, Y. Yamada. Electrochem *Solid-State Lett.***4** (2001) A5-A8.
10. O. Tanaike, H. Hatori, Y. Yamada, S. Shiraishi, A. Oya. *Carbon* 41 (2003) 1759-1764.
11. Y. Hanzawa, K. Kaneko, N. Yoshizawa, R. W. Pekala, MS Dresselhaus, *Adsorption* **4** (1998) 187-195.
12 H. Tamon, H. Ishizaki, M. Mikami, M. Okazaki. *Carbon* **35** (1997) 791-796.
13. T. Yamamoto, T. Nishimura, T. Suzuki T, H. Tamon. *Drying Tech* **19** (2001) 1319-1333.
14. M. Inagaki, H. Miura, H. Konno. *J. Europ. Ceram.* Soc. **18** (1998) 1011-1015.

15. M. Inagak, Y. Okada, V. Vignal, H. Konno. *Carbon* **36** (1998) 1706-1708.
16. M. Inagaki, S. Kobayashi, F. Kojin, N. Tanaka, T. Morishita, B. Tryba, **42** *Carbon* (2004) 3153-3158.
17. T. Morishita, R.Suzuki, T. Nishikara, T. Tsumura, M. Inagaki. *Tanso* **2005** (2005) 226-231.
18. T. Morishita, R.Suzuki, , T. Tsumura, H. Habazaki, M. Inagaki. *Tanso* (submitted)
19 H. Shi. *Electrochimica Acta* **41** (1996)1633-1639.
20 G. Gryglewicz, J. Machnikowski, E. Lorenc-Grabowska, G. Lota, Frackowiak *Electrochimica Acta* **50** (2005) 1197-1206.
21 L. Wang, M. Fujita, M. Inagaki. *Electrochimica Acta.* (in press)

Chapter 5

Preparation of carbon-coated tungsten and molybdenum carbides and their performance for electrode materials of electrochemical capacitors

5-1 Introduction

Electric double layer capacitors (EDLCs) have been used as a small energy storage device in different equipments, for memory backup and for the energy generated by solar cells. Most of EDLCs consisted of activated carbon electrodes because they could provide a very large surface area [1]. The capacitance was thought to depend principally on surface area of electrode carbons. Large surface area of carbon materials has been realized through activation process using either steam, CO_2 or KOH [2,3], and reached to be 1500-2000 m^2/g.

Recently, strong demands were arisen to get higher electric energy storage and so many efforts have been devoted to increase the capacitance through combining electric double layers with redox reactions, which are called supercapacitors [4,5]. Activated carbons mounted by ruthenium oxide were reported to have a high capacity [6,7]. Other metal oxides, such as manganese, tin and nickel oxides were also tried to be mounted on activated carbon electrodes [8-10]. Also the capacitors composed of two electrodes of different materials were proposed, the combination of activated carbon for one electrode with either graphite or metal oxide for another electrode, which were sometimes called hybridcapacitors [11-13].

A simple process to coat carbon onto various ceramics and metallic particles was developed; a powder mixture of carbon precursor, such as poly(vinyl chloride), with various oxides was heated above 700 °C in inert atmosphere [14]. Carbon-coated anatase type TiO_2 gave a hybrid photocatalysts which gave high photoactivity for some water contaminants together with high adsorptivity [15-17]. Oxides of transition metals, such as Fe_3O_4, Co_3O_4, NiO_2, were found to be reduced to metals by consuming a part of carbon coated, resulting in carbon-coated metals [18-20]. Coating of natural graphite particles by porous carbon was found to improve its anodic performance in Li ion rechargeable batteries [21]. Recently, the carbon coated on these ceramic particles was experimentally proved to be porous by dissolving out of MgO substrate [22]. Based on these experimental facts, a novel process was proposed to produce highly porous

carbons with BET surface area as high as 2000 m^2/g from thermoplastic precursors without applying any stabilization and activation processes [23,24]. The carbons thus prepared could have high EDLC capacitance in 1 mol/L H_2SO_4 electrolyte and a good rate performance [25] as shown in previous chapter.

In the present chapter, the same procedure for carbon coating of ceramic powders was applied to the mixture of a carbon precursor with either potassium tungstate or molybdate. The composite powders of porous carbon with either tungsten or molybdenum carbide were obtained. These composite powders were found to give a high capacitance when they were used as an electrode in electrochemical capacitor with 1 mol/L H_2SO_4 electrolyte.

5-2 Experimental

5-2-1 Preparation of carbon-coated tungsten and molybdenum carbides

The starting materials used were hydroxyl propyl cellulose (HPC) as carbon precursor, and K_2WO_4 and K_2MoO_4 powders of reagent grade as the precursor for tungsten and molybdenum carbide, respectively. The carbon precursor HPC was dissolved into water in a concentration of 10 mol/L and carbide precursor, either K_2WO_4 or K_2MoO_4, was dissolved into this HPC solution to have the mixture of two precursors in mass ratio of 5/5. The mixed precursor solutions thus prepared became gels at room temperature and dried at 100°C. The mixture of HPC with either K_2WO_4 or K_2MoO_4 thus prepared were heat-treated at a temperature between 800 and 1050 °C in Ar gas with a flow rate of 60 mL/min. After the heat treatment, the powders obtained were washed by 1 mol/L H_2SO_4 and then distilled water, in order to dissolve out the potassium metal, which might be remained in the powders.

The crystal structure of the carbon-coated substrate particles obtained was examined by X-ray powder diffraction (XRD) with CuKα radiation. Morphology and surface state of the carbon-coated particles were observed under transmission electron microscope (TEM) and field-emission-type scanning electron microscope (FE-SEM). Carbon content was determined from the ignition loss at 470 °C in a thermogravimeter (TG), up to this temperature both metal carbides, which were the products after the heat treatment, being not oxidized. Formation of carbide from the dried gels was also followed by TG-DTA under Ar gas atmosphere at 5°C/min. Adsorption/desorption isotherms of nitrogen gas on carbon-coated tungsten and molybdenum carbides were measured at 77 K and analyzed by BET method.

5-2-2 Electrode performance of carbon-coated tungsten and molybdenum carbides

The electrode for EDLC was prepared by mixing the sample powders with acetylene black as an electrical conductor and PTFE as a binder in a mass ratio of 80:10:10, which were blended

to be homogeneous by using acetone as solvent. The mixture thus prepared was pressed to be a thin film in approximate thickness of about 100 μm and then dried at 100 °C for 1 h under vacuum. Three-electrodes test cell with sample film as working electrode was used for the measurement of EDLC performance, where SCE as a reference electrode and a platinum wire as a counter electrode were equipped. The electrolyte used was 1M H_2SO_4. The performance of the sample powder as an electrode was determined from the cyclic voltammogram with a scanning rate of 1mV/sec and from the charge-discharge measurement with different current densities from 20 to 1000 mA/g at a potential window from 0.0 to 1.0 V. Capacitance of the sample powder was calculated from electric quantity discharged in the potential range of 0.7 to 0.4 V in discharge curve.

5-3 Results and discussion

5-3-1 Carbon-coated tungsten and molybdenum carbides prepared

In Fig. 5-1(a) and (b), changes in X-ray diffraction patterns are shown for the mixtures of HPC with K_2WO_4 and K_2MoO_4 in the ratio of 5/5, respectively, with heat treatment temperature. Fig. 5-2 shows TG-DTA curves for the same mixtures. Abrupt weight decrease at around 300 °C was due to pyrolysis of carbon precursor HPC to form carbonaceous materials, which coated the particles of K_2WO_4 (Fig. 5-2(a)). On further heating, K_2WO_4 was supposed to melt above 500 °C, because no diffraction peaks were detected on the sample quenched from 700 °C, and then these two components, molten K_2WO_4 and carbonaceous materials, reacted to form metallic W partly, but suddenly reacted at about 880 °C, associated with a sharp exothermal peak, to produce tungsten carbides W_2C and finally WC.

In the case of K_2MoO_4, very similar reaction process to that of K_2WO_4 was also suggested from change in XRD pattern and TG-DTA curve, except that the carbide finally formed was Mo_2C. Sudden weight loss was observed below 100 °C, which seemed to be due to loss of adsorbed water of the mixture (Fig. 5-2(b)). Above 500 °C after pyrolysis of HPC, K_2MoO_4 was supposed to be amorphous and then reacted with carbonaceous materials at around 800 °C to form carbide Mo_2C.

In Fig. 5-3(a) and (b), TEM images are shown for the sample prepared at 1000 °C from the mixture of HPC with K_2WO_4 and K_2MoO_4, respectively. The particles with irregular shape and dark contrast are reasonably supposed to be either WC or Mo_2C. The particles of WC had the size of 30 to 50 nm, but the particle sizes of Mo_2C was scattered in a large range from 5 to 200 nm. They seemed to be covered by carbon layer, which was supposed to be porous.

In Fig. 5-4(a) and (b), carbon content, which was determined from the ignition loss at 470°C in air, and BET surface area of carbon-coated WC and Mo_2C, respectively, are plotted against heat

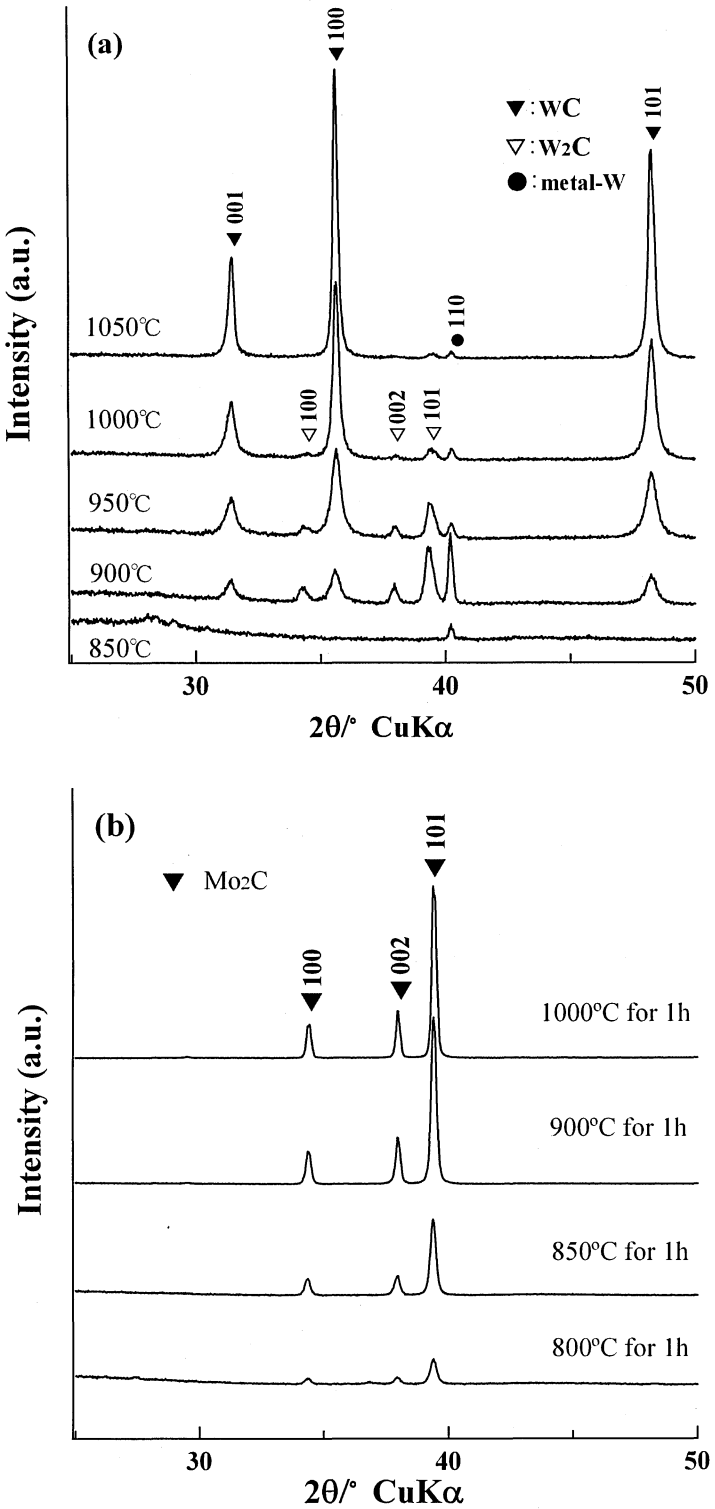

Fig. 5-1 Changes in X-ray diffraction pattern of the mixtures of HPC with K_2WO_4 (a) and with K_2MoO_4 (b) with heat treatment temperature.

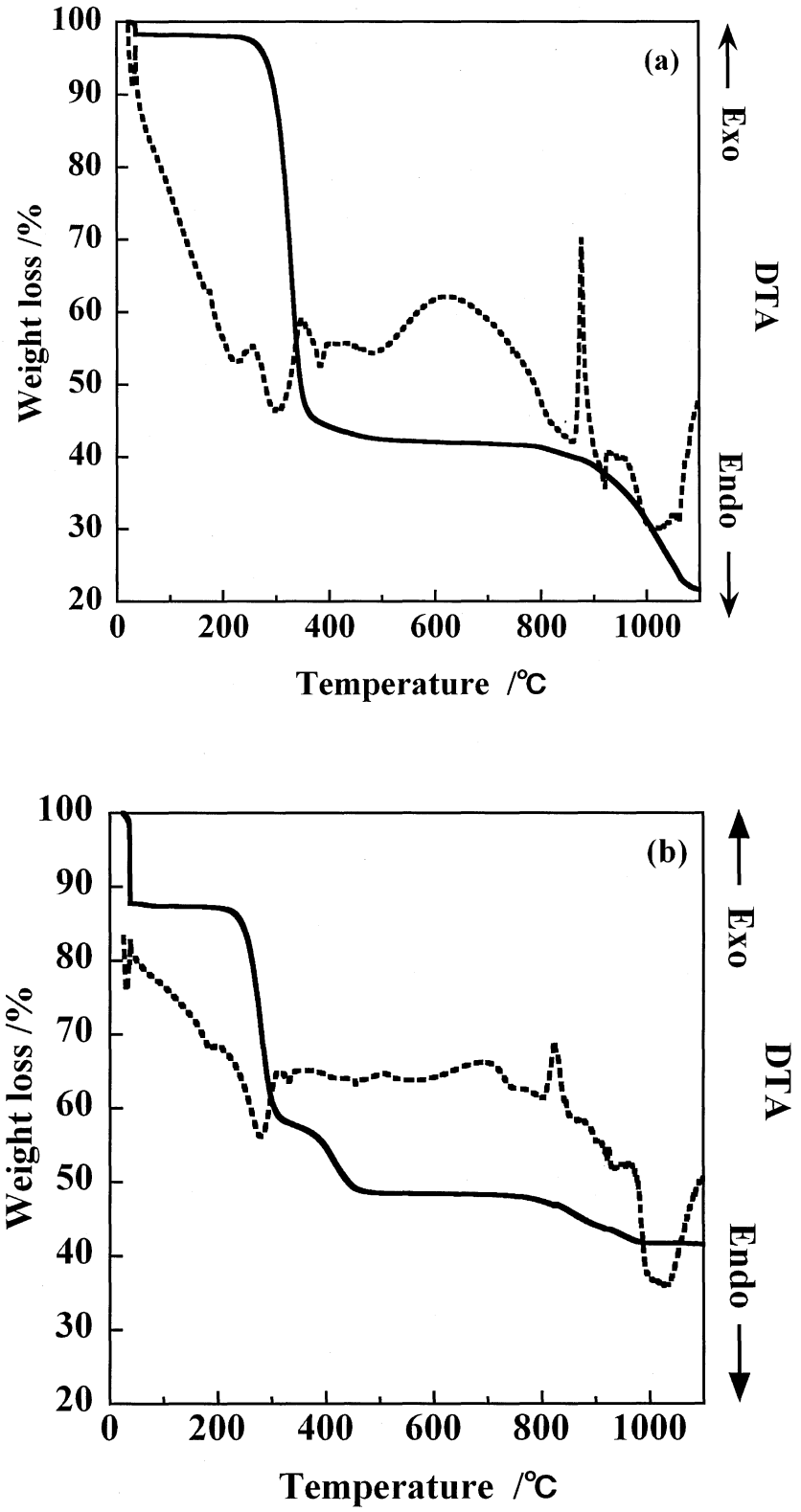

Fig. 5-2 TG-DTA curves for the mixtures of HPC with K_2WO_4 (a) and with K_2MoO_4 (b).

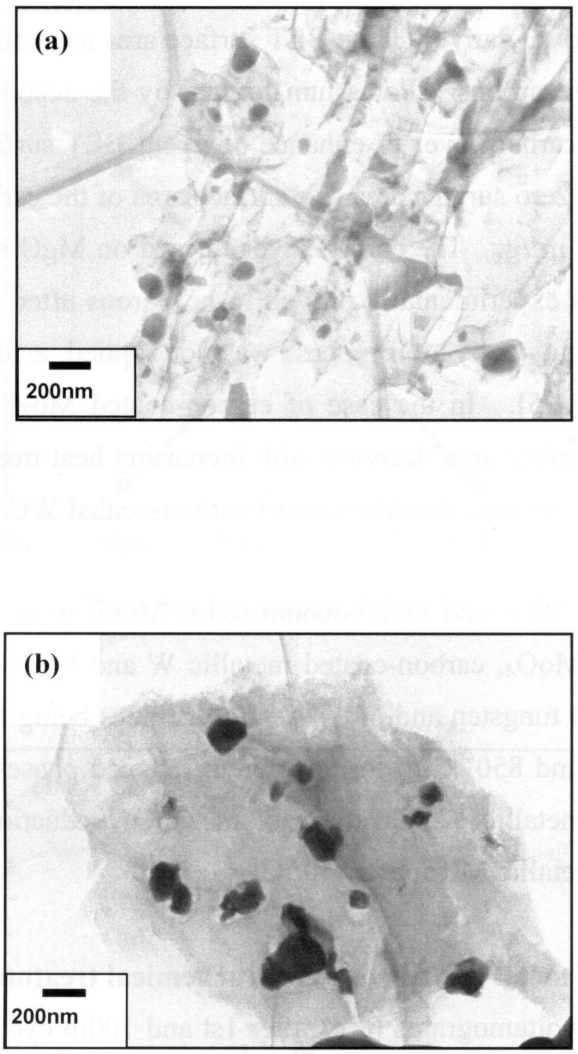

Fig.5-3TEM images of the samples prepared at 1050 °C from the mixtures of HPC with K_2WO_4 (a) and with K_2MoO_4 (b).

treatment temperature. On carbon-coated WC samples, carbon content decreases monotonically with increasing temperature, being consistent with TG curve in Fig. 5-2(a), probably due to carbonization and also consumption of carbon for the reduction of tungsten oxides. The powders prepared above 1000°C show relatively large BET surface area as about 170 m^2/g, suggesting the formation of highly porous carbons. Potassium formed by the decomposition of K_2WO_4 might act as activating agent of carbon layer to enhance apparent BET surface area. If the substrate WC were assumed to have zero surface area, the surface area of the carbon layer coated on WC is calculated to be about 770 m^2/g. The carbon layer formed on MgO substrate through the same process as the present was experimentally proved to be porous after dissolving out of MgO by sulfuric acid, even though any activation process was not applied, as described in Chapter 4 and reported in the papers [22-25]. In the case of carbon-coated Mo_2C, on the other hand, both carbon content and BET surface area decrease with increasing heat treatment temperature, noting that carbon content is much smaller than the case of carbon-coated WC, about 2 mass% after 1000 ^oC treatment.

When tungsten oxide WO_3 and molybdenum oxide MoO_3 were used as starting materials, instead of K_2WO_4 and K_2MoO_4, carbon-coated metallic W and Mo, respectively, were obtained after 1000 ^oC treatment, no tungsten and molybdenum carbides being formed. The reduction of WO_3 seemed to occur around 850 ^oC to form different reduced phases of WO_3, such as $W_{18}O_{49}$ and WO_2, and finally to metallic W. In the case of MoO_3, reduction to MoO_2 was observed above 700 ^oC and that to metallic Mo above 850 ^oC.

5-3-2 Structure change of metal carbides by electrochemical treatment

In Fig. 5-5(a), cyclic voltamograms (CV) after 1st and 100th cycles of charge-discharge are shown for a tungsten carbide powder (reagent grade) and that after 1st cycle for the carbon-coated tungsten carbide prepared from the mixture of HPC and K_2WO_4 at 1000 ^oC. In the carbide without carbon coating, redox peaks are clearly observed after 1st charge-discharge cycle, and after 100th cycle it becomes a little broad and also shift to low voltage side. On the other hand, the CV curve on the carbon-coated sample prepared from the mixture of HPC and K_2WO_4 are box-shape, typical for the formation of electric double layers, and no marked redox peaks are observed. No redox peaks were observed even in the charge-discharge process after 100th cycle.

For molybdenum carbide (reagent grade) and carbon-coated molybdenum carbide, cyclic voltamograms are shown in Fig. 5-5(b). Carbon-coated Mo_2C also shows box-shape curve and no redox peaks even after 1st charge-discharge cycle are observed, although two redox peaks are appeared clearly in molybdenum carbide (reagent grade) without carbon coating even after 100th cycle.

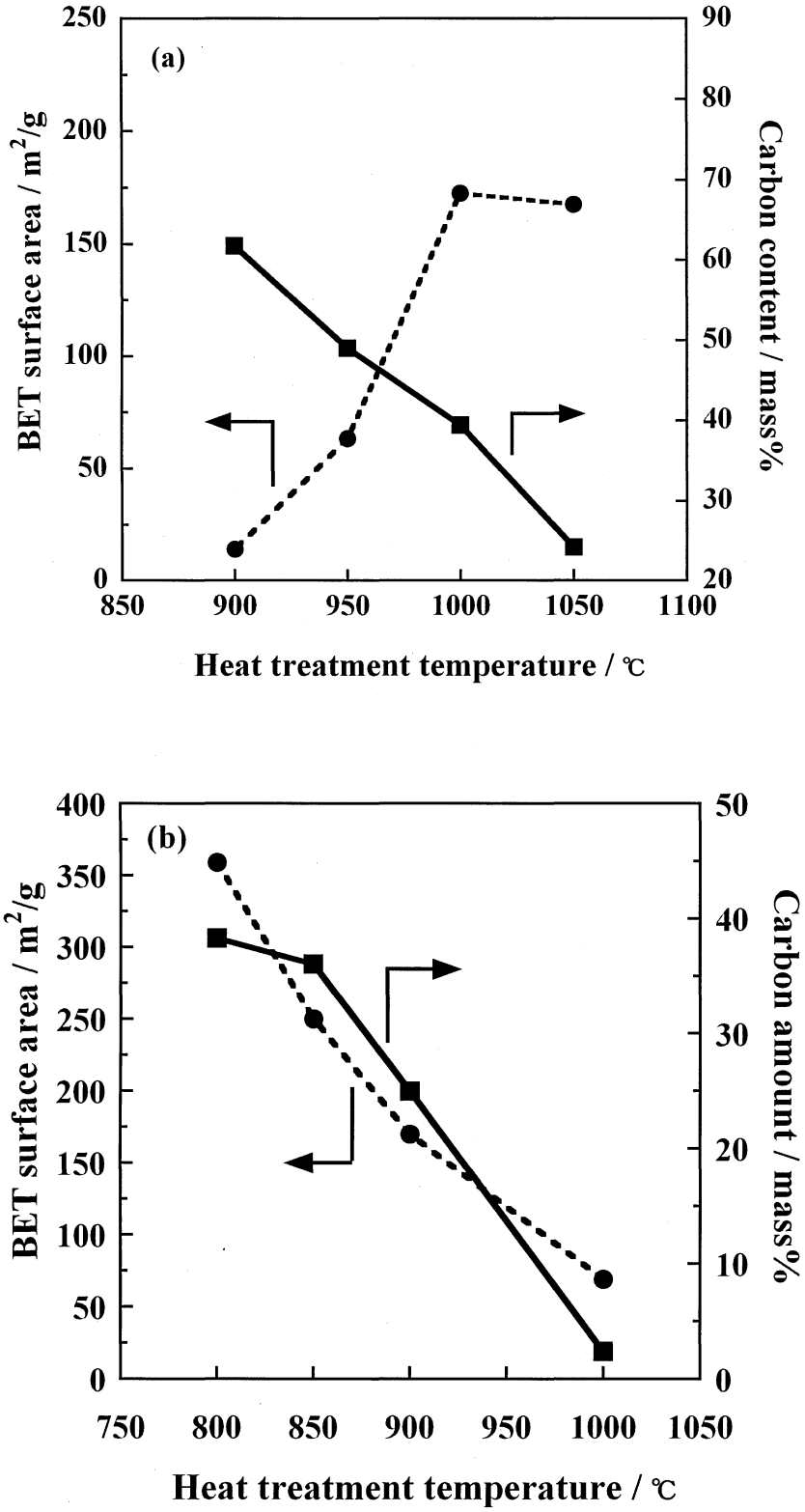

Fig. 5-4 Changes in carbon content and BET surface area of the carbon-coated tungsten carbide (a) and carbon-coated molybdenum carbide (b) with heat treatment temperature.

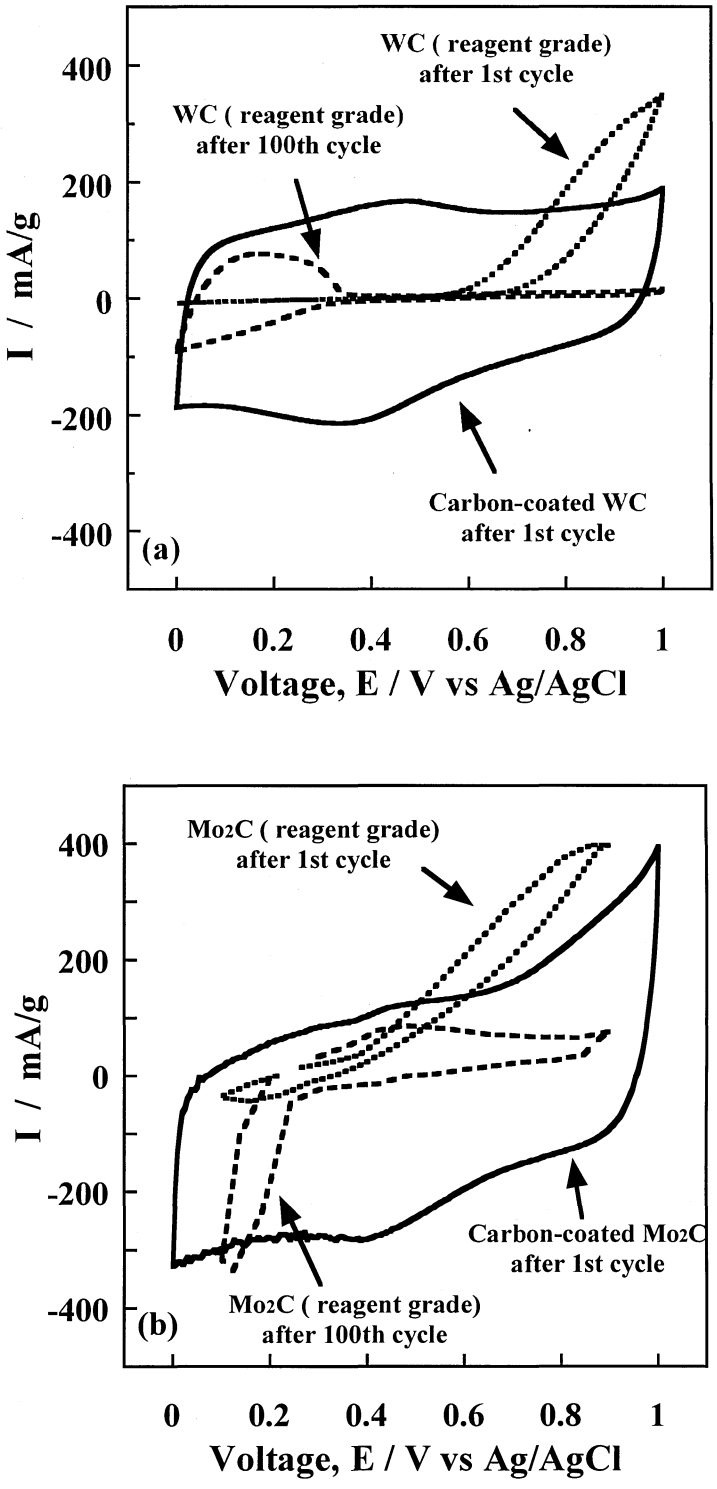

Fig. 5-5 Cyclic voltammograms of carbon-coated tungsten carbide prepared at 1000 °C and tungsten carbide powder without carbon coating (a), and of carbon-coated molybdenum carbide prepared at 850 °C and molybdenum carbide powder without carbon coating (b).

In Fig. 5-6, XRD patterns are shown for tungsten carbide without carbon coating and the carbon-coated tungsten carbide after the first charge-discharge cycle with a current density of 50 mA/g. In the electrodes recovered after the 1st cycle, various tungsten oxy-hydroxides were detected, such as $WO_{0.88}(OH)_{4.12}$, $WO_{1.84}(OH)_{2.22}$, etc. When tungsten carbide powder with the particle size of 1 μm without carbon coating was used as the electrode, it changed only partly to oxy-hydroxides after the 1st charge-discharge cycle, as shown in Fig. 5-6(a), and it needed many cycles, more than 100 cycles, to complete the transformation to oxy-hydroxides. Carbon-coated tungsten carbide, on the other hand, transformed completely to tungsten oxy-hydroxides even after the 1st cycle of charge-discharge (Fig. 5-6(b)). In carbon-coated tungsten carbide, carbide particles were very small as 30-50 nm and so could rapidly change to oxy-hydroxides by just 1st cycle of charge-discharge. Since these changes from carbide to oxy-hydroxides occur on the surface of carbide particles, large particles as reagent grade tungsten carbide used in Fig. 5-6(a) needed many cycles of charge-discharge to complete transformation to oxy-hydroxides. On carbon-coated Mo_2C, the diffraction peaks of the original Mo_2C disappeared completely after the 1st cycle of charge-discharge and no diffraction peaks were detected, suggesting that molybdenum oxy-hydroxides are in an amorphous state. These results reveal clearly that small particles of tungsten and molybdenum carbides coated by carbon layer transformed to oxy-hydroxides of respective metals during the 1st electrochemical treatment in 1 M H_2SO_4 electrolyte, because of their small particle sizes, and also that carbon coating was effective to keep carbide particles small. These oxy-hydroxides of respective metals are expected to perform the redox reactions during charge-discharge process.

5-3-3 Capacitor performance of carbon-coated metal carbides

In Fig. 5-7, charge/discharge curves are shown for the current density of 50 mA/g. The capacitance calculated from these curves was about 210 F/g. It has to be pointed out that the charge/discharge curves show a good linearity and any plateau corresponding to redox reaction was not observed, as no redox peaks were observed in cyclic voltamograms (Fig.5-5).

In Fig. 5-8(a) and (b), capacitance measured at the current density of 50 mA/g was shown as a function of heat treatment temperature on carbon-coated tungsten carbide and molybdenum one in the units of electric charge (F) per 1 g of carbon-coated metal carbide and also of charge (F) per 1 cm^3 of electrode films, which were prepared from the sample carbon-coated carbide with acetylene black and PTFE binder. In the case of tungsten carbide, capacitance value based on weight of the electrode increases abruptly above 950 °C, although carbon content decreases with increasing heat treatment temperature (Fig.5-4(a)). This increase in apparent capacitance is supposed to be due to the formation of tungsten carbide during heat treatment above 950 °C and

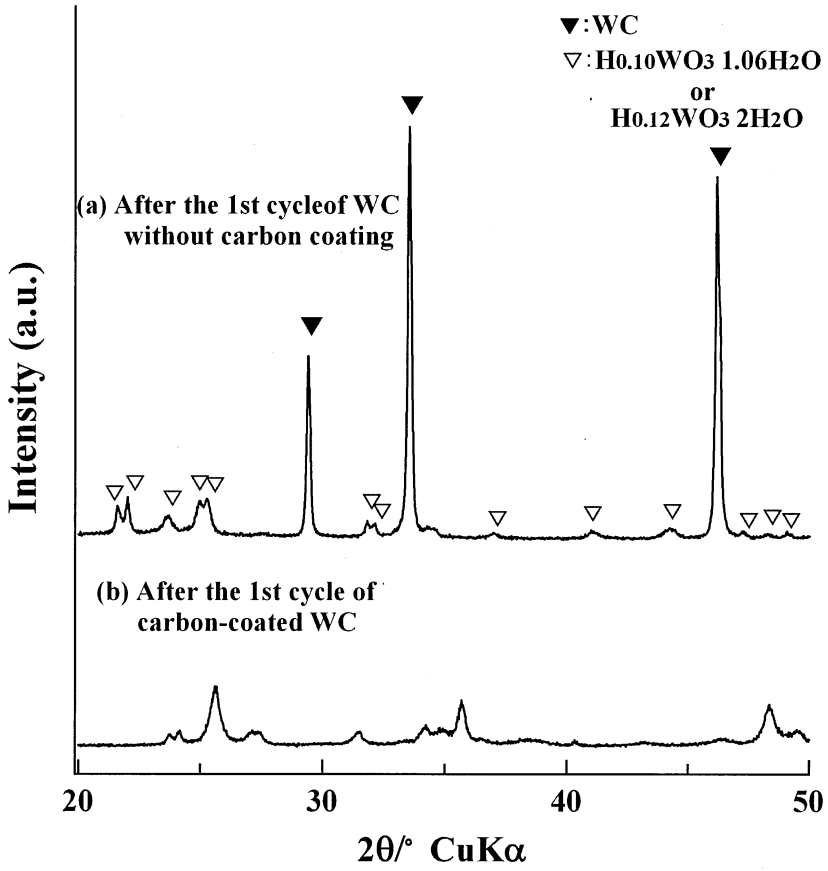

Fig. 5-6 XRD patterns of carbon-coated tungsten carbide before and after the first charge-discharge cycle.

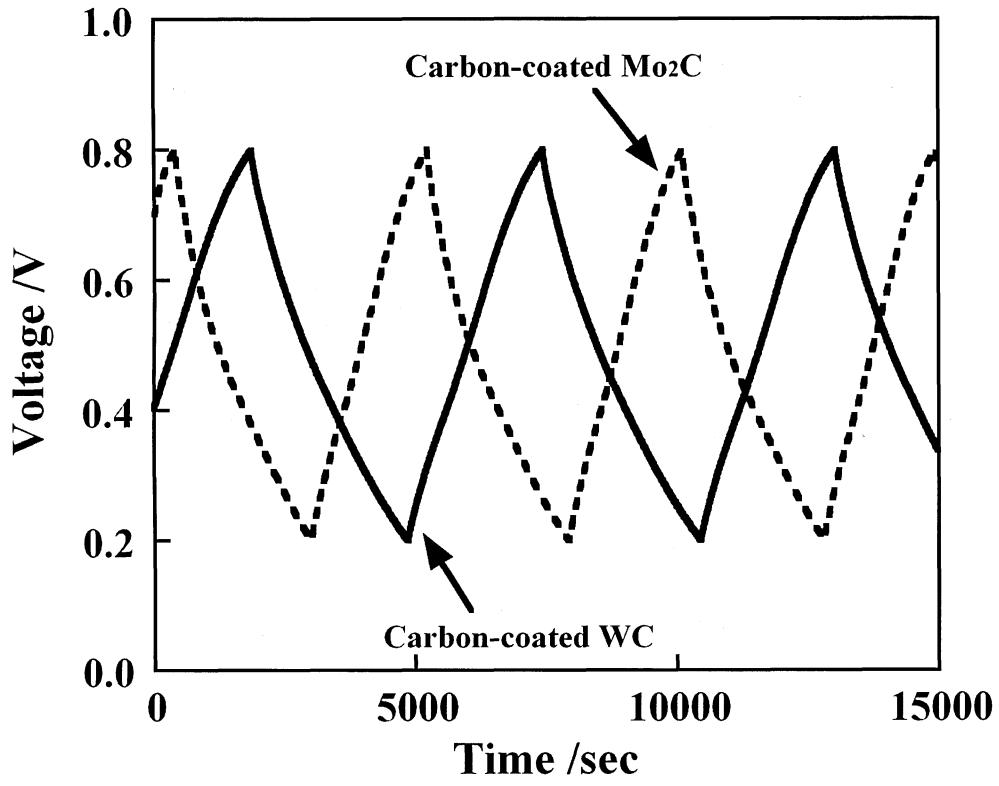

Fig. 5-7 Charge-discharge curves of carbon-coated tungsten and molybdenum carbide prepared at 1000 and 850 °C, respectively.

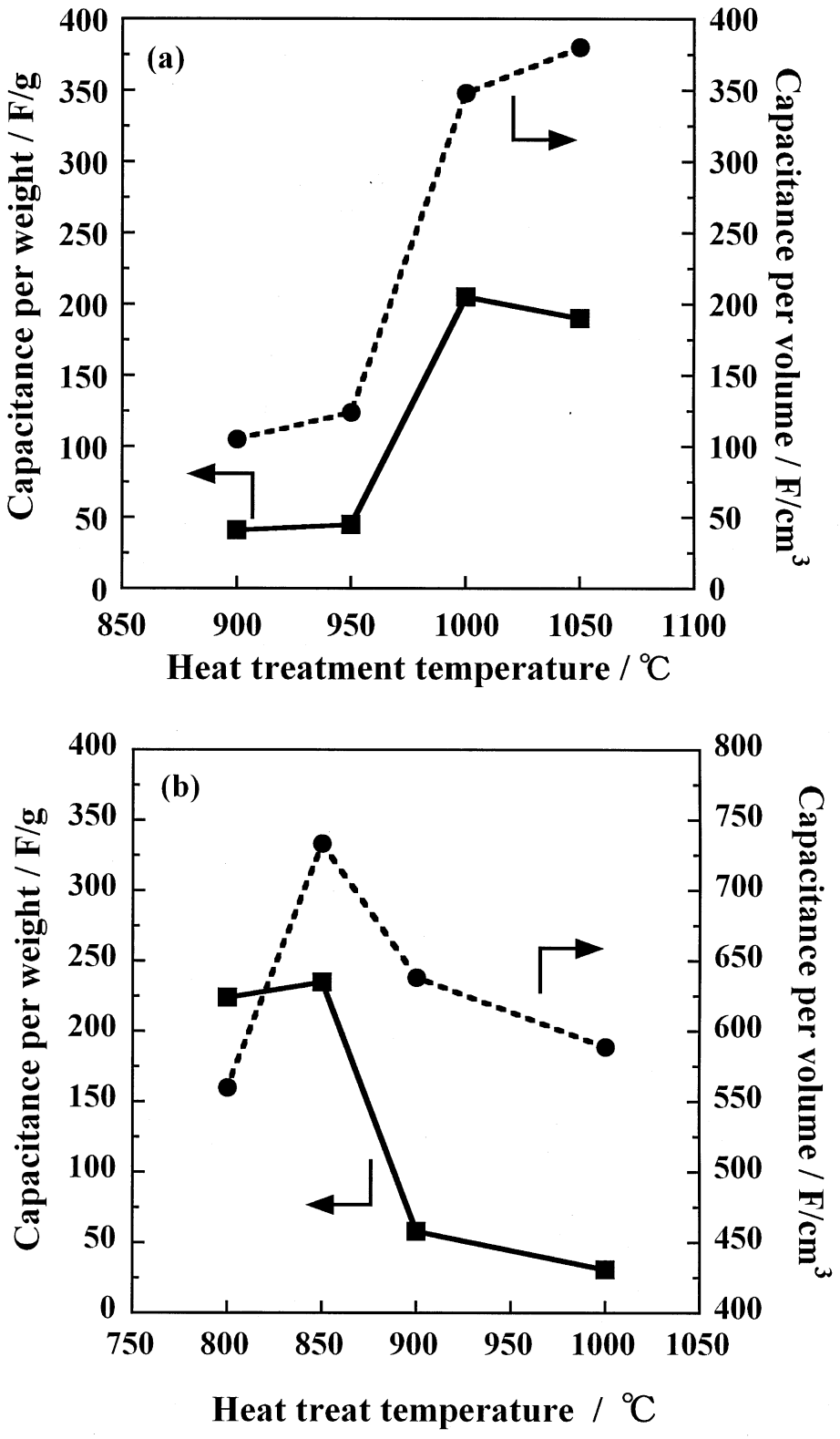

Fig. 5-8 Change in capacitance on the carbon-coated tungsten carbide (a) and carbon-coated molybdenum carbide (b) with heat treatment temperature.

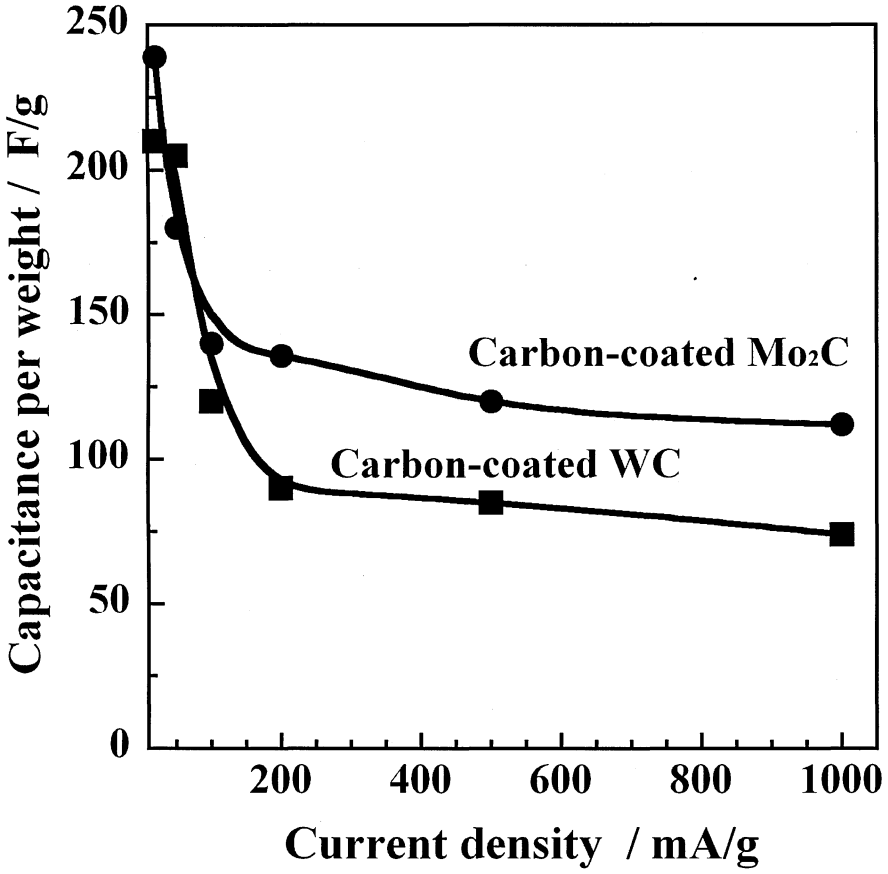

Fig. 5-9 Dependences of EDLC capacitance on current density for the carbon-coated tungsten and molybdenum carbides prepared at 1000 and 850 °C, respectively.

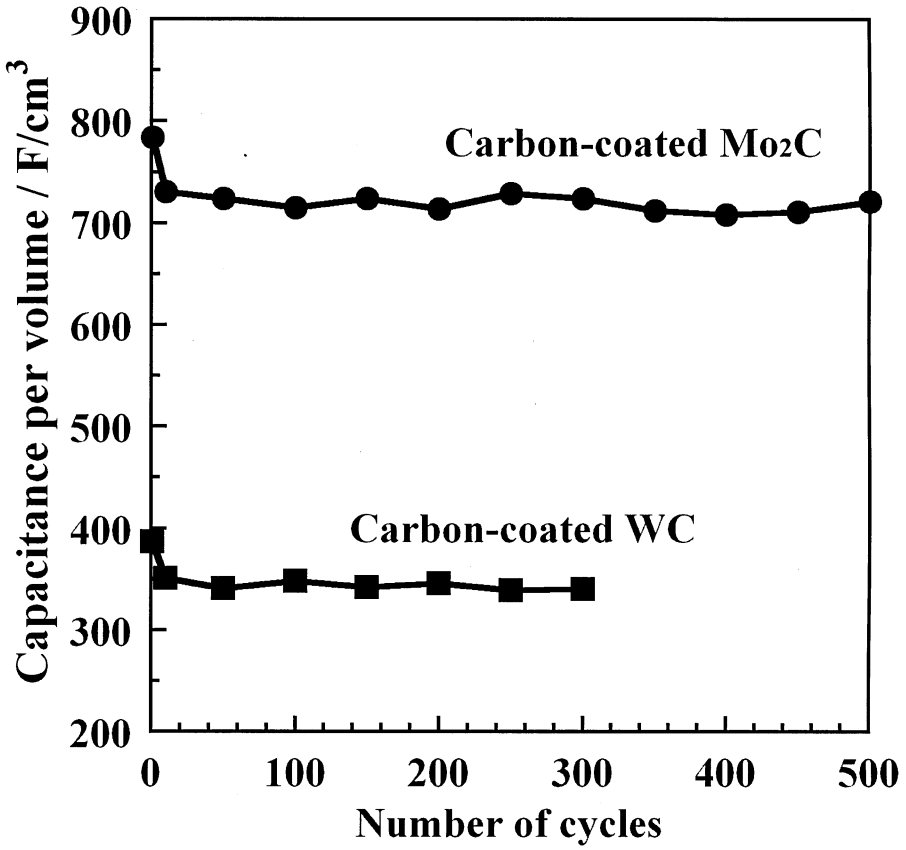

FIg.5-10 Cyclic performance of the carbon-coated tungsten and molybdenum carbide prepared at 1000 and 850 °C, respectively.

to the transformation of tungsten carbide to tungsten hydroxides during the first charge-discharge cycle, in other words, due to the overlapping of the redox capacitance of tungsten hydroxide to the electric double layer capacitance of porous carbon. In the case of molybdenum carbide, capacitance value based on weight of the electrode decreases with increasing heat treatment temperature (Fig. 5-8(b)), probably because of decreases in both carbon content and BET surface area (Fig. 5-4(b)).

Advantages on the present carbon-coated tungsten and molybdenum carbide electrodes were shown markedly by expressing the capacitance value on the basis of electrode volume, because of high bulk density of electrode films due to heavy metal carbides. The capacitance based on volume reached to more than 350 F/cm^3 in the case of tungsten carbide and 550-750 F/cm^3 in the case of molybdenum carbide. These capacitance values can be said to be very high in comparison with the value of 140 F/cm^3 in the case of porous carbons without any metal carbides [25].

For the carbon-coated tungsten and molybdenum carbides, which showed the highest capacitance values at the current density of 50 mA/g, the dependence of capacitance on current density was shown in Fig. 5-9. In low current density range, both samples give relatively large capacitances, but their capacitances decrease rapidly with increasing current density. This is supposed mainly due to the slow rate of redox reactions on tungsten and molybdenum hydroxides, although the capacitance due to electric double layer on pore walls of carbon also decreases with increasing current density.

In Fig. 5-10, cyclic performance in 1 M H_2SO_4 electrolyte with current density of 50 mA/g is shown on the carbon-coated tungsten and molybdenum carbides prepared at 1000 and 850 ^{o}C, respectively. Both samples showed good cyclic performance. On carbon-coated molybdenum carbide, particularly, high capacitance as about 730 F/cm^3 was kept even after 500 cycles. These good cyclic performances were supposed to be due to no agglomeration of tungsten and molybdenum hydroxide particles even by the repetition of redox reactions during charge-discharge cycles.

5-4 Summary

The powders prepared in the present work were the composite of tungsten and molybdenum carbides with porous carbon, where most of carbide particles were coated by porous carbon. The composite powders thus prepared gave relatively high capacitance in H_2SO_4 aqueous electrolyte, which was exhibited as the capacitance based on electrode volume. Changes from carbides to hydroxides of tungsten and molybdenum carbides were completed within the 1st cycle of charge-discharge because of their fine particles. Porous carbon coated on the particles inhibited

the growth of metal carbides during their formation, which made the transformation of metal carbide to metal hydroxides possible through 1st cycle of charge-discharge, and also disturbed the agglomeration of metal hydroxides during charge-discharge cycles, as well as acted as electrode materials for electric double layers. A scheme was shown on the formation of carbon-coated WC and tungsten hydroxides and the appearance of electric double layers, and redox reaction of tungsten hydroxides on carbon surface with charge and discharge process.

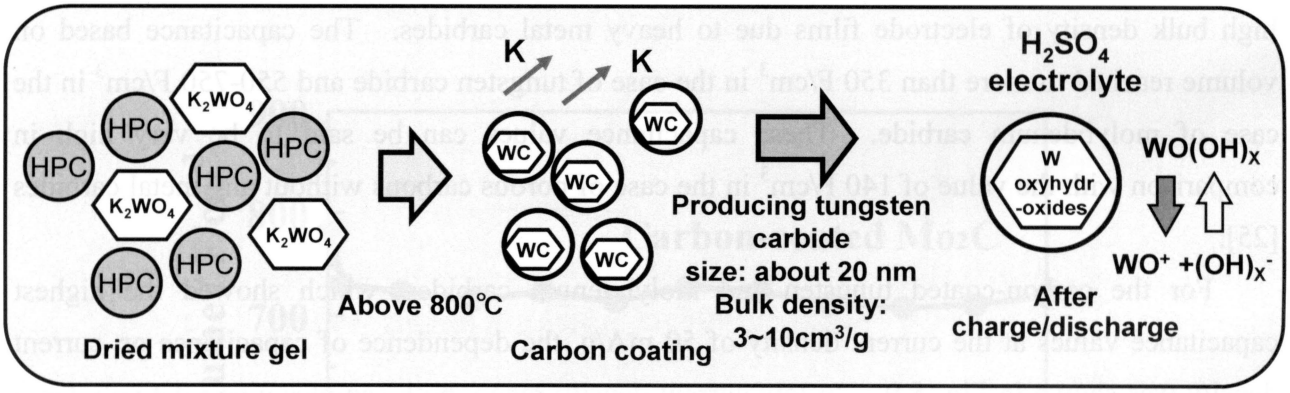

Fig. 5-11 Scheme of the process developed in the present chapter.

Reference

1. B. E. Conway, *Electrochemical supercapacitors*, Kluwer Academic, New York (1999).
2. F. Derbyshire, M. Jagtoyen, M. Thwaites, Acrivated Carbons - Production and Applications. In " Porosity in Carbons", PatrickJW, Ed. Edward Arnold, (1995) 227-252 .
3. F. Rodriguez-Reinoso. Activated Carbon. In "Introduction to Carbon Technologies", Marsh H, Heintz EA, Rodriguez- Reinoso F. Ed. Univ. Alicante, (1997) 35-61.
4 . J. P. Zheng and T. R. Jow., *J. Power Sources*, **62** (1996) 155-159.
5 . Y. Takasu, T. Nakamura, H. Ohkawauchi, and Y. Murakami, *J. Electrochem. Soc.*, **144** (1997) 2601.
6. M. Ramani, B. S. Haran, R. E. White, B. N. Popov and L.Arsov, *J. Power Sources*, **93** (2001) 209.
7. Y. Sato, K. Yomogida, T. Nanaumi, K. Kobayakawa, Y. Ohsawa, M. Kawai, *Electrochem. Solid-State Lett.*, **3** (2000) 113.
8. Y. Takasu, T. Ohnuma, W. Sugimoto and Y. Murakami, *Electrochem.*, **67** (1999) 1187.
9. J. H. Kim, K. H. Shin, C. S. Jin, D. K. Kim, Y. G. Kim, J. H. Park, Y. S. Lee, Y. S. Joo, and K. H. Lee, *Electrochem.* **69 (2001)** 853.

10. R. N. Reddy, and R. G. Reddy, *J. Power Sources*, **124** (2003) 330.
11. E. Raymundo-Piriero, E. V. Khomenko, E. Frackowiak and F Beguin, *J. Electrochem. Soc.*, (in press).
12. J. M. Miller and B. Dunn, *Langmuir,* **15**, (1999) 799.
13. H. B. Gu, J-U. Kim, H-W. Song, G-C. Park, and B-K. Park, *Electrochim. Acta,* **45** (2000) 1533.
14. M. Inagaki, H. Miura and H. Konno, *J. Europ. Ceram. Soc.,* **18** (1998) 1011-1015.
15. T. Tsumura, N. Kojitani, I. Izumi, N. Iwashita, M. Toyoda and M. Inagaki, *J Mater. Chem.,* **12**, (2002) 1391-1396.
16. M. Toyoda, T. Tsumura, Y. Nanbu, M. Omura and M. Inagaki, *Mizukannkyou Gakkaishi*, **26** [4], (2002) 209-214.
17. B. Tryba, A. W. Morawski, T. Tsumura, M. Toyoda and M. Inagaki, *J. Photochem. Photobio. A: Chem.*, **167** (2004) 127-135.
18. M. Inagaki, Y. Okada, H. Miura and H. Konno, *Carbon*, **37** (1999) 329-334.
19. M. Inagaki, K. Fujita, Y. Takeuchi, K. Oshida, H. Iwata and H. Konno, *Carbon* **39** (2001) 921-929.
20. H. Konno, K. Fujita, H. Habazaki and M. Inagaki, *TANSO* **2002,** (2002) 113-116.
21. T. Tsumura, A. Katanosaka, I. Souma, T. Ono, Y. Aihara, J. Kuratomi and M. Inagaki, *Solid State Ionics*, **135** (2000) 209-213.
22. M. Inagaki, S. Kobayashi, F. Kojin, N. Tanaka, T. Morishita and B. Tryba, *Carbon*, **42**, 3153-3158 (2004).
23. T. Morishita, R. Suzuki, T. Nishikawa, T. Tsumura and M. Inagaki, *Tanso* **2005** (2005) 226-231.
24. T. Morishita, R. Suzuki, T. Nishikawa, T. Tsumura and M. Inagaki, *Tanso* (submitted).
25. T. Morishita, Y. Soneda, H. Hatori, T. Tsumura and M. Inagaki, *Carbon* (submitted).

Chapter 6
Conclusions

6-1 Materials for electric energy storage

Electric power storage is one of the important technologies for diversification and increasing efficiency of electric energy use. Electric power storage devices, such as rechargeable batteries and capacitors, have to be improved for the concomitant uses in a hybrid car and steady electric power supply. It was important to select appropriate electrode materials for each electric energy device and so many materials and its preparation methods had been developed. Now, it is also important to take into account that the preparation methods for the electrode materials have to be energy saving and also environment friendly, in addition to their high performance for energy storage. Carbon materials and noble metal oxides are noted as attractive materials in advanced devices which are in the next generation of energy system and have already played the important role, such as lithium ion rechargeable batteries, electric double layer capacitors and fuel cells[1-4].

In the present thesis, MnV_2O_6 and carbon-coated Sn fine particles were developed for anode materials of lithium ion rechargeable batteries, and also mesoporous carbons and carbon-coated WC and Mo_2C were developed for electrode materials of electrochemical capacitors. For these materials, new preparation methods were developed, most of which were based on carbon coating process, by taking into consideration on the accountability for environment, simple processes at low temperature, possibility to use wasted materials. In Table 6-1, the results of the present thesis are summarized by showing characteristics on preparation and their electrode applications for the materials developed. These materials showed either larger electric energy storage and/or better charge-discharge performance than the conventional materials. These materials are believed to contribute the future development of electric energy storage devices.

Brannerite-type crystalline powders of anhydrous manganese vanadate MnV_2O_6 were successfully precipitated by mixing V_2O_5 with $Mn(CH_3COO)_2$ powders in water medium below 200 °C under hydrothermal and coprecipitation conditions. The advantages of these two preparation methods were lower energy consumption, simple and easy process and higher reproducibility. Charge and discharge capacities of the anhydrous MnV_2O_6 which showed strong 110 diffraction line in X-ray powder pattern and consisted of rod-like particles gradually increased with cycling, though the frist cycle gave relatively low discharge capacity and low Columbic efficiency. Beyond 25th cycles, both charge and discharge capacities reached more than 600

mAh/g.

Carbon-coated Sn powders were prepared from the powder mixtures of thermoplastic precursor poly(vinyl alcohol) (PVA), SnO_2 and MgO. SnO_2 was reduced to metallic Sn on the course of heating to carbonize PVA, and its particle size in carbon shell was around 30 to 100 nm. MgO existence hindered the agglomeration of molten metallic Sn and made the dispersion of metallic Sn as fine particles possible. They showed high anodic performance in lithium ion rechargeable batteries; high charge capacity as 500 mAh/g even after 10th cycle and stable cyclic performance. The spaces left in carbon shell by MgO after its dissolution were supposed to absorb a large volume expansion and contraction of Sn metal particles by Li alloying and dealloying during charge and discharge cycles. When carbon-coated Sn loaded onto graphite flakes, metallic Sn contributed to the increase in capacity.

Porous carbons with high surface area were successfully prepared from thermoplastic precursors, such as poly(vinyl alcohol) (PVA), hydroxyl propyl cellulose (HPC) and poly(ethylene terephthalate) (PET), by the carbonization of mixtures with MgO at 900 ^{o}C in inert atmosphere. MgO in the carbonization products was easily dissolved out by using a diluted sulfuric acid. Mixing of carbon precursors with MgO precursors (reagent grade MgO, magnesium acetate and citrate) was done either in powder (powder mixing) or in aqueous solution (solution mixing). The BET surface area of the carbons obtained through solution mixing could reach to very high value, such as 2000 m^2/g, even though any activation process was not applied. Pore structure of the resultant carbons was found to depend strongly on the mixing method; the carbons prepared through solution mixing were rich in mesopores, but those through powder mixing were rich in micropores. The size of mesopores was found to be almost the same as that of MgO particles, suggesting the possibility to control mesopore size in resultant carbons. The porous carbon with a BET surface area of 1900 m^2/g prepared at 900 ^{o}C through solution mixing of Mg acetate with PVA showed pretty high EDLC capacitance, about 300 F/g with a current density of 20 mA/g and 210 F/g with 1000 mA/g. Rate performance was closely related to the relative amount of mesoporous surface area.

New electrode materials for electrochemical capacitors, composite powders of porous carbon with metal carbides, either tungsten carbide WC or molybdenum carbide Mo_2C, were prepared through carbon coating process. In these composite powders, most of particles of metal carbide were supposed to be coated by porous carbon and changed to hydroxide during the first charge-discharge cycle in H_2SO_4 aqueous electrolyte, which showed redox reaction in further charge-discharge cycles, in addition to electric double layers on carbon surface. These composite powders gave a high capacitance in 1 M H_2SO_4 electrolyte, as about 350 F/cm^3 for carbon-coated WC and 550 - 250 F/cm^3 for carbon coated Mo_2C. Coating by porous carbon

inhibited the growth of metal carbide particles during their formation and also the agglomeration of hydroxides during charge-discharge cycles.

6-2 Carbon coating on ceramic particles

Carbon coated on ceramic particles through the carbonization of various thermoplastic resins in the mixtures with different substrate ceramics endued with new characteristics for complex materials i.e., carbon materials [5-8]. The characteristics of this method were that coated carbon layer were served as various functions, *e.g.* possessing of high surface area, inhibition of grain growth on substrate materials, separating between substrate particles, keeping a functional space as in the case of carbon-coated Sn, etc. In addition, thermoplastic resins could be used as carbon sources. Disposal resins such as PET tips could be used as carbon precursor.

In order to get a high surface area, activation process of carbon has usually been employed. In addition, there have been reported various precursors and processes to prepare porous carbons without any activation process. Microporous and mesoporous carbons were prepared by using various templates, such as zeolites and silicas [9, 10]. For these template processes, however, it was pointed out that the template had to be dissolved out by strong acids after carbonization and that large amount of production was not easy, although the pores with a specific size were easily obtained. The method, developed in the present thesis using MgO substrate, was very simple and easy process to prepare mesoporous carbons. In this process, even the design of pore size distribution is possible by selecting suitable magnesium salts. The process for the preparation of porous carbons from thermoplastic precursors is expected to be developed as a novel process for the production of porous carbons, including conventional activated carbons.

6-3 Prospect

While an economic activity and social activity become large scale, consumption of energy and resources increases and global environment problems, such as environmental pollution and warming, have been actualizing. So, electric energy storage as rechargeable batteries and electrochemical capacitors have to be investigated and developed for future.

Therefore materials prepared and carbon coating process developed in the present thesis is attractive materials and methods. Furthermore, carbon coating process can be expect for other many application the exception of electric energy device.

Table 6-1 Results in the present thesis for the materials developed.

Chapter	Materials developed	Preparation method	Materials used	Electric energy device applied	Results in the present thesis	
					Preparation	**Electrode properties**
2	Anhydrous MnV_2O_6	Autogenous hydrothermal and coprecipitation	$Mn(CH_3COO)_2$, V_2O_5	Anode for Li ion rechargeable batteries	Direct preparation below 200 °C. Characteristic XRD pattern. Rod-like particles.	High capacity of > 600mAh/g. Capacity increase with cycling. *Large irreversible capacity at 1st cycle.*
3	Carbon-coated Sn		SnO_2, MgO, thermoplastic precursor PVA		Autogenous reduction of SnO_2 to Sn during carbon coating. Fine particles of Sn.	High capacity as ~50mAh/g. Good cyclic performance. *Large irreversible capacity at 1st cycle.*
4	Mesoporous carbons	Carbon coating process	MgO, Mg salts, thermoplastic precursors (PVA, HPC, PET)	Electric double layer capacitors, EDLC	Mesopore size control by MgO precursors. High surface area without activation (~2000m^2/g). Thermoplastic precursors. Recycling of MgO.	High EDLC capacitance as ~300 F/g. Good rate performance above 75 %.
5	Carbon-coated WC and Mo_2C		K_2WO_4, K_2MoO_4, HPC	Electrochemical capacitors	Autogenous formation of carbides during carbon coating. Fine particles of WC and Mo_2C.	Redox capacitance due to metal hydroxide and double layer capacitance. High capacitance per volume (~550F/cm_3).

Reference

1. J. R. Dahn, A. K. Sleegh, H. Shi, B. M. Way, W, J, Weydanz, J.N. Reimers, Q, Zhong, U. von Sacken,Lithium Batteries, G. Pistoia, *editor, Elsevier* (1993) p.1-44.
2. M. Wakihara, *Material Sci. and Engineering* **33** (2001) 109-134.
3. B. E. Conway, *Electrochemical supercapacitors*, Kluwer Academic, New York (1999).
4. K. Kinosihta, In "Carbon: electrochemical and physicochemical properties" John Wiley Sons, New York, NY (1988).
5. M. Inagaki, H. Miura and H. Konno, *J. Europ. Ceram. Soc.,* **18** (1998) 1011-1015.
6. T. Tsumura, N. Kojitani, I. Izumi, N. Iwashita, M. Toyoda and M. Inagaki, *J Mater. Chem.,* **12**, (2002) 1391-1396.
7. M. Toyoda, T. Tsumura, Y. Nanbu, M. Omura and M. Inagaki, *Mizukannkyou Gakkaishi*, **26** [4], (2002) 209-214.
8. B. Tryba, A. W. Morawski, T. Tsumura, M. Toyoda and M. Inagaki, *J. Photochem. Photobio. A: Chem.*, **167** (2004) 127-135.
9. M.S. Mel'gunov, E.A. Mel'gunova, V.I. Zaikoviskii, V.B. Fenelonov. *Langmuir* **19** (2003) 10426-10433.
10. T. Kyotani, T. Nagai, S. Inoue, A. Tomita, *Chem. Mater* **9** (1997) 609-615.

List of Publications

[1] Michio Inagaki, Takahiro Morishita, Masanori Hirano, Vinay Gupta, Tsuyoshi Nakajima
"Synthesis of MnV_2O_6 under autogenous hydrothermal conditions and its anodic performance"
Solid State Ionics **156** [3-4] 2003 275-282

[2] Takahiro Morishita, Kayo Nomura, Tokuo Inamasu Michio Inagaki
"Synthesis of anhydrous MnV_2O_6 powder by coprecipitation and its anodic performance for lithium secondary battery"
Solid State Ionics **176** 2005 2235-2241

[3] Takahiro Morishita, Rieko Suzuki, Tetsuo Nishikawa, Tomoki Tsumura, Michio Inagaki,
"Preparation of Porous Carbons by Carbonization of the Mixtures of Thermoplastic Precursors with MgO"
Tanso **2005**, 2005 226-231.

[4] Takahiro Morishita, Masamitsu Hirabayashi, Yuta Nisihoka, Tomoyuki Okuni, Naoto Ota, Michio Inagaki
"Preparation of carbon-coated Sn powders and their loading onto graphite flakes for lithium-ion secondary battery"
Journal of Power Sources, (in press)

[5] Takahiro. Morishita, Yasusshi. Soneda, Hiroaki Hatori, Tomoki Tsumura, Michio Inagaki,
"Preparation of porous carbons from thermoplastic precursors and their performance for electric double layer capacitors"
Carbon (submitted).

[6] Takahiro Morishita, Yasushi Soneda, Hiroaki Hatori, Michio Inagaki
"Carbon-Coated Tungsten and Molybdenum Carbides for Electrode of Electrochemical Capacitor"
Electrochimica Acta (submitted)

[7] Takahiro Morishita, Rieko Suzuki, Tetsuo Nishikawa, Tomoki Tsumura, Michio Inagaki,
"Preparation of Mesoporous Carbons by Carbonization of the Mixtures of Poly(vinyl alcohol) with Magnesium salts"
Tanso (submitted)

Others

[1] Michio Inagak Takahiro Morishita, Akitoshi Kuno, Takayuki Kito, Masanori Hirano ,Taisuke Suwa, Kouichi Kusakawa
"Carbon foams prepared from polyimide using urethane foam template"
Carbon **42** (2004) 497-502

[2] Michio Inagaki, Shingo Kobayashi, Fumi Kojin, Nobuhiro Tanaka, Takahiro Morishita, Beata Tryba.
"Pore structure of carbons coated on ceramic particles"
Carbon **42** (2004) 3153-58

[3] Hidetaka Konno, Takahiro Morishita, Syuya Sato, Hiroki Habazaki, Michio Inagaki
"High-capacity negative electrode materials composed of Si-C-O glass-like compounds and exfoliated graphite for lithium ion battery"
Carbon, **43** 2005 1111-14

---------- Acknowledgment ---------

The present study was accomplished in Graduate School of Engineering, Aichi Institute of Technology, in the period from 2001 to 2006. The author has been helped by ceramics laboratory's staffs and many student members.

The author is profoundly grateful to *Professor Michio Inagaki* who gave investigation of materials science to me and engaging in the present study, and would like to express his sincere gratitude for beneficial advices, discussion and consultation.

The author is greatly indebted to *Professor Tsuyoshi Nakajima*, *Professor Yuichi Kobayashi* and *Professor Masanori Hirano* for their kind helps and useful advices for making this thesis.

The author wishes to express many thanks to *Dr. Yasushi Soneda* of National Institute of Advanced Industrial Science and Technology and *Dr. Tomoki Tsumura of NARD Institute Ltd.,* for their kind helps, useful advices and many teaching.

The author wishes to express his gratitude to *Professor Hidetaka Konnno* and *Professor Hiroki Habazaki* of Hokkaido University, for measurements of XPS and TEM.

The author wishes to express his thanks to *Dr. Yasuo Izumi* of Tokyo Institute of Technology, for measurements of XAFS analysis.

The author thanks to *all the student members of ceramics laboratory,* where he had a very fulfilling time with them.

Finally, the author expresses his special thanks to his parents for longstanding their support.

January, 2006

Takahiro Morishita